Aus dem Physiologischen Institut

der Julius-Maximilians-Universität Würzburg

DFG Emmy Noether Gruppe von Dr. Robert J. Kittel

Hebbian plasticity at neuromuscular synapses of Drosophila

Dissertation

zur Erlangung des naturwissenschaftlichen Doktorgrades

der Julius-Maximilians-Universität Würzburg

Dmitrij Ljaschenko

geboren in Syr-Darja, Usbekistan

Würzburg 2013

Eingereicht am: 2013.10.10

Mitglieder der Promotionskommission:

Vorsitzender: Prof. Dr. Christian Wegener beauftragt von Dekan Prof. Dr. Markus Engstler

Gutachter : Prof. Dr. Manfred Heckmann

Gutachter: Prof. Dr. Erich Buchner

Tag des Promotionskolloquiums: 2014.01.15

Doktorurkunde ausgehändigt am:

Ehrenwörtliche Erklärung (September 2013):

Ich versichere hiermit ehrenwörtlich, dass ich die vorliegende Doktorarbeit selbständig verfasst habe und keine anderen als die angegebenen Hilfsmittel verwendet habe. Stellen, die wörtlich oder sinngemäß aus anderen Schriften entnommen wurden, sind gekennzeichnet. Die Arbeit hat weder komplett, noch auszugsweise, in gleicher, oder ähnlicher Form einer anderen Prüfung vorgelegen. Ich habe bisher keine akademische Grade erworben oder versucht zu erwerben.

Dmitrij Ljaschenko

Danksagung

Zuallererst möchte ich dem Betreuer meiner Dissertation, Robert Kittel danken, bei dem ich so viel lernen durfte. Bei ihm habe ich erst verstanden was konsequentes wissenschaftliches Denken und effizientes, professionelles Arbeiten bedeutet. Außerdem möchte ich mich bei Manfred Heckmann bedanken, der mich in die Welt der Elektrophysiologie eingeführt hat, an dessen Institut ich arbeiten durfte und der in der entscheidenden Publikationsphase wertvolle Ratschläge gab.

Ich bedanke mich auch bei Erich Buchner, der mit seinen Vorlesungen die Grundlagen für mein neurobiologisches Verständnis gelegt hat und sich bereit erklärt hat die Zweitkorrektur zu übernehmen. Bei Claudia Wirth und Nadine Ehmann, die mir viel Arbeit abgenommen haben und Tobi Langenhan für seine Hilfsbereitschaft. Bei Brian Miller, der das Korrekturlesen übernahm.

Bei meinen Kollegen und Freunden: Nadine Ehmann, Jenny Gehring, Nici Hartmann, Martin Pauli, die die Physiologie Würzburg zu einem Zuhause gemacht haben.

Nicht zu vergessen bei meinen Eltern Irina und Stanislaw, ohne deren Mut nach Deutschland auszuwandern und ihre harte Arbeit, die mir das Studium erst ermöglicht hat, mein Leben wohl ganz anders verlaufen wäre.

Bei meinen Schwestern Katya und Lina für die moralische und noch wichtiger viktualische Unterstützung, bei meinen beiden besten Freunden Johannes und Christoph, die mit mir den gleichen Weg gegangen sind.

Und nicht zuletzt bei Sabrina, die immer bei mir ist.

to Pauline

Hebbian plasticity at neuromuscular synapses of *Drosophila*

1. Summary

Synaptic plasticity determines the development of functional neural circuits. It is widely accepted as the mechanism behind learning and memory. Among different forms of synaptic plasticity, Hebbian plasticity describes an activity-induced change in synaptic strength, caused by correlated pre- and postsynaptic activity. Additionally, Hebbian plasticity is characterised by input specificity, which means it takes place only at synapses, which participate in activity. Because of its correlative nature, Hebbian plasticity suggests itself as a mechanism behind associative learning.

Although it is commonly assumed that synaptic plasticity is closely linked to synaptic activity during development, the mechanistic understanding of this coupling is far from complete.

In the present study channelrhodopsin-2 was used to evoke activity *in vivo*, at the glutamatergic *Drosophila* neuromuscular junction. Remarkably, correlated pre- and postsynaptic stimulation led to increased incorporation of GluR-IIA-type glutamate receptors into postsynaptic receptor fields, thus boosting postsynaptic sensitivity. This phenomenon is input-specific.

Conversely, GluR-IIA was rapidly removed from synapses at which neurotransmitter release failed to evoke substantial postsynaptic depolarisation. This mechanism might be responsible to tame uncontrolled receptor field growth. Combining these results with developmental GluR-IIA dynamics leads to a comprehensive physiological concept, where Hebbian plasticity guides growth of postsynaptic receptor fields and sparse transmitter release stabilises receptor fields by preventing overgrowth.

Additionally, a novel mechanism of retrograde signaling was discovered, where direct postsynaptic channelrhodopsin-2 based stimulation, without involvement of presynaptic neurotransmitter release, leads to presynaptic depression. This phenomenon is reminiscent of a known retrograde homeostatic mechanism, of

inverted polarity, where neurotransmitter release is upregulated, upon reduction of postsynaptic sensitivity.

2. Zusammenfassung

Das Phänomen der synaptischen Plastizität bestimmt die Entwicklung funktionaler neuronaler Schaltkreise. Die meisten Neurowissenschaftler betrachten synaptische Plastizität als die neuronal Grundlage von Lernen und Gedächtnis. Es gibt viele Ausprägungsarten synaptischer Plastizität, eine davon ist die sogenannte Hebb'sche Plastizität. Diese ist definiert durch eine aktivitätsinduzierte, langanhaltende Veränderung der Stärke einer synaptischen Verbindung, verursacht durch korrelative Aktivierung der Prä- und der Postsynapse. Zusätzlich ist die Ausbreitung der Hebb'sche Plastizität synapsenspezifisch, d.h. nur die Synapsen, die an der korrelativen Aktivierung teilnehmen, erfahren auch die Veränderung. Das Wachstumssignal breitet sich also nicht auf benachbarte Synapsen aus. Der korrelative Wesenszug der Hebb'schen Plastizität macht sie zu einem naheliegenden zellulären Mechanismus assoziativen Lernens.

Es wird angenommen, dass synaptische Aktivität und synaptische Plastizität während der Entwicklung neuronaler Schaltkreise eng gekoppelt sind. Das mechanistische Verständnis dieser Kopplung ist jedoch weitgehend unverstanden.

In der vorliegenden Arbeit wurde das lichtaktivierbare Kanalrhodopsin-2 verwendet, um Aktivität an der glutamatergen neuromuskulären Synapse in der lebenden, sich frei bewegenden, *Drosophila melanogaster* Larve auszulösen. Wenn die Prä- und die Postsynapse korrelativ aktiviert wurden, führte dies zur verstärkten Integration von Glutamatrezeptoren des GluR-IIA Typs in die postsynaptischen Rezeptorfelder, was in einer Erhöhung der postsynaptischer Empfindlichkeit mündete. Dieses Platizitätsphänomen wurde als synapsenspezifisch identifiziert und damit als Hebb'sch.

Im Gegenzug, wurde der gleiche Rezeptortyp entfernt, wenn Neurotransmitterfreisetzung nicht zu einer erheblichen Depolarisation der Postsynapse führte. Dieser Mechanismus könnte für die Kontrolle des Rezeptorfeldwachstums verantwortlich sein.

Es wurde ein physiologisches Modell erarbeitet, bei dem Hebb'sche Plastizität das Wachstum postsynaptischer Rezeptorfelder während der Entwicklung leitet und sporadische, nicht synchronisierte Neurotransmitterfreisetzung die Rezeptorfeldgröße stabilisiert, indem sie das Wachstum Dieser begrenzt.

Zusätzlich wurde eine neue Modalität der synaptischen Plastizität an der neuromuskulären Synapse entdeckt: Ein retrograder Signalweg wird aktiviert wenn die postsynaptische Seite, unter Umgehung der Präsynapse, direkt, lichtinduziert aktiviert wird. Dieser Signalweg führt zur präsynaptischen Depression. Das Phänomen erinnert stark an einen bereits bekannten retrograden homöostatischen Mechanismus, reziproker Polarität, bei dem Neurotransmitter Freisetzung hochreguliert wird, wenn die Empfindlichkeit der Postsynapse verringert wird.

3. Introduction

3.1 Learning and memory

3.1.1 General

Men ought to know that from nothing else but thence [from the brain] come joys, delights, laughter and sports, and sorrows, griefs, despondency, and lamentations. And by this, in an special manner, we acquire wisdom and knowledge, and see and hear, and know what are foul and what are fair, what are bad and what are good, what are sweet and what unsavoury. [...] And by the same organ we become mad and delirious, and fears and terrors assail us, some by night, and some by day, and dreams and untimely wanderings, and cares that are not suitable, and ignorance of present circumstances, desuetude, and unskilfulness. All these things we endure from the brain, when it is not healthy [...] In these ways I am of opinion that the brain exercises the greatest power in the man (Adams, 1849).

Hippocrates 460-377 B.C., On the sacred disease (Epilepsy)

Consciousness and processes underlying learning and memory are and will probably remain the phenomena most challenging to analyse in Neurobiology. The human brain is the most complex system known to science; it contains billions of neurons each connected to other neurons by an enormous number of contacts. This elaborate structure gives rise to our perceptions, emotions, determines the rules by which we learn and remember.

3.1.2 Declarative and non-declarative memory

Memory is the preservation of learned information, a phenomenon psychologists have extensively studied and classified by the nature of stored information (Bear et al., 2007a). Based on these studies, two main categories of memory were defined, non-declarative (implicit) and declarative (explicit) memory. The latter saves facts that we remember during our lifetime, i.e. the capital of Mali, the name of Tupac's 1996 album (semantic knowledge), or personal events (episodic, autobiographic memory). Memories like these are widely distributed throughout the brain and the

storage and retrieval of these memories greatly depends on consciousness. Non-declarative memory, in contrast, is stored and recalled on a less conscious basis and is subdivided into several classes (Bear et al., 2007a). The four most prominent are:

(1) Non-associative memory comes in two subclasses, (1a) habituation, which is decreasing the response to a stimulus after repeated presentations and the opposite effect (1b) sensitisation, which is increasing the response to a stimulus after repeated presentations (Schacter and Wagner, 2012).

(2) Associative memory, as in (2a) classical conditioning, which is to learn to associate a strong response-evoking stimulus to a neutral stimulus. There, a strong stimulus (unconditioned stimulus) like food is presented shortly after an otherwise neutral stimulus, e.g. sound of a metronome. This stimulus now becomes the conditioned stimulus and can alone evoke a response, which normally is evoked by the unconditioned stimulus (Pavlov, 1927). (2b) Operant conditioning (term coined by B.F. Skinner) is another subclass of associative learning, which is learning to associate a coincident action with a meaningful stimulus like a reward and as a result increasing the frequency of this behaviour (Thorndike, 1901).

(3) Priming is improved recalling of learned information, when a small part of the information is presented as a hint. For example: individuals are presented a list of words to learn. Later, if they are given the first three letters of a word as a hint to remember words from the list, they perform better than in free recall. Interestingly, amnesiac patients, who do not even remember having learned these words, perform as well as healthy patients in this task. This speaks for an unconscious mechanism behind priming (Schacter and Wagner, 2012).

(4) Procedural memory is unconscious remembering of certain trained skills and habits (Bear et al., 2007a; Schacter and Wagner, 2012).

3.1.3 Long-term, short-term and working memory

Another way to classify memory is by its persistence. Memories that last for days, months or years are usually referred to as long-term memory. Short-term memories last for seconds or hours and are vulnerable to disruption, e.g. by head trauma or electroconvulsive shock (Schacter and Wagner, 2012). The instability of short-term memory led to the idea that short-term memory can be transferred to long-term memory by a process termed consolidation (Schacter and Wagner, 2012). A direct transfer of sensory information into long-term memory, however, is also possible (Bear et al., 2007a).

Memories, which are stable for even shorter periods are referred to as working memory. There, information is stored temporarily for seconds, its capacity is very limited and it requires rehearsal to keep the memory 'alive', e.g. keeping a phone number 'in mind' by repeating it. Working memory is often studied by measuring a person's digit span, which is a list of randomly chosen numbers, a person can repeat after hearing it. The normal digit span is 7, plus or minus two numbers (Bear et al., 2007a).

3.2 Synaptic plasticity

3.2.1 Synaptic plasticity in general

Since the brain is governed by natural laws, the obvious questions to ask as a neuroscientist are: what are the physiological processes behind learning and memory and what is the physical representation of memory, in other words, a memory trace or engram?

Synapse (Greek: syn- together, hapsis- joining), a term coined by C.S. Sherrington, describes the communication connections between neurons, or neurons and other cells. 1897, it first appeared in written form (Tansey, 1997) in a Physiology textbook by M. Foster (Foster M., 1897). Sherrington, who contributed to the book, already recognised the contact site between nerve cells as an "opportunity for some change

in the nature of the nervous impulse". Later, when it was realised that synapses change their properties upon stimulation, it was tempting to view these structures not just as the place of signal interpretation, but also as the location of memory storage.

3.2.2 The electrical synapse

To distinguish between the two sides of a synapse and indicate the direction of signal propagation, the terms pre- and postsynapse were introduced. Signals typically propagate from the pre- to the postsynapse.

Synapses are subdivided into two major classes: the chemical and the electrical synapse. The latter are comparably simple in terms of structure and function; they allow direct ion flow between two cells, which is possible in both directions. Although there are rectifying electrical synapses, which means current flows preferentially in one direction (Hormuzdi et al., 2004).

Specialised proteinaceous pores, called gap junctions, provide the connection between the cells in an electrical synapse. The cells are electrically coupled, which means ions flow directly from one cell to the other. Thus, a depolarisation of one cell is mirrored by a kinetically similar depolarisation of the connected cell (Bear et al., 2007b). This mechanism guarantees almost instantaneous information transfer, only slowed by diffusion of ions through the relatively large 1-2 nm pore (Bear et al., 2007b).

3.2.3 The chemical synapse

In a chemical synapse the presynaptic side generally consist of an axon terminal, where the arriving action potential triggers an electrochemical gradient driven inflow of Ca^{++} ions through voltage-gated Ca^{++} channels into the presynapse. This leads to fusion of neurotransmitter (NT) filled vesicles with the cell membrane and release of neurotransmitter into the synaptic cleft.

The molecules governing presynaptic exocytosis are reviewed in (Jahn and Fasshauer, 2012). In short, the fusion of vesicles with the presynaptic membrane is mediated by a molecular machinery, which consists of several proteins: the so-called SNARE complex (vesicular and presynaptic membrane proteins SNAP25, Synaptobrevin and Syntaxin) is responsible for the close placement and final fusion of the cell- and vesicle membranes. Synaptotagmin 1 is the Ca^{++} sensing protein, which controls fusion. Both the SNARE proteins and Synaptotagmin additionally increase the curvature of the vesicle, thus, increasing the probability of fusion (Martens and McMahon, 2008). A substantial number of other proteins is involved in control of synaptic exocytosis (Jahn and Fasshauer, 2012).

Presynaptic exocytosis takes place at specialised areas of the presynapse, the active zones, which are characterised by an electron-dense membrane. Active zones, additionally, often harbour electron dense proteinaceous structures, which project into the cytosol. These structures are believed to facilitate tethering, docking, and fusing of vesicles (Zhai and Bellen, 2004).

Postsynaptic receptors are localised opposite active zones in electron-dense membranes called postsynaptic densities (PSD). Receptors can be directly gated ion channel receptors (proteinaceous pores), which are responsible for fast signal transmission, or G-protein coupled receptors (slower action via second messengers). A wide array of neurotransmitters, of diverse chemical origin are involved at different synapses, such as acetylcholine, glutamate, dopamine, to name only a few (Schwartz and Javitch, 2012). Intriguingly, glutamate, the main excitatory neurotransmitter of the vertebrate brain also acts excitatory at the *Drosophila* neuromuscular junction (NMJ; Jan and Jan, 1976a).

The selectivity to ions in directly gated ion channel receptors dictates whether neurotransmitter binding to the receptor leads to excitation (depolarisation) or inhibition (hyperpolarisation) of the postsynapse (Hille, 2001). The electrical-to-chemical-to-electrical translation of the signal in chemical synapses and the corresponding involvement of many proteins and other molecules render the

chemical synapse a very flexible site for changing signals travelling through the nervous system. At the same time, the chemical synapse is the site of action for many neuro-toxins (Bear et al., 2007b).

The transmission parameters and morphology of synapses are not static; usually they can change as a function of prior activity. This phenomenon is called synaptic plasticity and is nowadays thought to be one of the most important features of chemical synapses and the ultimate correlate of memory storage (Kandel and Siegelbaum, 2012).

3.2.4 The Hebbian learning rule

Before it was known how synapses change their transduction properties upon stimulation, the Canadian psychologist Donald O. Hebb proposed a postulate for the cellular basis of learning, which was to become enormously influential during the rise of cellular neurosciences: "When an axon of cell A is near enough to excite a cell B and repeatedly or persistently takes part in firing it, some growth process or metabolic change takes place in one or both cells such that A's efficiency, as one of the cells firing B, is increased" (Hebb, 1949).

The broad interpretation range of this hypothesis lead to a plethora of investigations, which demonstrated Hebbian plasticity at synaptic level, in a wide range of experimental setups. Today, most neuroscientist would probably agree on the following three defining characteristics of Hebbian plasticity on synaptic level: (1) a long-term change in synaptic strength, that (2) depends on simultaneous activation of the pre- and postsynaptic side and, that (3) acts independently at individual synapses (Abbott and Nelson, 2000).

This synaptic learning rule provides an attractive mechanism for models of neuronal network formation, learning and memory (Abbott and Nelson, 2000; Sejnowski, 1999). The Hebbian mechanism seems especially promising as a cellular explanation for memory formation in associative learning paradigms.

Much of the work on Hebbian synaptic plasticity and synaptic plasticity in general has been concentrated on cellular and molecular mechanisms, which underlie activity-dependent, functional changes in synaptic function. The major molecular effectors of synaptic plasticity are discussed below.

3.2.5 Molecular basis of presynaptic plasticity in invertebrates

In the 1970s, scientists around Eric R. Kandel started a systematic investigation of synaptic mechanisms underlying habituation and sensitisation at the cellular level. It was found that in *Aplysia californica*, a large marine slug, habituation of the gill and siphon withdrawal reflex (upon a mild tactile stimulus to the siphon) is accompanied by depression of the monosynaptic connection between the central sensory neuron and the motoneurons that mediate this reflex (Castellucci et al., 1970). The depression was attributed to a decrease in transmitter release from the sensory neuron, therefore a presynaptic effect (Castellucci and Kandel, 1974). The sensitisation of the same pathway (upon a noxious stimulus) was also shown to be based on a presynaptic modulation (Castellucci and Kandel, 1974).

Protein kinase A (PKA), protein kinase C (PKC) and many downstream effectors in the presynaptic terminal are responsible for both effects (Byrne and Kandel, 1996; Royer et al., 2000). The same presynaptic pathways are involved in classical conditioning in *Aplysia* (Hawkins et al., 1983; Walters and Byrne, 1983). Long-term structural changes of the synapse were shown to depend on transcription factors CREB and C/EBP and protein synthesis (Dash et al., 1990; Kandel, 2001; Montarolo et al., 1986).

Intriguingly, the same molecules and molecular pathways are involved in learning deficit mutants in *Drosophila*, which were identified later in forward genetic screens: the first two identified genes were *dunce* and *rutabaga*, coding for a cAMP-dependent phosphodiesterase and an adenylyl cyclase, respectively (Davis, 2005). PKA (cAMP-dependent protein kinase 1) also plays a role in associative olfactory learning in *Drosophila* (Aszodi et al., 1991; Drain et al., 1991; Li et al., 1996), and the CREB

pathway turned out to be important for long-term olfactory memory in *Drosophila* (Yin et al., 1994).

3.2.6 Molecular basis of postsynaptic plasticity in vertebrates

The two most promising candidates for a cellular mechanism of learning and memory in vertebrates are long-term potentiation (LTP) and long-term depression (LTD; Malenka and Bear, 2004). Experimentally, LTP was first demonstrated in 1973. Bliss and Lømo showed that tetanic stimulation of the perforant pathway to the dentate gyrus of the hippocampus, leads to stronger evoked postsynaptic potentials in the dentate gyrus for hours (Bliss and Lømo, 1973).

The importance of the hippocampus in acquisition of explicit memory was first shown with patient H.M. After surgical removal of his hippocampi, parahippocampal gyrus, and amygdalae in an attempt to cure his epilepsy, the patient was unable to acquire new episodic long-term memory, his short-term memory and procedural memory acquisition remained intact. Interestingly, already acquired explicit memories remained intact (Corkin et al., 1997; Schacter and Wagner, 2012). The fact, that Hebbian LTP was discovered in the hippocampus first, led to the popularity of Hebbian plasticity as a research topic. LTP has been identified at many classes of excitatory synapses, in many areas of the vertebrate brain: hippocampus, amygdala, cerebellum and cerebral cortex (Malenka and Bear, 2004).

Among several LTP inducing mechanisms, the most prominent depends on activation of so-called NMDA-type (N-methyl-D-aspartate) glutamate receptors. The NMDA receptor (NMDA-R) is blocked by Mg^{++} ions when the membrane is negatively polarised, the block is removed upon depolarisation. If glutamate binds additionally, the channel opens. The channel, therefore, acts as a coincidence detector of membrane depolarisation (postsynaptic side) and glutamate release (presynaptic side), thus, detecting correlation between the post- and the presynapse. The NMDA-R opening leads to Ca^{++} influx and activation of protein kinases and can ultimately promote insertion of additional AMPA-type (α-amino-3-hydroxy-5-

methyl-4-isoxazolepropionic acid) glutamate receptors into previously silent synapses by lateral diffusion or postsynaptic exocytosis (Kessels and Malinow, 2009). AMPA receptors are the major current carrying postsynaptic ion channel receptors during excitatory synaptic transmission at vertebrate glutamatergic synapses. Increasing AMPA receptor numbers therefore increases the current.

Activity-dependent reduction of synaptic strength, LTD can be evoked by low frequency firing (Feldman, 2012). The critical requirement for both LTP and LTD is thought to be presynaptic spiking (action potential firing) and postsynaptic depolarisation. While strong postsynaptic depolarisation leads to LTP, weak postsynaptic depolarisation leads to LTD (Feldman, 2012). This led to the conclusion that the level of postsynaptic Ca^{++} elevation determines the direction of synaptic strength change: weak elevation of postsynaptic Ca^{++} leads to LTD, strong elevation to LTP (Feldman, 2012).

3.2.7 General molecular model for learning related plasticity

Although some studies had indicated a role of the postsynapse during synaptic plasticity in *Aplysia* (Bailey and Chen, 1988; Glanzman et al., 1990), until the mid 1990s research in *Aplysia* concentrated on the presynapse.

An increasing number of reports, however, showed postsynaptic plasticity in invertebrates: a postsynaptically mediated Hebbian mechanism of synaptic plasticity was shown in *Aplysia* (Lin and Glanzman, 1994). In leech (*Hirudo medicinalis*) multiple forms of NMDA-dependent LTP and LTD (Burrell and Sahley, 2004) and a Hebbian, but NMDA independent mechanism in *Octopus vulgaris* (Hochner et al., 2003) and honeybee, *Apis mellifera* (Menzel and Manz, 2005) were demonstrated.

New data support a role of NMDA receptor activity in associative learning in *Aplysia* (Antonov et al., 2003; Murphy and Glanzman, 1997), *Drosophila* (Xia et al., 2005), *Caenorhabditis elegans* (Kano et al., 2008) and Hebbian LTP in associative learning in *Octopus vulgaris* (Shomrat et al., 2008). Habituation and Sensitization in *Aplysia* (Li et al., 2009; Li et al., 2005) and habituation in *C. elegans* (Rose et al., 2003),

both previously thought to rely solely on the presynapse, were also shown to involve postsynaptic AMPA receptors. Even on the level of protein synthesis the importance of the postsynaptic side was shown in long-term facilitation in *Aplysia* (Cai et al., 2008).

Research in vertebrates is also starting to shift towards less thoroughly explored terrain: the presynapse. There is evidence that LTD and LTP may well involve changes on the presynaptic side like alteration of vesicle fusion, recruitment of empty release sites and enlargement of release sites (Krueger and Fitzsimonds, 2006).

The NMDA receptor independent LTP at the mossy-fiber-to-CA3 synapse is mediated primarily presynaptically, whether presynaptic plasticity is also at work in the CA1 region or the dentate gyrus, remains debated (Krueger and Fitzsimonds, 2006). When several phenomena are involved in a mechanism, scientific publications reasonably tend to show the most obvious effects first. This might be one reason for the presynaptic focus of invertebrate researchers and the postsynaptic focus of vertebrate researchers.

What makes matters even more complex is that synapses can also communicate in the opposite direction, from post- to presynapse. The corresponding retrograde signals were found in vertebrates (Regehr et al., 2009), in *Aplysia* e.g. during long-term facilitation (Antonov et al., 2003; Cai et al., 2008) and in *Drosophila* during homeostatic synaptic processes (Davis, 2006).

Additionally, there is anterograde communication (presynapse to postsynapse) during synaptic plasticity, besides the one mediated by neurotransmitters. EphB receptors and presynaptic B-ephrins were shown to be necessary for the induction of mossy fibre LTP, which is mediated presynaptically (Contractor et al., 2002).

It's becoming obvious that vertebrates and invertebrates share not only the same mechanisms in action potential propagation and synaptic transmission, but also mechanisms for alteration of synaptic strength (Glanzman, 2010).

3.3 Limitations of the synaptic plasticity hypothesis

Memorising new facts and events is a process in which information entering the brain causes specific physical changes within it. The commonly accepted view among most neuroscientists is that memory is stored in structural modifications of synaptic connections; this results in changes of synaptic efficiency and in new patterns of neural activity (Kandel and Siegelbaum, 2012).

The synaptic plasticity hypothesis (SPH), however, has always faced criticism. In 1972 the Australian neurophysiologist John Eccles formulated it as follows: "The simple concept that disuse leads to regression of spine synapses and excess usage to hypertrophy can be criticised because […] almost all cells […] are discharging continuously. One can imagine therefore that there would be overall hypertrophy of all synapses under such conditions […] Evidently frequent synaptic excitation could hardly provide a satisfactory explanation of synaptic changes involved in learning." (Arshavsky, 2006).

To counter this criticism several phenomena were presented as mechanisms to tame uncontrolled synaptic hypertrophy, e.g. spike-timing dependent plasticity (STDP), where the precise timing of pre- and postsynaptic depolarisation can lead to strengthening or weakening of the same synapse (Abbott and Nelson, 2000).

However, there are still many points of criticism of synaptic plasticity, especially as the mechanism of long-term memory storage. Y.I. Arshavsky summarised the seven most important points in his view (Arshavsky, 2006). Four of which I would like to present here:

(1) Synaptic plasticity cannot explain life-long persistence of memory, basically because of the contradiction between the need for stability of life-long memory and the unstable-plastic nature of synaptic plasticity. Put differently: the fast turnover rate of protein structures implied in plasticity contradicts the stability of synaptic

connections, e.g. at the level of spine morphology (Grutzendler et al., 2002; Zuo et al., 2005).

(2) The SPH demands that the same circuitry runs storage and recall of memory (no artificial memory device does this). This leads to several problems, one of which is, that the recall of information might change the circuit where the information is stored. Constant spontaneous firing poses another problem to stability of newly formed circuitry. Additionally, the resistance of long-term memory to epileptic seizures and electroshocks is hard to explain. Basically all circuits should be changed after electric events like that, but they do not affect long-term memory.

(3) The different localisation of explicit memory storage (neocortex) and memory formation and consolidation (medial temporal lobe, hippocampus) poses another explanation difficulty to the SPH.

(4) Different time scales of synaptic (hours) and long-term memory consolidation processes (weeks or months) is another inconsistency, which is hard to resolve.

A large part of memory research concentrates on molecular mechanisms of synaptic plasticity, more or less silently assuming that this is the ultimate correlate of memory. Additionally, there is a lack of rival hypotheses for long term storage of memory, which might be one of the reasons SPH has not only been used to explain learning and initial memory consolidation, but also permanent consolidation. The author proposes the genomic DNA as the only known cellular substrate stable enough to account for the properties of long term memory (Arshavsky, 2006).

3.4 *Drosophila* neuromuscular junction

3.4.1 Background

The common fruit fly, *Drosophila melanogaster* (Greek: dew-δρόσος loving-φίλος; dark-μέλας belly -γαστήρ) has been the topic of research in biology for over a century. Especially in the field of neuroscience, *Drosophila* research lead to

groundbreaking discoveries, which influenced many areas of neurobiological research (Bellen et al., 2010; Weiner, 2000).

The fruit fly as an experimental model combines many advantages, which made the animal one of the most popular in neuroscience: there is a great variety of genetic techniques and a sequenced genome (Adams et al., 2000) available. Quick generation of transgenic animals is possible. Thousands of mutated flies exist, and scientists in the field are willing to share their transgenic flies and genetic tools (Ashburner et al., 2005).

Drosophila offers several developmental stages, with different sets of advantages.

(1) Optical accessibility during the developmental window between the fertilised egg and the embryo has proved itself very useful in developmental studies (Nusslein-Volhard and Wieschaus, 1980).

(2) The large 3rd instar larva is accessible to electrophysiology, with its transparency to imaging. Studies of simple behaviour and learning are easily performed.

(3) The early pupa has the advantage that it does not move, nor contract muscles upon motoneuron stimulation, while the electrophysiological properties of the neuromuscular junction (NMJ) are preserved (Jan and Jan, 1976a).

(4) The adult fly, with a large repertoire of innate and learned behaviour is valuable, especially to study the neurobiological basis of learning and behaviour.

Furthermore, *Drosophila* is very practical in terms of maintenance. It is small, easy to breed, has a short life cycle (**Figure 1A**) and is cheap to keep in large numbers. The animals are kept in vials containing egg-laying medium (**Figure 1B**), which supplies flies and larvae with food. Female flies lay eggs on laying medium, from which larvae develop. Larvae transform into pupae, from which adults eclose. Regular transfer of adult flies to new vials ensures a constant supply of embryos, larvae, pupae and adults at any developmental stage.

The life cycle of the fly is illustrated in **Figure 1A**. Female flies lay or insert eggs (length: 0.5 mm) into the medium. About 24 h after egg laying (AEL) the 1st instar larva hatches. There are three larval stages 1st-3rd instar, 1st and 2nd larval stages last 24 hours each, the 3rd lasts 48 h. The larva grows and moults twice before climbing to a dry place to form a pupa (5 days AEL) and remains in this stage for 4 days. Eclosion occurs at day 9 AEL. Within 12 hours the fly reaches fertility, pairs and the cycle begins anew. (Ashburner et al., 2005)

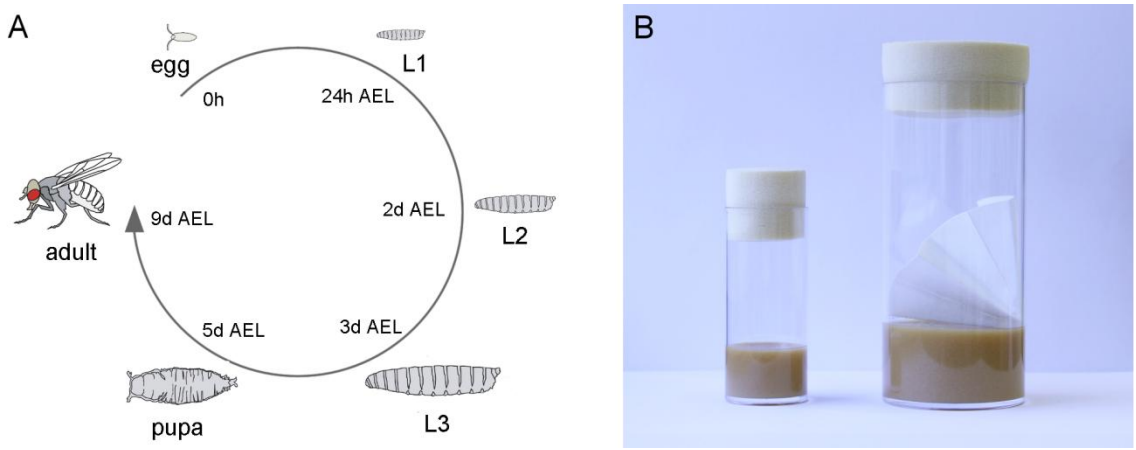

Figure 1 *Drosophila* life cycle and vials with laying medium. (A) Life cycle of *Drosophila* under optimal conditions, at 25°C (Ashburner and Roote, 2007). The adult fly lays eggs, up to 100/day (Ashburner and Roote, 2007). 24h after egg-laying (AEL) 1st instar larvae hatch. They undergo three rounds of growth and two rounds of moulting to reach the level of third instar larvae 3 d AEL. 5 d AEL the larvae pupate and after 4-4.5 more days in this stadium of metamorphosis adults ecclose at day 9 AEL. At 18 °C, the development takes around twice as long (Ashburner et al., 2005; Ashburner and Roote, 2007) Figure adapted from (Wolf, 2012). (B) Culture vials for *Drosophila* breeding with egg laying medium: small 6.4 cm (height) x 2.6 cm (inner ∅) and large vial 10.5 cm (height) x 4.6 cm (inner ∅) with filter paper.

3.4.2 Anatomy and Physiology of the neuromuscular junction

The *Drosophila* larval neuromuscular junction (NMJ) came under increased focus by neuroscientists when the feasibility of electrophysiology was demonstrated at this synapse for the first time (Jan and Jan, 1976b). Due to ever improving genetic tools, this synapse remains one of the most thoroughly studied synapses (Budnik and Ruiz-Canada, 2006).

Several factors have contributed to its popularity: the optical and electrophysiological accessibility, the typical, easily tractable structure, with well-defined innervation patterns, which allows investigating the same NMJ in many individuals, or the same NMJ during development of one individual and not least the availability of sophisticated genetic tools and resources.

The *Drosophila* body wall neuromuscular system consist of about 400 striated multinuclear muscle cells (10-20 nuclei), the arrangement of these muscles is constant (**Figure 2**). All electrophysiology in the present work was done at the ventral longitudinal muscle 6 (VLM 6, **Figure 2C**). In late 3rd instar larvae this muscle is about 400 µm long, 80 µm wide and 25 µm thick. The innervating nerves terminate in boutons with diameters of 2-6 µm (**Figure 3**), which contain several synapses. The boutons are surrounded by complex infoldings of the muscular membrane, the sub-synaptic reticulum (Hertweck, 1931; Osborne, 1967). The synaptic cleft is 20 nm wide.

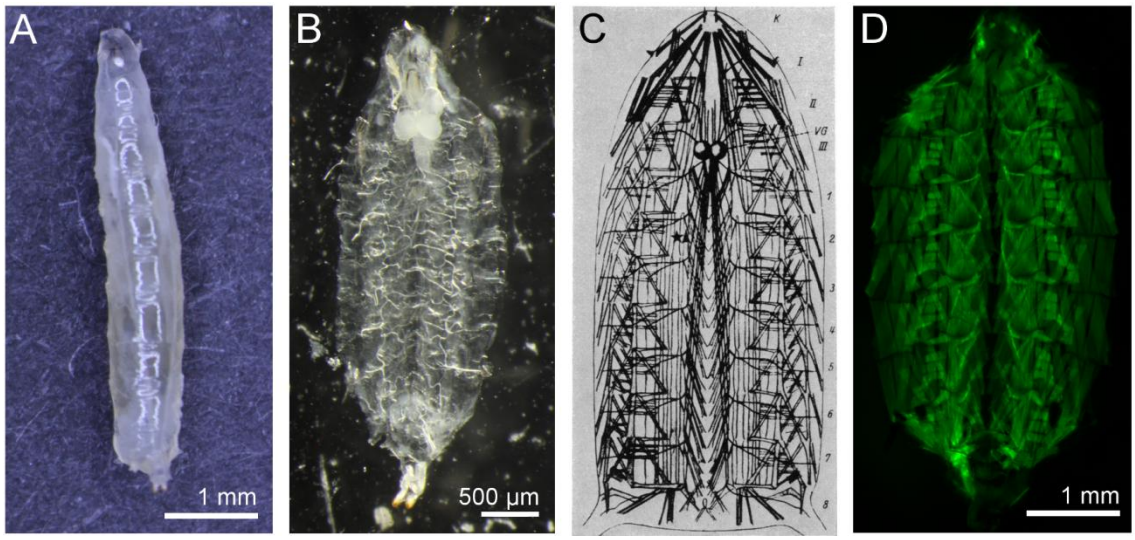

Figure 2 The *Drosophila* body wall muscle system. (A) A large 3rd instar *Drosophila* larva. (B) Dissected larva, innards removed. (C) Drawing of the larval neuromuscular system from (Jan and Jan, 1976b), which the authors adopted from (Hertweck, 1931). The thoracic segments are marked with Roman numbers, the abdominal segments with Arabic numbers, K marks the head, VG marks the ventral ganglion (CNS). Star marks the VLM 6 and arrowhead the VLM 7 of the second abdominal segment. (D) Epifluorescence image of a dissected larva with *g7-GAL4* driven EGFP expression.

VLM 6 is an isopotential muscle cell with a resting membrane potential (V_m) of -54 mV in normal saline and a specific muscle capacitance of 7.1 µF/cm², which results in 2000-5000 pF for this muscle (Jan and Jan, 1976b; Stewart et al., 1994). V_m depends on external Na^+ concentration and K^+ concentration, it obeys the Goldman-Hodgkin-Katz equation with a permeability coefficient of $P_{Na}/P_K = 0.23$. Cl^- is thought to distribute passively between the two sides of the cell membrane. The membrane resistance is typically between 5 and 10 MΩ. The transmission at this synapse is quantal and the Ca^{++} concentration dependence of release is to the power of 4. The main excitatory transmitter at the synapse is glutamate (Jan and Jan, 1976a).

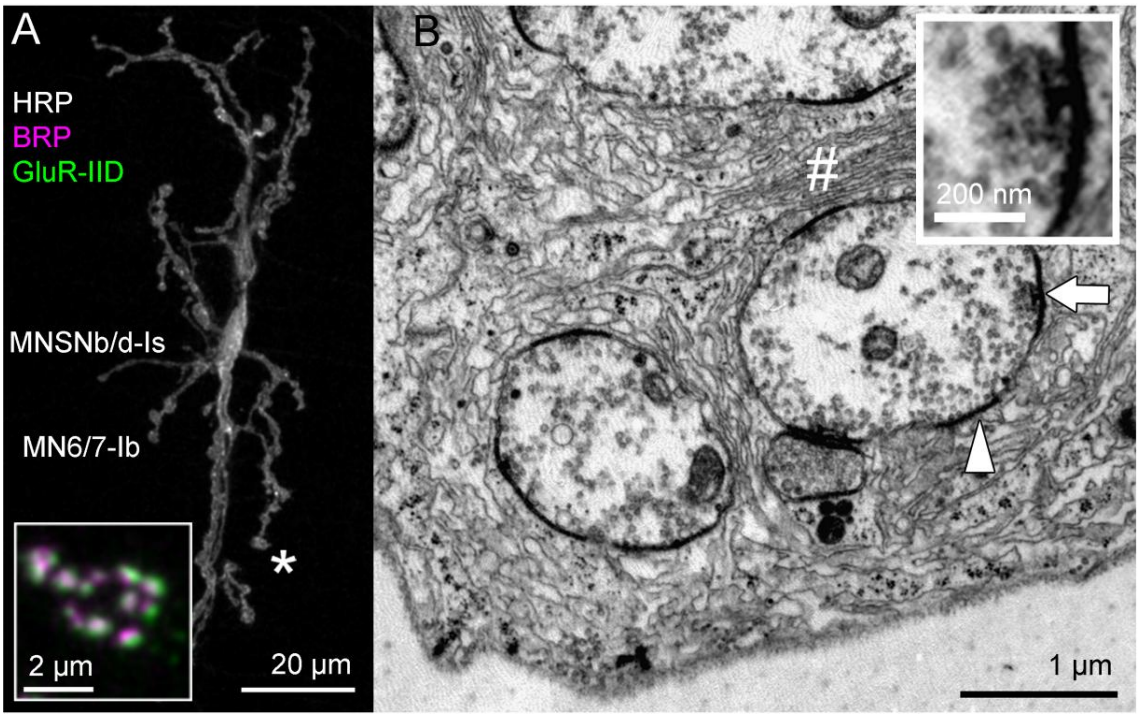

Figure 3 Example *Drosophila* larval NMJ. (A) Muscle 6/7 NMJ of segment A2 is shown. Anti horse radish peroxidase (HRP, grey) stains reliably the neuronal membrane, thus showing the overall morphology of the NMJ. For one bouton, marked with an asterisk, the staining against Bruchpilot (magenta) and GluR-IID (green), an essential subunit of the postsynaptic non-NMDA-type receptor is shown in the inset. One branch with MN6/7-Ib innervation (large boutons) and one branch with MNSNb/d-Is innervations (small boutons) are marked. (B) Transmission electron microscopic (TEM) image of a bouton. # marks the sub-synaptic reticulum, the arrowhead shows an active zone without a visible T-bar and the corresponding PSD, the arrow marks an active zone with a T-bar, which is enlarged in the inset. Vesicles are concentrated around the T-bar. Dr. Nicole Wagner (University of Würzburg) kindly provided the TEM image.

Muscle 6 is innervated by the nerve SNb/SNd harbouring two motoneurons: MN6/7-Ib, which forms large Ib boutons (3-6 μm diameter) and MNSNb/d-Is, which forms small Is boutons (2-4 μm diameter; Hoang and Chiba, 2001). Every bouton harbours several monadic synapses. Thus, the muscles 6 and 7 receive input from more than 1000 synapses (estimation from electron-microscopic data), but probably only a fraction of them contribute to synaptic transmission in physiological conditions (Atwood et al., 1993; Atwood and Wojtowicz, 1999).

The active zone and the PSD are identified as two closely aligned membranes with higher electron-densities than the surrounding membrane. The electron densities are 400-600 nm in diameter. On the presynaptic side some active zones display electron dense projections, called T-bars (**Figure 3B**). The T-bars are thought to play a major role in synaptic transmission. The protein BRP which is a major component of the T-bar is required for proper T-bar formation, it clusters Ca^{++} channels with its N-terminal side (oriented towards the membrane) and tethers vesicles with its C-term (oriented away from the membrane), the latter property is important for a fast vesicle replenishment at high action potential firing rates (Hallermann et al., 2010a; Hallermann et al., 2010b; Kittel et al., 2006; Wagh et al., 2006). T-bars are also found in other dipteran species (Feeney et al., 1998; Trujillo-Cenóz, 1969).

The PSD consists of scaffolding proteins, which cluster receptors opposite active zones (Kennedy, 1997). This adds to the high fidelity of synaptic transmission.

The extracellular matrix of the synaptic cleft contains cell adhesion proteins to keep the pre and the postsynapse tightly associated. Among scaffolding proteins Discs-large (Dlg; Lahey et al., 1994) is the most prominent at the NMJ. It has a pleiotropic function. The protein interacts, among others, with Fasciclin II (FasII, a homophilic cell adhesion protein; Schuster et al., 1996). CaMKII is thought to act upstream of Dlg (Koh et al., 1999). Integrins, which mediate cell-to-cell and cell-to-matrix adhesion seem to operate even further upstream of Dlg and are thought to be involved in synaptogenesis and plasticity (Beumer et al., 2002; Clegg et al., 2003). A

downstream function of Dlg is to bind the Shaker K^+-channel and secure the proper localisation of this channel (Zito et al., 1997).

One major determinant of synaptic strength at the *Drosophila* NMJ is the relative abundance of different types of glutamate receptors in PSDs (DiAntonio et al., 1999). The *Drosophila* genome encodes 30 putative glutamate receptor subunits, 18 AMPA and kainate type, 2 NMDA, 4 δ type and 6 without a homologue in mammals (Petersen et al., 1997). A number of non-NMDA type glutamate receptor subunits are expressed at the PSD of the NMJ, where receptors probably form tetramers from GluR-IIC (GluRIII), GluR-IID, GluR-IIE and either GluR-IIA or GluR-IIB (DiAntonio et al., 1999; Featherstone et al., 2005; Marrus et al., 2004; Petersen et al., 1997; Qin et al., 2005; Schuster et al., 1991).

3.4.3 Plasticity at the neuromuscular junction

Drosophila muscles increase their area 100-fold between the 1st and the 3rd instar larval stage (Petersen et al., 1997), the innervation must keep pace to ensure reliable transmission, therefore the bouton number, synapse number per bouton (Schuster et al., 1996) and number of vesicles within each bouton increases (Prokop, 1999). These developmental changes are referred to as developmental plastic changes, or developmental plasticity.

At receptor field level, developmental plasticity was elegantly shown in studies using fluorescently labelled glutamate receptor subunits in combination with live imaging on completely intact, anesthetised larvae. At individual synapses, most receptor fields initially grow by incorporating GluR-IIA type receptors. Meanwhile, the presynapse matures by increasing the BRP content of its active zones and additionally, incorporation of GluR-IIB receptors starts to increase. The incorporation of GluR- IIA slows down, until an even ratio between GluR-IIA and GluR-IIB is reached (Rasse et al., 2005; Schmid et al., 2008). While the physiological cues for these processes remain unknown, synaptic activity is thought to play a major role.

When the larval NMJ is disturbed genetically, it shows plastic changes, which affect structure and function of the junction. *Ether a go-go* (*Eag*), a Potassium channel mutation which leads to defective action potential repolarisation kinetics and firing of multiple APs instead of one, leads to increased branching of the NMJ and increased number of boutons (Budnik et al., 1990). Additionally, it was shown that a chronic increase (genetically) of neuronal activity can trigger local postsynaptic protein synthesis leading to elevated levels of GluR-IIA receptors (Sigrist et al., 2000), which is thought to be an important mediator of long-term synaptic plasticity at the larval NMJ (Sigrist et al., 2002).

Due to the extent and chronic nature of genetic manipulation, however, it cannot be said whether the products of the above mentioned genes are also at work in plastic changes during natural development, or whether the observed phenotypes are just results of developmental disturbances. To circumvent this limitation, heat shock-induced mutations (*shibire* or *paralytic*) were devised. With help of these tools, changes in protein levels can be induced in an acute manner. Unfortunately, it was shown that higher temperature alone already has a substantial effect on larval locomotor behaviour and morphology (increased movement, larger NMJs, more glutamate receptors at higher temperatures; Sigrist et al., 2003).

To acutely trigger plastic changes at the NMJ, activity can be induced directly by electrical stimulation of the nerve in the semi-intact preparation (dissected larva). The obtained results, however, might reflect phenomena which do not take place *in vivo*. It is known for example that the composition of the extracellular solution has a strong effect on the observed release probability and therefore on interpretation of electrophysiological data (Borst, 2010). Additionally, unknown substances of the haemolymph might influence plasticity phenomena in living animals.

The next step towards studying activity-dependent induction of plasticity *in vivo,* was to investigate whether natural crawling might have an effect on NMJ properties. Steinert and colleagues showed that larvae, if put on food-free medium, start to crawl faster. While one part of them returns to slower movement after some time,

others keep up a fast crawling speed. Between 40 and 80 minutes after the start of the experiment the permanent fast crawlers show increased mEJP amplitudes (miniature excitatory junctional potentials, evoked by neurotransmitter spontaneously released by one vesicle). Evoked junctional potentials (eEJP) are therefore also increased. After 80 minutes, mEJPs acquire the original smaller amplitudes, while eEJPs are still large, which means that the quantal content (number of released vesicles) must have increased (Steinert et al., 2006).

This experiment, however, still does not address activity-dependent plasticity. The authors emphasise that these "[…] changes, which are triggered *in vivo* by potentially multiple natural cues including nerve activity, muscle activity, and/or other factors."(Schuster, 2006). Therefore authors preferred to name the observed changes experience-dependent and the question whether they directly depend on activity of motoneurons remained open.

The next logic step to induce activity *in vivo* was the use of channelrhodopsin 2 (ChR2, a light-gated ion channel; Nagel et al., 2003) in living *Drosophila* larvae (Schroll et al., 2006). Ataman and colleagues have shown that ChR2 based stimulation of the motoneurons can lead to morphological changes of the NMJ. At the functional level, however, induced changes remained marginal: slightly increased quantal size (mEJP amplitude,), without affecting the quantal content (Ataman et al., 2008).

3.5 Approach of the study

This work aimed to provide a better mechanistic understanding of activity-induced synaptic plasticity, using the larval *Drosophila* neuromuscular junction as an example synapse. Although many published papers have improved the understanding of synaptic plasticity at this synapse, most of them have dealt with genetically induced plasticity (Budnik and Ruiz-Canada, 2006).

The authors used genetic tools (e.g. knockouts) to chronically change expression levels of proteins, this lead to changes in synaptic function and plasticity behaviour. Finally, the authors deduced an important function of the protein in activity-induced synaptic plasticity (Budnik and Ruiz-Canada, 2006). This reasoning is seriously flawed: synaptic plasticity is an important function of most synapses. A serious disturbance of important proteins in the synapse will have an effect on synaptic plasticity. However, this does not necessarily mean reciprocally that the very same protein is at work during naturally occurring activity-dependent synaptic plasticity phenomena.

In this study, a different approach was chosen. ChR2 stimulation was used to induce activity-dependent, synaptic changes in a quantifiable manner, in living, freely moving larvae. This work demarcates itself from short-term synaptic plasticity work, developmental plasticity, experience-dependent plasticity and activity-induced plasticity in the dissected animal. It is also a step towards inducing plasticity in the central nervous system of *Drosophila* in a quantifiable manner *in vivo,* which will be necessary to test the hypothesis that more complex memories are stored in changes of strength of synaptic connections.

4. Experimental procedures

4.1 Fly breeding and retinal supplementation

Drosophila were raised in 10.5 cm (height) x 4.6 cm (∅) transparent tubes; with laying medium (recipe see Solution formulas) and some dry baker's yeast. Additionally, a paper filter was put on top of the medium to provide a larger dry surface for wandering third instar larvae and for pupation.

To raise larvae destined for experiments, typically around 20 virgin female flies were crossed with 7-9 male flies in 6.4 cm x 2.6 cm tubes, a small paper filter was spanned above the laying medium to ensure that the flies do not stick in the stirred medium when transferred to a fresh tube. Fly transfer was done every day to ensure similar larva densities.

Drosophila larvae need all-*trans*-retinal (RAL) supplementation to the diet, to express functional ChR2 (Schroll et al., 2006). Therefore RAL was added to the laying medium. Larvae eat the laying medium; RAL is taken up into the system and built into the opsin protein. For most experiments, larvae were either raised at 25 °C and in food containing 0.1 mM RAL (standard conditions) or at 29 °C and in food containing 1 mM RAL (enhanced expression conditions).

4.2 Genotypes, nomenclature and basic fly genetics

Drosophila has four pairs of chromosomes: a pair of 2nd, 3rd and 4th chromosomes, females have additionally a pair of X chromosomes. Males have one X and one Y chromosome. The genotype of a chromosome is indicated if there is a variation to the chromosome. In *Drosophila* nomenclature, semicolons separate chromosomes. Commas separate names of rearrangements, mutations and transgenes on the same chromosome. In this work following genotypes were used:

w^{1118}: A mutation of the *white* gene, leading to white eyes. Transgenic flies are usually created from flies, which carry a mutation in the white gene (white background). In order to distinguish flies, which inserted a transgene of interest into their genome, a so-called mini-white gene is coupled to the transgene, leading to red eyes in flies with white background. A fly line with a *white* mutation is therefore the proper control line for most transgenic flies.

P{UAS-Chop(315)2} in short *UAS-chop2*: An insertion of a truncated *channelopsin-2* (Schroll et al., 2006) gene variant (*chop2-315* c-terminally truncated after amino acid 315; Nagel et al., 2003) on the third chromosome. The *chop2* gene is under control of the upstream activating sequence (UAS). All channelopsin flies, which were used in this study carry the truncated variant of the *channelopsin-2* gene and are referred to as *chop2*.

ok6-GAL4: On the second chromosome there is an *ok6-GAL4* motoneuron driver construct. If crossed with a UAS reporter line, the UAS controlled construct is transcribed in motoneurons of the larval ventral nerve cord.

g7-GAL4/CyO w-GFP (w^{-}*)*: On the second chromosome a *g7-GAL4* muscle driver construct. The homologous 2nd chromosome carries the balancer *CyO*, additionally there is a GFP inserted, under the promoter of the white gene, which leads to the transcription of the GFP gene where the white gene is normally transcribed. There is no mini-white gene (*w*$^{-}$) fused to the GFP. The *g7-GAL4* line was a gift from Aaron DiAntonio, Washington University.

g7-GAL4/CyO w-GFP (w^{-}*); P{UAS-Chop(315)2}/TM6B, Tb* in short *g7-GAL4/CyO w-GFP (w*$^{-}$*); UAS-chop2/Tb*: A *g7-GAL4* driver on the 2nd over the above-mentioned *CyO* balancer chromosome. On the 3rd chromosome the *chop2* construct is balanced over *TM6B* with the marker *Tb* (tubby), a dominant marker, which leads to tubby larvae.

P{w[+mW.hs]=GawB}tey[5053A]/TM6B, Tb, in short *m12-GAL4/Tb*: The *m12-GAL4* driver is active in the larval muscle 12. The construct is integrated into the

third chromosome and balanced by TM6B, marked by the above-mentioned marker Tb. The stock was created from flies out of the Bloomington collection (Bloomington # 2702).

UAS-2xEGFP/y; ; UAS-CD8::GFP. An EGFP construct on the 1st chromosome under the control of the UAS Promoter. On the 3rd, a CD8-GFP fusion under control of the UAS promoter. CD8 is a transmembrane glycoprotein from mice. This reporter line, if crossed to a GAL4 driver, leads to fluorescence in the GAL4 expressing cells and therefore can be used to analyse the expression pattern of the GAL4 driver line.

For most experiments the binary GAL4/UAS system (Brand and Perrimon, 1993) was used to create the desired genotypes. The *GAL4* gene encodes the yeast transcription activator protein GAL4. *UAS* (upstream activation sequence) is a small section of the promoter. Binding of GAL4 to UAS activates the transcription of the gene downstream of UAS. The *GAL4* gene can be brought into the genome of a fly randomly via p-element insertion. The *p-GAL4* construct can hit the genome just downstream of a genomic enhancer and stay there (enhancer detection or trapping; O'Kane and Gehring, 1987). If this happens, the GAL4 transcription factor is produced at the temporal and spatial distribution as controlled by the genomic enhancer. For instance if the genomic enhancer is active in motoneurons, the GAL4 protein will also be produced there.

The GAL4 fly line (driver) is crossed with a UAS (effector) fly line and the gene under the control of the UAS promoter will be transcribed at the temporal and spatial pattern dictated by the GAL4 line. Till present, an innumerable number of GAL4-driver and UAS-effector lines have been created by different labs. Thus, basically any tissue in *Drosophila* can be specifically targeted by this system. In the present work it was used to express ChR2 in motoneurons, muscles or both. To visualise the expression pattern of the GAL4 lines, UAS-GFP reporter lines were employed.

Genotypes used for experiments are listed below:

w^{1118}

'Pre': *ok6-GAL4/+; UAS- chop2/+*

'Post': *g7-GAL4/+; UAS-chop2/+*

'Pre & Post': *ok6-GAL4/g7-GAL4; UAS-chop2/+*

'Pre & M12-Post': *ok6-GAL4/+; m12- GAL4/UAS-chop2*

To visualise expression:

'Pre & M12-Post': y/*UAS-2xEGFP; ok6-GAL4/+; m12-GAL4/UAS-CD8::GFP*

'Post': y/*UAS-2xEGFP; g7-GAL4/+, UAS-CD8::GFP/+*

4.3 Channelrhodopsin-2 based photo-stimulation

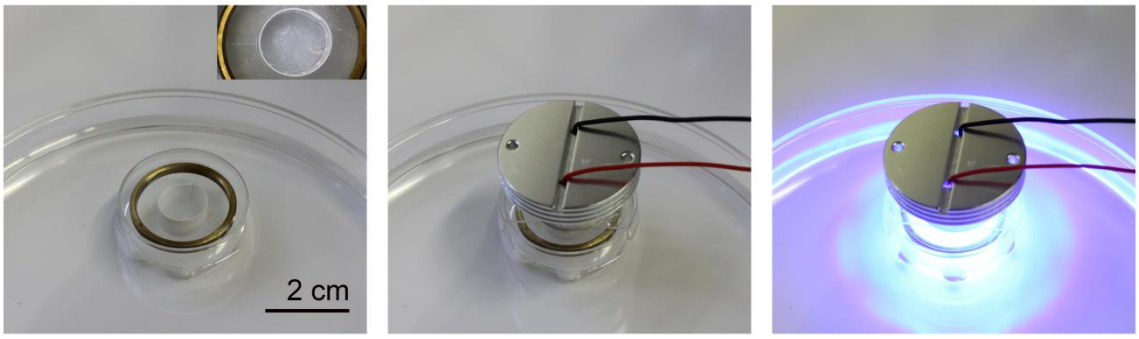

Figure 4 Photo-stimulation Arena. Left, the arena consists of a white plastic hollow cylinder (∅1.3cm, height 0.8cm), with holes at the side to allow air supply. It is placed in a small petri dish (∅ 3.5cm) containing a moist filter paper; the cylinder is covered by a cover glass, which in turn is weighted by a brass ring. The inset shows the area from above, with a larva placed inside. The small petri dish stands on 6mm feet and is immersed in a large water reservoir. The strong blue light LED (middle) is placed on top of the arena. In the right panel the light is turned on.

For experiments, the largest 3rd instar larvae that still crawled in the laying medium and that showed a clear contraction upon blue light stimulation (~1 mW/mm² at

460nm) were chosen. The photo-stimulation was done in a custom built stimulation arena, where larvae could move freely on a moist filter paper (**Figure 4**). In order to minimise heating of the larvae, the arena was cooled by a large water reservoir from below.

For experiments two types of blue light LEDs were used: a standard multi array LED 12V, 1.8W (weak LED; **Figure 5A** left; from LED-Light®) at a distance of 8cm to the larva, or as for most experiments a low emission angle 3W LED (strong LED; **Figure 5A** right; from LEDxON®) at a distance of 1.5cm. The weak LED produced a light intensity of around 40µW/mm² at 460nm in the arena. The strong LED unfolded an intensity of 1.7mW/mm².

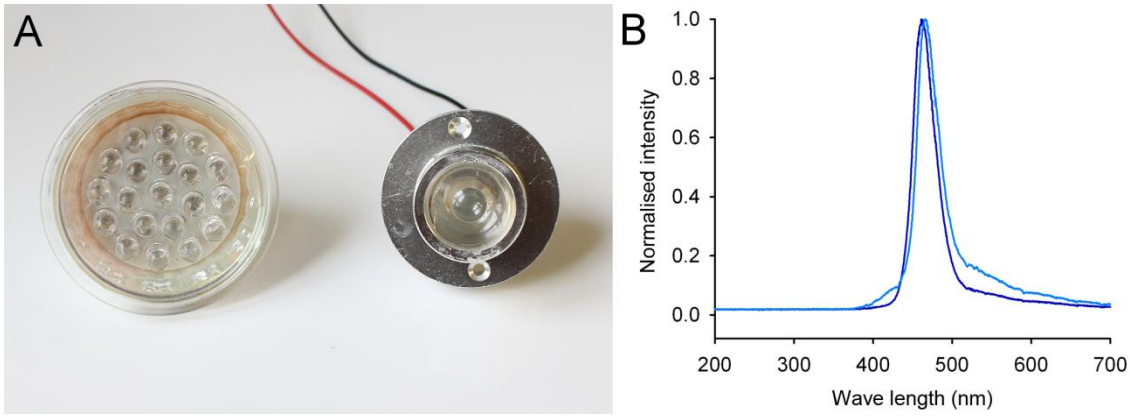

Figure 5 Blue light LEDs. (A) Weak LED (40µW/mm2) left, strong LED (1.7mW/mm2) right. (B) Emission spectra of weak LED (light blue) and the strong LED (dark blue) measured by a spectrometer (Ocean Optics, USA).

The irradiance was measured with a power meter (model # 3803; New Focus, USA) and verified with a different model (fieldmate laser power meter; Coherent Inc; USA). The weak LED had to be set up at a distance of 8cm to allow homogeneous illumination. The strong LED reaches a powerful and homogenous illumination at a short distance due to the built in lens and a low emission angle. Both LEDs showed similar emission spectra (**Figure 5B**).

Larvae were photostimulated according to two different protocols: the first protocol (standard light-stimulation protocol; **Figure 6A**) was the same as used in Vivian Budnik's lab (Ataman et al., 2008; Koon et al., 2011). The stimulation pulses of the second protocol (short pulse light-stimulation protocol) were reduced, from 2 s to 15 ms (**Figure 6B**).

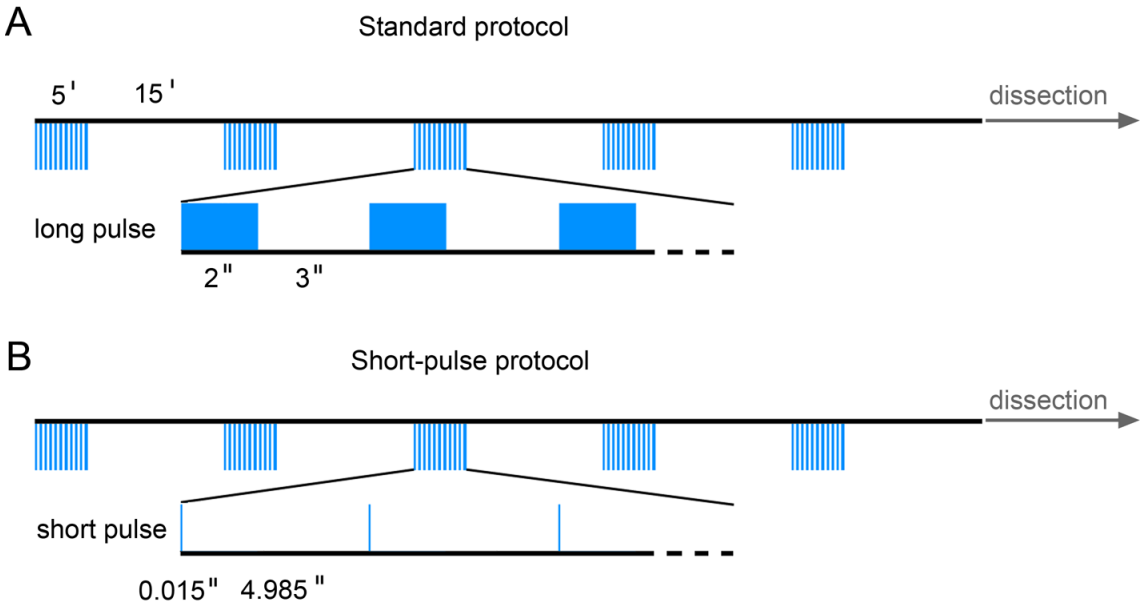

Figure 6 Photo-stimulation protocols. (A) The standard protocol consists of 5 stimulation periods each 5 min long with intermittent 15 min breaks. During the stimulation period the LED oscillates between 2 s pulses and 3 s breaks. (B) In the short-pulse protocol, the light pulse is reduced from 2 s to 15ms.

For a better understanding of currents induced by light-stimulation, larvae were dissected and electrophysiological measurements were performed as described in 'Electrophysiological recordings'. Blue light was applied by a mercury lamp (Nikon intensilight C-HGFI) and filtered by a 460-500 nm filter, which had the advantage of conveniently adjusting irradiance by neutral density filters.

4.4 Solutions

Expression of functional ChR2 demands feeding *Drosophila* larvae with RAL. It is, however, insoluble in water, therefore a 50 mmol/l stock in pure Ethanol was prepared and stored at -20 °C. This solution was intermixed with laying medium just before transferring flies to a new tube. In order to control for possible side effects of alcohol supplementation, a corresponding amount of ethanol was added to tubes of control larvae.

HL-3 (see Solution formulas) is a standard solution, developed for stable electrophysiological measurements at the semi-intact larval neuromuscular preparation (Stewart et al., 1994). In the present study, it was used for electrophysiological measurements, following plasticity inducing light-stimulation. The Ca^{++} concentration was chosen to be 1 mmol/l to allow comparison to previous results (Kittel et al., 2006; Schmid et al., 2008). At this concentration, dynamic phenomena like paired pulse facilitation or depression are detected more easily, compared to solutions with 1.5 mmol/l Ca^{++}. The Ca^{++} concentration was adjusted by adding the corresponding volume of 1 mol/l Ca^{++} stock solution to Ca^{++}-free HL-3 at the day of the experiment.

However, when ChR2 was expressed presynaptically in motoneurons and light stimuli were applied on dissected larvae in HL-3, light-evoked excitatory junctional currents (lEJCs) were detected only sporadically. In contrast, the same stimuli lead to contraction of the intact larva. This was probably due to shielding effects exerted by divalent cations (20 mM Mg^{++} in HL-3) on neuronal membranes (Feng et al., 2004). After reducing the magnesium concentration to 5 mmol/l (HL-3.1, see Solution formulas; Feng et al., 2004; Yoshihara and Littleton, 2002), lEJCs could be measured. HL-3.1 was developed to circumvent some disadvantages of HL-3 to standard saline, in particular, a reduced neuronal membrane excitability (Feng et al., 2004). We assume that HL-3.1 matches the fly haemolymph more closely than HL-3 and it is sensible to use HL-3.1 for measurements where nerve excitability and signal

conduction is of importance. Therefore HL-3.1 was used for measurements during light application.

For immunohistochemical stainings, larvae were fixed either in ice cold PBS (phosphate buffered saline, an isotonic, not strictly formulated solution, see Solution formulas) containing 4% PFA (paraformaldehyde) or in pure Methanol at -20°C.

All steps after the fixation were carried out in PBS solutions containing 0.05% (v/v) Triton X100, a detergent, used to permeabilise membranes. This solution will be referred to as PBT (see Solution formulas). In order to block unspecific binding a normal goat serum (NGS) solution (5% v/v) in PBT was used (see Solution formulas). It is reasonable to block with NGS since all secondary antibodies were raised in goat.

4.5 Semi-intact preparation of 3rd instar larvae

For experiments following the photo-stimulation protocol, dissection of larvae was performed in ice-cold Ca^{++} free HL-3 (Stewart et al., 1994). For electrophysiological measurements during light application, ice cold Ca^{++} free HL-3.1.

Late, non-wandering 3rd instar larvae (the biggest, which crawled in the laying medium) were immobilised at both ends, using fine pins on a Sylgard® pad, the dorsal side showing up. Two small holes were cut with fine scissors perpendicular to the dorsal midline close to the pins. The larva was cut open along the dorsal midline, the body wall opened to the sides and pinned down with 4 more pins. The innards were removed cautiously, while cutting the tracheal connections to the body wall.

The CNS was also removed cautiously while cutting the motoneuron nerves, except for measurements where light-induced currents were measured in 'Pre' or 'Pre & Post' animals. Here, to reduce endogenous motoneuron activation, the brain was

removed, while the ventral nerve cord was left intact to induce lEJCs. To prevent overall muscle contraction while photo-inducing lEJCs, all motoneuron nerves leaving the ventral nerve cord were cut, besides those innervating the muscles of the segment at which recordings were made.

4.6 Electrophysiological recordings

4.6.1 Current clamp recordings

For electrophysiological recordings sharp electrodes with resistances varying between 9 and 21 MΩ were used. The intra-electrode solution was 3 mol/l KCl, to reduce the pipette resistance. The electrode shape is a compromise between being sharp enough to penetrate the muscle without causing too much damage and having a resistance, low enough to allow fast current application in voltage clamp mode.

The electrodes were pulled with a DMZ-Zeitz-Puller (DMZ, Germany) from filamented Borosilicate glass pipettes (GB 150-8P; Science products, Germany) with an outer diameter of 1.5 mm and an inner diameter of 0.8 mm.

To measure cell membrane potential, modern amplifiers (Axoclamp 2B or the Axoclamp 900A were used) operate in current-clamp mode, where a voltage follower is used as the primary amplifier. A voltage follower is a special operational amplifier (op-amp, **Figure 7A-C**). In the required circuit, the output voltage is linearly proportional to the input voltage and the op-amp is called buffer. In this configuration the amplifier measures both the voltage drop across the membrane (V_m) and additionally the voltage drop at the tip of the pipette ($V_t=R_p*I$, where R_p is pipette resistance). To remove V_t from the signal a second amplifier is introduced to give a counter current to V_t (**Figure 7D**). This is done in the bath before the cell is impaled by the electrode.

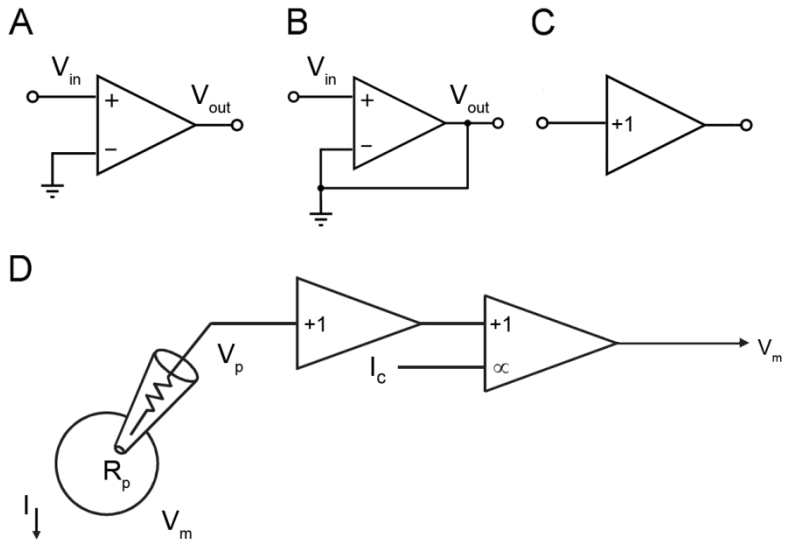

Figure 7 Operational amplifier and potential measurement. (A) Operational amplifier (op-amp): the input voltage (V_{in}) is measured and amplified hundreds or thousands of times to the output voltage (V_{out}). (B) In this op-amp configuration, V_{out} is linear proportional to V_{in} (unity gain) is called buffer and can be used as voltage follower. (C) A simplified depiction of a unity gain buffer/voltage follower. (D) Voltage follower with an additional operational amplifier to give a current (I_c) in order to cancel out the voltage drop across the pipette ($I*R_p$) from the overall measured voltage drop (V_p). Thus, the voltage-drop over the membrane (V_m) caused by current (I) can be measured. To adjust I_c the voltage drop has to be measured and compensated in the bath before penetrating the cell. Adapted from (The-Axon-Guide, 2008).

4.6.2 Two-electrode voltage clamp recordings

The current clamp technique is very practical but has some major disadvantages for measuring synaptic events:

(1) Since the measured potential is directly proportional to membrane resistance (Ohm's law: voltage = current x resistance), one does not know whether a difference in eEJP amplitude (evoked excitatory junctional potentials) or mEJPs (miniature excitatory junctional potentials) stems from a changed synaptic current or from a change in membrane resistance. Therefore, the membrane resistance needs to be measured to check whether it is comparable in the control and the experimental group.

(2) When current flows through a biological membrane, the capacitance of the membrane is loaded first, therefore the potential becomes proportional to the

current later during measurement (**Figure 8A**). The time course of the loading is proportional to the product of resistance and capacitance (time constant: τ = resistance x capacitance). Since synaptic currents are fast compared to τ, the resulting EJPs are rounded and do not represent the time course (kinetics) of synaptic currents.

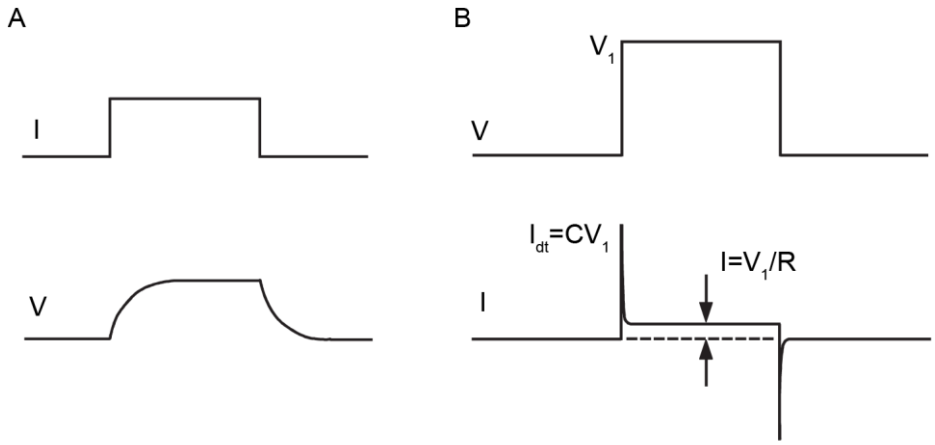

Figure 8 Current clamp and voltage clamp. (A) Current application (I) to a cell and the resulting voltage response (V) in the current clamp mode. First, the membrane capacitance is loaded, then membrane potential reaches steady-state level. When current is turned off, the capacitance unloads before voltage reaches baseline level. The same phenomena take place when synaptic currents occur and the voltage is measured. Thus, potential measurements in current clamp mode do not precisely reflect kinetics of synaptic currents. (B) Application of a voltage step to a cell in voltage clamp mode leads to a fast decaying capacitive current, its change in time I_{dt} is proportional to capacitance C of the system (cell + device) and the step size V_1. After the capacitive current I_{dt} has decayed, the current I will be proportional to applied V_1 and the resistance R. The capacitive current I_{dt} can be compensated in amplifiers. The same phenomena take place when synaptic currents cause voltage drops. Thus, voltage clamp measurements reflect the genuine kinetics of synaptic currents, if the voltage clamp is fast enough and capacitive currents are compensated. Adapted from (The-Axon-Guide, 2008).

For these reasons, most of the measurements were performed in the so-called Two-electrode voltage clamp configuration (TEVC). The properties of a voltage clamp are shown in (**Figure 8B**). In TEVC capacitive currents are fast and can be removed by appropriate capacitance cancellation circuitry, available in modern amplifiers.

The mechanism behind TEVC is shown in (**Figure 9A**). For clarity reasons, the circuit to compensate the potential drop at the electrode resistance (**Figure 7D**) and the capacitance cancellation circuit are omitted. The membrane potential (V_m), sensed by microelectrode 1 (ME1), it is amplified by the unity gain buffer (A1), the value is fed into the minus input of the negative feedback amplifier (A2), which compares it to the command potential (V_{cmd}, e.g. -60 mV). The difference ε is amplified and given out at the output of A2. This current (I_{TEVC}) is measured at the current monitor and applied to the cell to keep the cell potential stable. It is inversely proportional to the current, which flows over the membrane (I).

Thus, the membrane current is measured indirectly. Given good capacitance compensation (not shown in the circuit) and a fast voltage clamp, the circuitry measures real kinetics of synaptic currents.

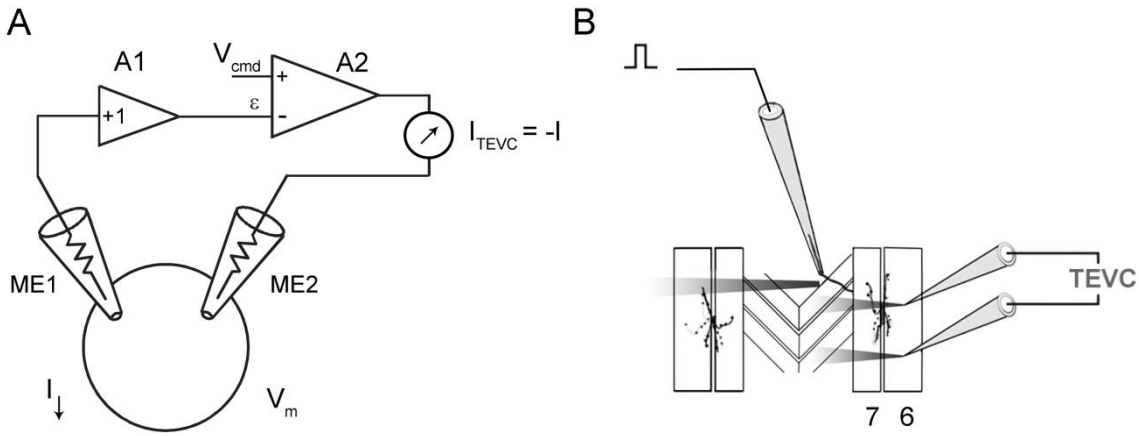

Figure 9 Two-electrode voltage clamp. (A) Simplified two-electrode voltage clamp circuit. ME1 microelectrode (voltage electrode) measures the potential (V_m) via the unity gain buffer A1. The difference ε between this potential and command voltage (V_{cmd}) is measured by the negative feedback amplifier A2. It gives a corresponding current I_{TEVC} via ME2 (current electrode) to keep membrane voltage at command potential level. I_{TEVC} is inversely proportional to the membrane current I. Adopted from (The-Axon-Guide, 2008). (B) Schematic depiction of the TEVC measurement configuration on muscle 6. The nerve can be stimulated via the suction electrode (SE) to elicite evoked excitatory junctional currents (eEJCs). Adapted from (Pawlu et al., 2004).

In TEVC measurements the voltage was clamped to -60 mV for eEJC (evoked excitatory junctional currents) and lEJCs (light evoked excitatory junctional currents). For mini (miniature junctional currents) measurements cell potential was clamped to -80 mV, in order to increase signal to noise ratio.

A voltage clamp needs a certain speed to accurately measure the time course of synaptic currents. The speed of a voltage clamp is assessed by measuring the time it takes to apply a defined voltage step to the cell by the voltage clamp. For eEJCs the speed of the voltage clamp was adjusted to follow a voltage step of -10 mV (-60 mV to -70 mV; applied by the amplifier) within 0.75 ms. A gain of 2400 V/V (which is V_{output} of A2 per ε; **Figure 9A**) resulted in a voltage error of about 5 mV at currents around -100 nA. Since the measured eEJCs are typically smaller in 1mol/l Ca^{++}, this voltage error should be acceptable and not lead to a large drop in the driving force for ions.

Figure 9B shows a schematic depiction of the TEVC configuration in a larva with ME1, ME2 and a stimulation electrode with a nerve inside to stimulate the motoneurons for eEJC recordings. All electrophysiological measurements were performed on muscle 6, segments A2 and A3.

To evoke currents, a 300 μs voltage pulse was given. In order to ensure reliable stimulation, the pulse was around 1.5 times higher than necessary to activate both motoneurons (MN6/7-Ib, MNSNb/d-Is), which innervate the muscle 6/7 NMJ. This resulted in a stimulation voltage of typically 10 V. Electrical stimulation was done with the Grass S88 or S48 stimulator (Astro-Med Inc., USA).

Minis were measured at a holding potential of -80 mV for 90 s without any stimulation. In order to be able to measure minis, the signal to noise ratio was minimised by reducing the gain below 600 V/V, but it was kept high enough to follow the -10 mV step within 1.5 ms. This resulted in gains between 300 and 600 V/V.

Due to a destabilising effect by the non-ideal nature of biological membranes and the resulting oscillations of the clamp, a so-called phase lag correction is introduced in amplifiers (The-Axon-Guide, 2008). It reduces oscillations (therefore noise) and thus, improves signal-to-noise ratio, which is especially important in mini recordings (Phase Lag 0.3 ms). Phase lag, however, slows down the clamp. For evoked currents, phase lag was reduced to minimum, since signal to noise is not limiting for these large currents.

Light-evoked currents were also measured at low gains (300-600 V/V) and a phase lag of 0.3 ms, to be able to resolve minis, comparably small steady state 'Post' currents and lEJCs at the same time.

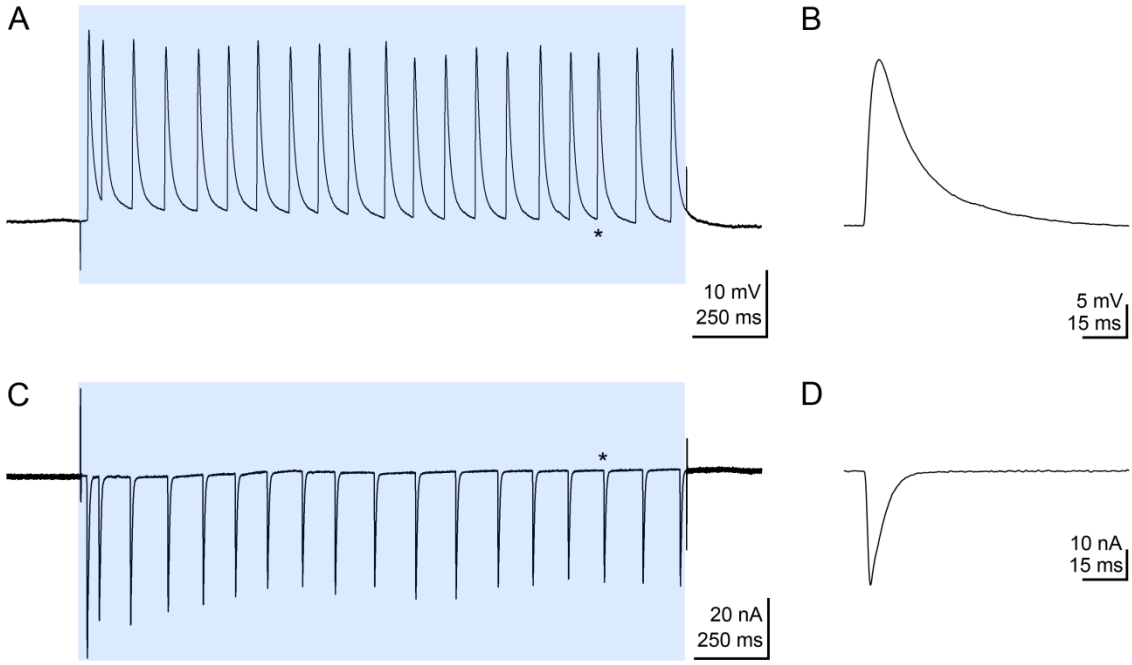

Figure 10 Light-induced potentials and currents in a 'Pre' larva. Larvae were raised at 29 °C and 0.1 mM RAL. Blue boxes indicate light application. (A) lEJPs induced in muscle 6 by blue light (1.7 mW/mm² LED, at 460nm), asterisk marks an lEJP shown in (B) on a shorter time scale. (C) lEJCs induced in the same muscle by the same LED, asterisk marks the lEJC shown in (D) on a shorter time scale. lEJPs show slower kinetics compared to lEJCs. lEJC kinetics are similar to currents evoked directly by electrical stimulation (eEJCs), which confirms an AP like stimulation of the motoneuron synapse by continuous light in 'Pre' animals

Figure 10 shows presynaptically light-induced junctional potentials (lEJPs; current clamp) and currents (lEJCs; voltage clamp). lEJPs show slower rise- and decay times compared to lEJCs. lEJCs (**Figure 10D**) demonstrate fast rise time and fast decay kinetics similar to electrically evoked eEJCs. This confirms synchronous neurotransmitter release, as in AP evoked stimulation of the NMJ.

All measurements were done with Axoclamp 900A or Axoclamp 2B amplifiers and digitised by the Digidata 1440 analog-digital converter, using Clampex 10 (all four Molecular Devices, USA).

4.6.3 Analysis of electrophysiological recordings

The determination of basic parameters of synaptic currents was performed in Clampfit 10 (Molecular Devices, USA). To analyse basal synaptic transmission typically 15 eEJCs, measured at 0.2 Hz, were averaged. The rise time was defined as the time between 10 % and 90 % of the rising slope.

The decay time constant (decay τ) was determined by fitting a mono-exponential function to the 60-0 % of the decaying slope, the part of the current mainly defined by closing of postsynaptic receptors, as shown in (Pawlu et al., 2004). Due to the large number of analysed decays in **Figure 21C**, a macro was written in Origin Labtalk script language to automate the analysis.

Minis were detected by the Clampfit template search algorithm and averaged for one recording to determine rise times and decay time constants as described above for eEJCs.

Quantal content was estimated by dividing the mean amplitude of eEJCs evoked at 0.2 Hz by the corrected mean amplitude of minis measured in the same cell (Hallermann et al., 2010a). The correction factor of 0.75 was necessary to compensate the higher ionic driving force at stronger depolarisation used in mini recordings (Hallermann et al., 2010a). Statistical data analysis and display of results were done in Sigmaplot 12 (Systat, USA) and Origin 8 (Originlab, USA).

4.7 Immunohistochemistry

The staining procedure was basically performed as previously described (Schmid and Sigrist, 2008), in short: for stainings against GluR-IIA in connection with HRP, dissected larvae were fixed in pure Methanol for 5 min at -20 °C. For all other stainings larvae were fixed in ice cold 4 % paraformaldehyde (in PBS) for 10 min. After fixation, larvae were kept in PBT until all larvae were dissected and fixed.

To block unspecific binding, a blocking solution of 5 % normal goat serum (NGS, from Jackson Immunoresearch, USA) in PBT was used for 30 min. The antibody reactions were carried out in 5 % NGS containing PBT. The primary antibodies were applied over-night at 4 °C, the secondary for 2h at room temperature. The washing procedure was done with PBT, two times short, three times for 20 min.

The monoclonal anti-ChR2 antibody (15E2, mfd diagnostics, Germany) was used as a supernatant at a 1:1 dilution. The monoclonal anti-BRP antibody (nc82, a gift from Erich Buchner, University of Würzburg) was used at a 1:250 dilution. The monoclonal mouse anti-GluR-IIA antibody was used at dilutions of 1:100 or 1:200 (8B4D2, Developmental Studies Hybridoma Bank, University of Iowa). The polyclonal rabbit anti-GluR-IIB (a gift from Aaron DiAntonio, Washington University) was used at 1:2500. The polyclonal rabbit anti-GluR-IID (a gift from Stephan J. Sigrist, FU Berlin) was used at 1:1000.

The following secondary antibodies were used: Alexa 488 goat anti-rabbit (Invitrogen), Alexa 488 goat anti-mouse (Invitrogen), Cy3 goat anti-rabbit (Dianova), Cy3 goat anti-mouse (Dianova), Cy5 goat anti-rabbit (Dianova), Cy5 goat anti-mouse (Dianova), Cy3 goat anti-HRP (Dianova), Cy5 goat anti-HRP (Dianova) and Atto 647N goat anti-mouse (Attotec).

The stained larval preparations were embedded in Vectashield mounting medium H1000 (Vector Laboratories Inc., USA). All larvae from one experiment were stained equally in the same vial and mounted to the same slide.

4.8 Confocal laser scanning microscopy

ChR2 in combination with HRP stainings were imaged with an upright line scanning confocal microscope (LSM 5, Zeiss, Germany), with a 1.25 numerical aperture, 63x oil immersion objective. The zoom was adjusted to give a pixel size of 100 nm. The z-step size was 400 nm for NMJ stacks and 1 μm for VNC stacks. This experiment was performed by Nadine Ehmann, Universtiy of Würzburg

All other stainings were imaged with an inverse SP5 line scanning confocal microscope (Leica Microsystems, Germany), equipped with a 1.4 numerical aperture, 100x oil immersion objective. The pixel size was 75 nm, z-step size 420 nm.

To ensure comparability, all image acquisition was done at the same laser and imaging settings for compared groups, alternating between control and RAL fed larvae.

4.9 Analysis of imaging data

Analysis of imaging data was carried out in ImageJ (rsbweb.nih.gov/ij/) essentially as previously described (Schmid et al., 2008; Schmid and Sigrist, 2008). For analysis of BRP punctae and receptor clusters, the confocal stacks were maximum projected, the individual background subtracted and the image was Gaussian blurred (radius 0.9 pixel). In contrast to the cited protocols, the images were neither normalised, nor recalculated to original maximum intensity. An intensity threshold was applied to remove background. Non-synaptic staining was removed manually.

Single spots (receptor clusters or BRP spots) were detected with the "Find Maxima" command, the resulting mask was used to segment the blurred and thresholded image. Particles in the segmented image were automatically analysed with the

"Analyze Particles" command, which gave among other parameters the number, the size and the mean intensity of the detected receptor clusters or BRP spots.

The whole analysis process except subtracting background and removal of non-synaptic staining was automated. All images from one channel of an experiment were analysed with the same settings. Thus, no bias was introduced by the experimenter. In connection with the same laser power and imaging settings identical conditions were created for control and RAL fed animals, which made quantitative comparisons feasible.

HRP signal quantification was done with the "Measure" command after maximum projecting the confocal stacks, subtracting the background, thresholding the image and manually removing non-synaptic staining. All settings for this analysis were the same for all NMJs from one fluorescent channel of one experiment.

Stainings with a mean background intensity of the maximum projected confocal stack higher 25 out of 256 a.u. were excluded from analysis.

4.10 Statistical analysis

Comparisons of independent groups were performed with t-tests, unless data was not distributed normally, or showed a different variability between the compared groups. In these cases a Mann-Whitney rank-sum test (rs-test) was used. The levels of significance are marked with asterisks: * $P \leq 0.05$, ** $P \leq 0.01$, *** $P \leq 0.001$. Groups of measurements (electrophysiology or imaging) from the same larva, e.g. muscle 12 vs. muscle 13, or muscle 6 vs. muscle 7, were compared using paired t-tests. Data is presented as mean ± standard error of the mean (sem), except in **Figure 17**, where error bars represent standard deviation.

5. Results

5.1 Electrical activity-induced acceleration of synaptic currents

During continuous low frequency electrical stimulation (0.2 Hz), in TEVC measurement at muscle 6 (**Figure 11A**), a kinetic change in evoked currents was observed. The decay time constant was significantly reduced by more than 25% within 20 min. (**Figure 11B**; average decay τ of 10 eEJCs at t = 0: 4.99 ± 0.14 ms, n = 10; at t = 20 min: 3.86 ± 0.10 ms, n = 10, $P < 0.001$, paired t-test). We next turned to the identification of a molecular correlate of this kinetic change.

It is known that the proportion of slowly desensitising GluR-IIA-type receptors in the postsynapse correlates with the length of decay time constants of synaptic currents (DiAntonio et al., 1999; Schmid et al., 2008). Correspondingly, anti GluR-IIA stainings revealed a smaller average GluR-IIA cluster size on the voltage-clamped muscle 6 compared to its neighbouring muscle 7, which also received electrical stimulation, but was not voltage-clamped (**Figure 11C**; M7: 0.212 ± 0.030 μm^2, n = 6; M6: 0.163 ± 0.031 μm^2, n = 6, P = 0.001, paired t-test).

Both muscles are innervated by the same nerve bundle, which indicates that preventing postsynaptic depolarisation during neurotransmission led to lower levels of GluR-IIA. No difference in the average GluR-IIA cluster sizes was seen on the contra-lateral side between M6 and M7, and the cluster sizes there tended to be larger than on the stimulated side (M7: 0.2819 ± 0.0143 μm^2, n = 6; M6: 0.2726 ± 0.0261 μm^2, n = 6, P = 0.505, paired t-test).

Such comparably rapid glutamate receptor dynamics have not been observed during imaging of NMJ development *in vivo* (Rasse et al., 2005; Schmid et al., 2008). To attain a better understanding of the role of activity in glutamate receptor dynamics, ChR2-based stimulation was employed to induce quantifiable photo-stimulation of the intact, freely moving larva.

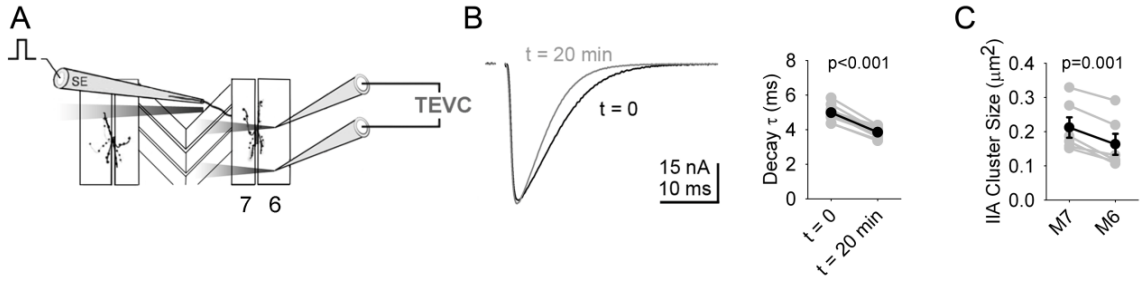

Figure 11 Activity-dependent GluR-IIA removal from postsynaptic densities. (A) TEVC recordings were made from muscle 6, while the hemisegment was electrically stimulated via the sucked-in nerve (SE, suction electrode) at 0.2 Hz. Adapted from (Pawlu et al., 2004). (B). Representative traces (averages of the first and the last 10 eEJCs during a 20 min long electrical stimulation period at 0.2 Hz, black and grey respectively) and summary of all experiments (grey, single experiments; black, mean with SEM) show significant stimulus-induced reduction of eEJC decay τ. (C) Staining showed smaller GluR-IIA receptor clusters on muscle 6 (voltage clamped) compared to adjacent muscle 7 after 20 min electrical stimulation at 0.2 Hz (grey, single experiments; black, mean with SEM). (Ljaschenko et al., 2013).

5.2 Cell-specific channelrhodopsin expression

To gain control over the pre- and the postsynapse *in vivo*, ChR2 was expressed, using the bipartite GAL4/UAS system (Brand and Perrimon, 1993), in motoneurons, in muscle cells or in both compartments. **Figure 12** shows ChR2 distribution (anti-ChR2 stainings) in the three genotypes. When driven with *ok6-GAL4*, ChR2 is visible in motoneuron cell bodies, localised in the ventral nerve cord. ChR2 was not detected in boutons at the NMJ.

Postsynaptically driven ChR2 expression (*g7-GAL4*) leads to immunoreactivity in the muscle, especially around the boutons. No staining in the VNC was detectable. The 'Pre & Post' situation shows, as expected, staining in both compartments.

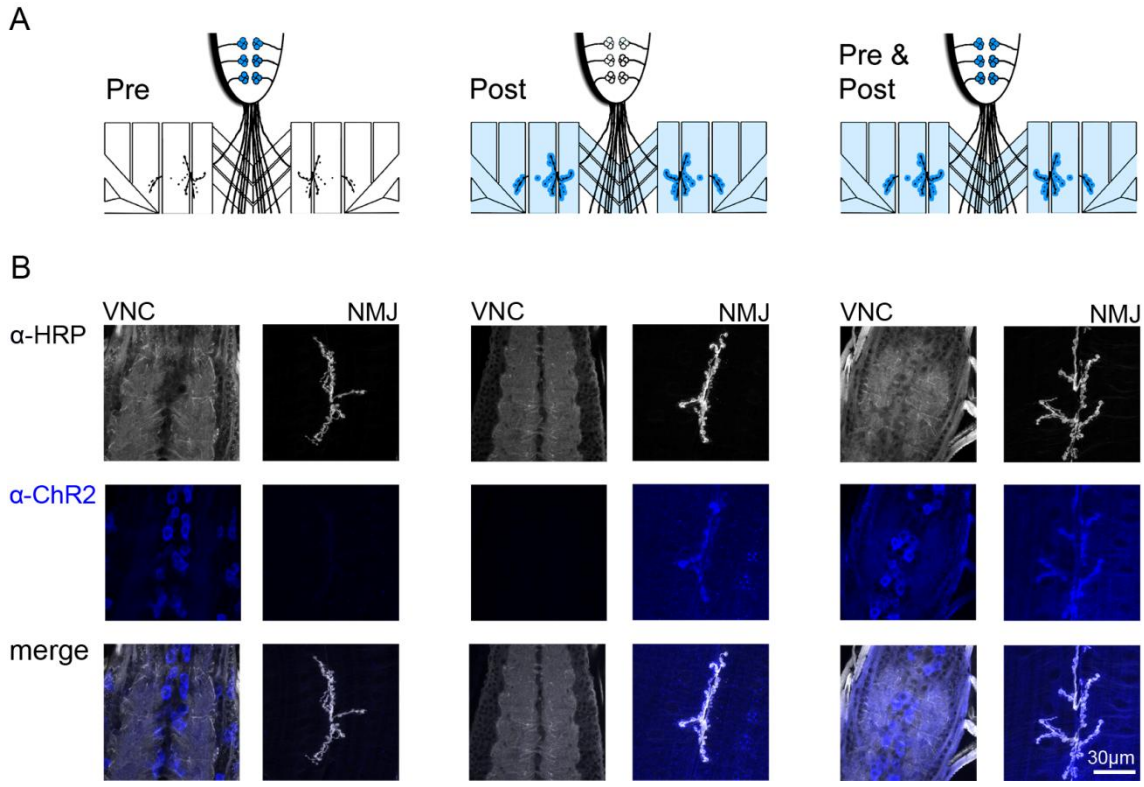

Figure 12 Targeted ChR2 expression. (A) Schematic depiction of ChR2 expression in three different genotypes (presynaptic ChR2 'Pre'; postsynaptic ChR2 'Post'; combined 'Pre & Post') based on (B) anti-ChR2 and anti-HRP (neuronal membrane marker) stainings at the ventral nerve cord (VNC) and the NMJ. Larvae were raised under standard conditions. (Ljaschenko et al., 2013).

5.3 Quantification of light-induced channelrhodopsin currents

Before effects of plasticity inducing light protocols on synaptic transmission were assessed, light-induced currents were measured in semi-intact preparations and analysed. **Figure 13A** shows frequencies of measured lEJCs in 'Pre' larvae under different conditions. Hardly any lEJCs could be detected in HL-3, therefore HL-3.1 was used to assess influence of different RAL concentrations in food and temperatures at which larvae were raised. HL-3.1 is believed to be closer to natural haemolymph in its action potential (AP) propagation properties (Feng et al., 2004). As expected, the frequencies of lEJCs (measured in HL-3.1) increased when temperature was raised at which larvae were bred, or when more RAL was added to the laying medium (**Figure 13A**).

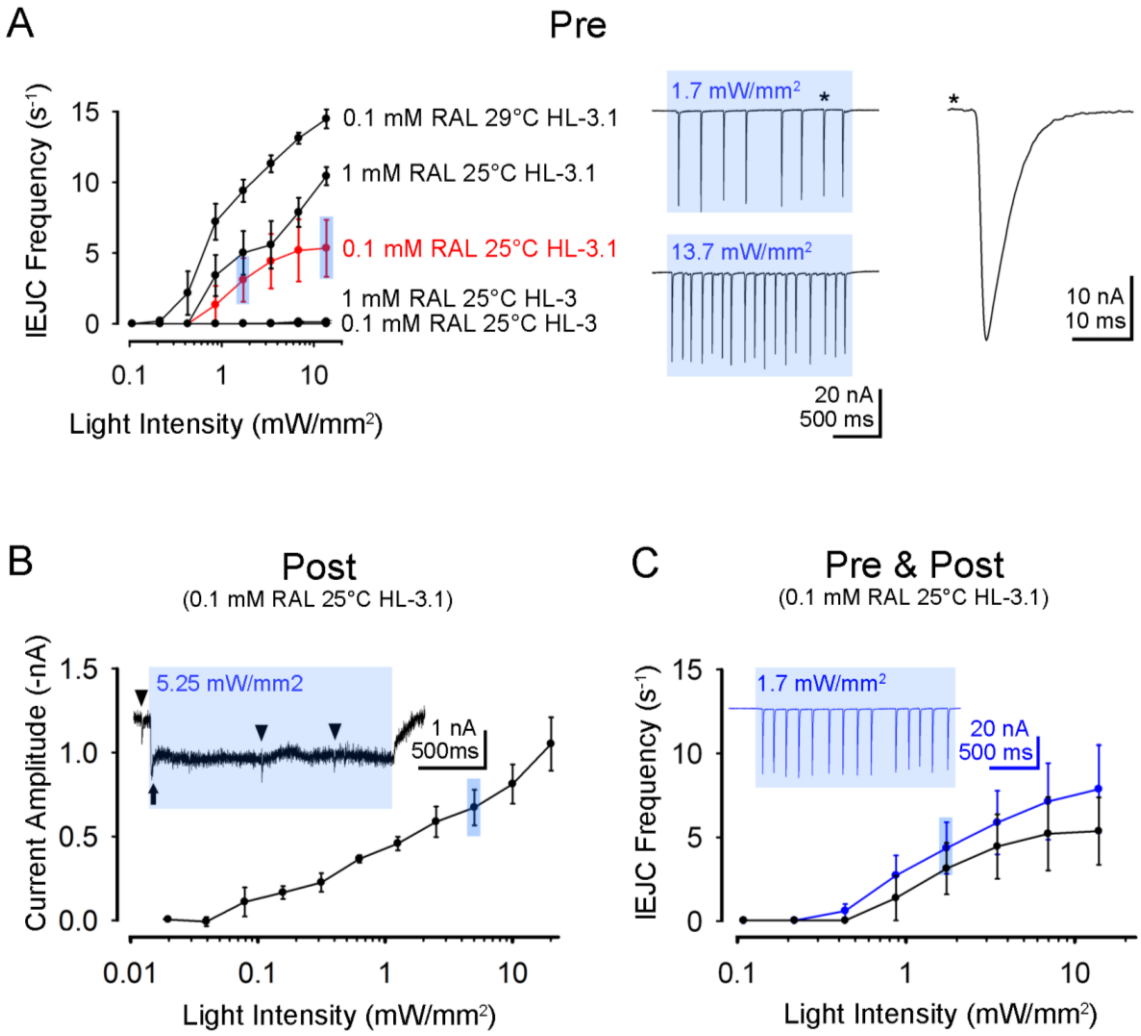

Figure 13 TEVC measurements during light-stimulation. Measurements were performed at muscle 6. (A) Measured frequencies of lEJCs in 'Pre' 3rd instar larvae, raised under different conditions. Recordings were done in two different salines (HL-3 and HL-3.1). Hardly any lEJC could be evoked in HL-3. Red curve shows lEJC frequencies in larvae, raised under standard conditions. Inset shows example lEJCs measured in the same animal, but at two different light intensities, which are highlighted blue in the frequency diagram. The light pulses are indicated as blue rectangles. Asterisk marks an example lEJC, shown at shorter timescale. (B) Light-evoked postsynaptic steady-state currents in larvae with postsynaptically expressed ChR2. Larvae were raised under standard conditions. Inset shows an example trace of a postsynaptically light-evoked current, light pulse is indicated as a blue rectangle. Arrow indicates the ChR2 photocurrent typical transient, arrowheads point to minis. (C) Comparison between frequencies of lEJCs in 'Pre' (black) and 'Pre & Post' larvae (blue), raised under standard conditions. Inset shows example trace measured from a 'Pre & Post' larva, blue rectangle indicates the applied light pulse. (Ljaschenko et al., 2013).

Postsynaptically light-evoked currents (**Figure 13B**) show a ChR2 typical peak (indicated with an arrow) followed by a steady state current. As expected, the amplitude increases with increasing light intensity.

In the 'Pre & Post' situation, the measured currents appear as a linear summation of pre- and postsynaptically evoked currents (**Figure 13C**). Indeed, the frequency of lEJCs in 'Pre & Post' animals shows no difference compared to the frequency in 'Pre'.

5.4 Quantal size increase by weak presynaptic photo-stimulation

In order to induce synaptic plasticity, a standard stimulation protocol (**Figure 6A**), implemented in an earlier publication (Ataman et al., 2008) was used. As a light source, an easily available weak blue LED lamp (40μW/mm2, **Figure 5A** left) was utilised. With this stimulation, the electrophysiologically observed effects in the afore mentioned publication could be reproduced in 'Pre' larvae, raised under standard conditions. The amplitude of minis was slightly but significantly increased (Control minis 0.74 ± 0.05 nA, n = 11 NMJs, 'Pre' minis 0.81 ± 0.03 nA, n = 13, P = 0.040 rs-test;), eEJCs were unchanged and the reduction of quantal content did not reach statistical significance. The paired pulse ratio, a measure for release probability also remained unchanged (Supplemental data **Table 1**).

5.5 Strong photo-stimulation-induced functional plasticity

Since photo-stimulation with the weak lamp induced only minor changes in the electrophysiological footprint, a significantly stronger LED (1.7 mW/mm2, **Figure 5A** right) was used for the following experiments. All three genotypes, raised under standard conditions, were subjected to the standard photo-stimulation protocol (**Figure 6A**). At this point, photo-stimulation led to very pronounced changes in

synaptic currents (**Figure 14**; Supplemental data **Table 2**). In 'Pre' and also 'Post' larvae, photo-stimulation led to a substantial decrease in eEJC amplitudes (**Figure 14A**, Supplemental data **Table 2**). The mean mini amplitudes remained unaltered, which resulted in a reduction of quantal content (**Figure 14B**; Supplemental data **Table 2**).

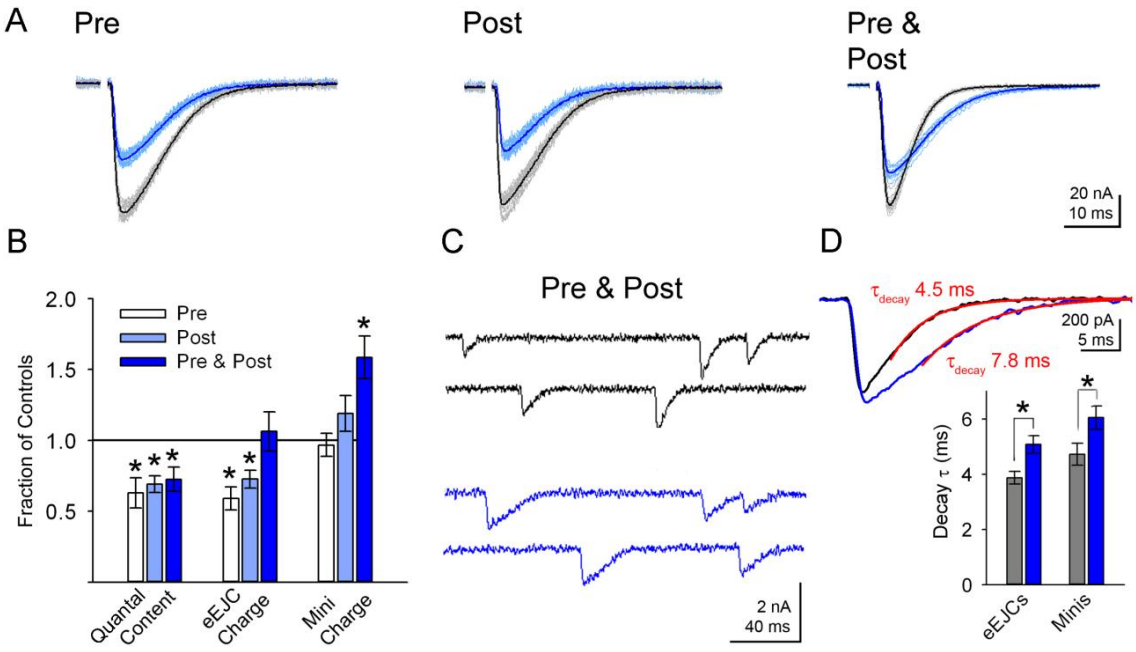

Figure 14 Induction of functional synaptic plasticity *in vivo*. (A) Representative eEJCs recorded following the standard *in vivo* photo-stimulation protocol. Mean traces of representative recordings in black (control) and dark blue (RAL) with corresponding individual traces from the same recordings in grey (control) and light blue (RAL) are shown. Stimulation artefacts were removed for clarity reasons. (B) Relative change of quantal content, charge carried by eEJCs and minis are shown ('Pre' white, 'Post' light blue, 'Pre & Post' dark blue) compared to their respective controls. (C) Representative recordings of minis in control (black) and 'Pre & Post' NMJs (blue) show different decay kinetics. (D) Representative examples of averaged mini recordings at control (black) and 'Pre & Post' NMJs (blue) with monoexponential functions fitted to the decaying part (60-0%, see Experimental procedures) of the current. Below, statistical comparison shows increased mini and eEJC decay τ in 'Pre & Post' (blue) larvae compared to controls (grey). (Ljaschenko et al., 2013).

The 'Pre & Post' animals also showed a significant decrease in quantal content. Additionally, eEJCs displayed a kinetic change, induced specifically by combined pre- and postsynaptic photo-stimulation, namely a protraction of the decay τ

(**Figure 14A,D**; Control eEJCs 3.87 ± 0.23 ms, n = 11 NMJs, 'Pre & Post' eEJCs 5.08 ± 0.32 ms, n = 10, P = 0.006 t-test;). Minis also showed a decay τ prolongation (**Figure 14C,D**; Control minis 4.72 ± 0.40 ms, n = 11, 'Pre & Post' 6.05 ± 0.42 ms, n = 11, P = 0.01 rs-test), which corresponded to a ~60 % increase in mini charge transfer (**Figure 14B**). This protraction of quantal events lifted the eEJC charge to the control level, despite a strongly reduced quantal content (**Figure 14B**). Thus, correlation between pre- and postsynaptic activity led to functional plasticity at the level of quantal synaptic transmission.

5.6 Standard synaptic markers unaffected by photo-stimulation

The standard photo-stimulation protocol led to substantial functional changes of the synapse in all three genotypes (**Figure 14**; Supplemental data **Table 2**). To test for a corresponding structural change at the level of synaptic proteins, an immunohistochemical analysis of standard synaptic markers was performed. Bruchpilot (BRP) a major component of the presynaptic release site (Kittel et al., 2006; Wagh et al., 2006) and Glutamate receptor IID subunit (GluR-IID), which is presumably present in all NMJ ionotropic glutamate receptor types (Featherstone et al., 2005; Marrus et al., 2004; Qin et al., 2005), were visualised. The overall structure of the NMJ was made visible by the anti HRP antibody, which reliably marks the presynaptic membrane of motoneurons (Jan and Jan, 1982).

Larvae were raised under standard conditions and subjected to the standard photo-stimulation protocol (**Figure 6A**). The analysis of maximum projections of confocal stacks revealed no significant differences between control and RAL fed larvae (**Figure 15**; Supplemental data **Table 3**). The size of the NMJ was unchanged, as measured by the total HRP area (**Figure 15C**). No change in size or number of BRP spots and size or number of GluR-IID clusters was resolved (**Figure 15B,C**).

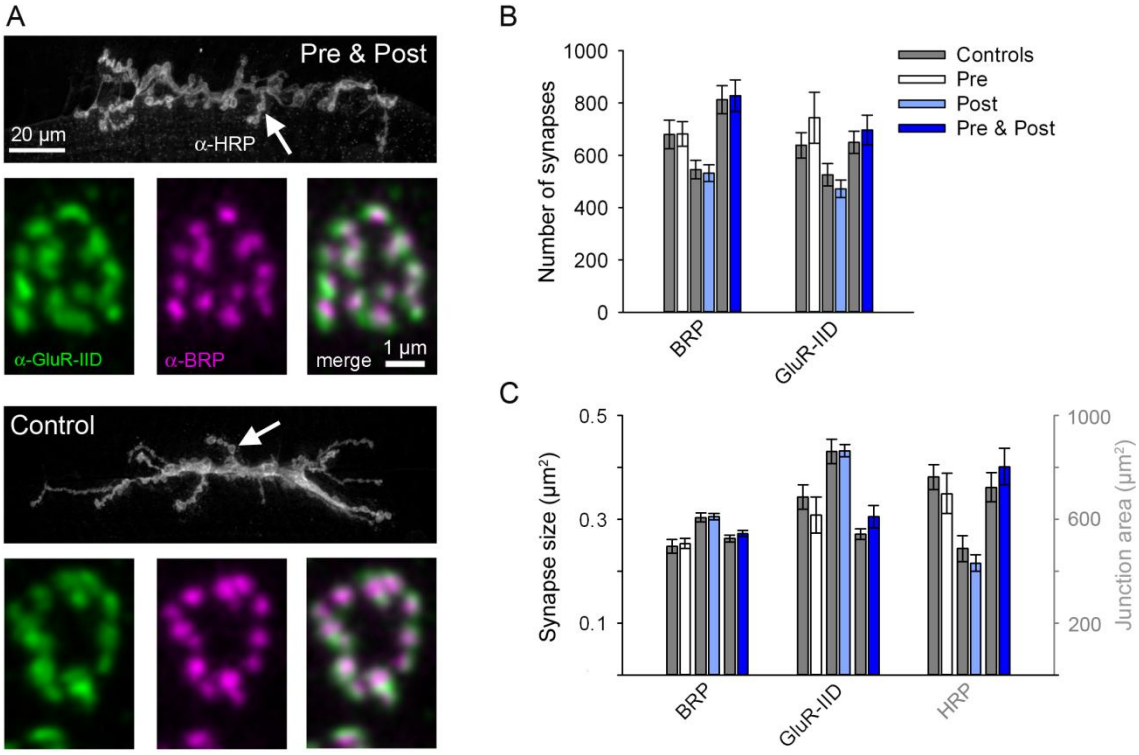

Figure 15 Immunohistochemical stainings of standard synaptic markers. Maximum projections of confocal images from triple stainings of the shared muscle 6/7 NMJ (segments A2 and A3). Larvae were raised under standard conditions and stimulated with the standard photo-stimulation protocol. (A) Representative staining from 'Pre & Post' (upper panels) and control larvae (lower panels) against HRP (α-HRP, grey), against GluR-IID (α-GluR-IID, green) and against BRP (α-BRP, magenta). Arrows indicate the enlarged boutons. (B) Number of synapses, presynaptically marked with α-BRP and postsynaptically with α-GluR-IID. (C) Synapse size i.e. mean size of single BRP spots and GluR-IID clusters. Junctional area, i.e. area covered by α-HRP. (Ljaschenko et al., 2013).

5.7 Paired photo-stimulation induced GluR-IIA receptor field growth

Two types of ionotropic glutamate receptor channels are known to be present at the *Drosophila* NMJ. Both types are tetrameric and contain GluR-IIC (also called GluR-III), IID, IIE subunits and additionally either GluR-IIA or GluR-IIB (Featherstone et al., 2005; Marrus et al., 2004; Qin et al., 2005). The GluR-IIA type receptors mediate a much larger charge transfer due to substantial slower desensitization kinetics (DiAntonio et al., 1999).

Motivated by this finding and the discovered link between the acceleration of decay τ and decreased content of GluR-IIA in electrical stimulation-induced removal of IIA-type receptors (**Figure 11**), stainings against the IIA and the IIB subunits were performed to investigate whether the prolonged decay τ, observed after 'Pre & Post' stimulation, correlated with increased GluR-IIA content. In agreement with the prolonged decay τ, stainings against the GluR-IIA subunit showed a 54% increase in numbers of detected clusters (**Figure 16A**; Control 481 ± 54 clusters, n = 25 NMJs; 'Pre & Post' 742 ± 67 clusters, n = 21, P = 0.002 rs-test). Furthermore, this increase was accompanied by a 41 % growth of the mean GluR-IIA cluster size (**Figure 16A**; Control 0.173 ± 0.009 μm2, n = 25 NMJs; 'Pre & Post' 0.244 ± 0.007 μm2, n = 21, P < 0.001 t-test).

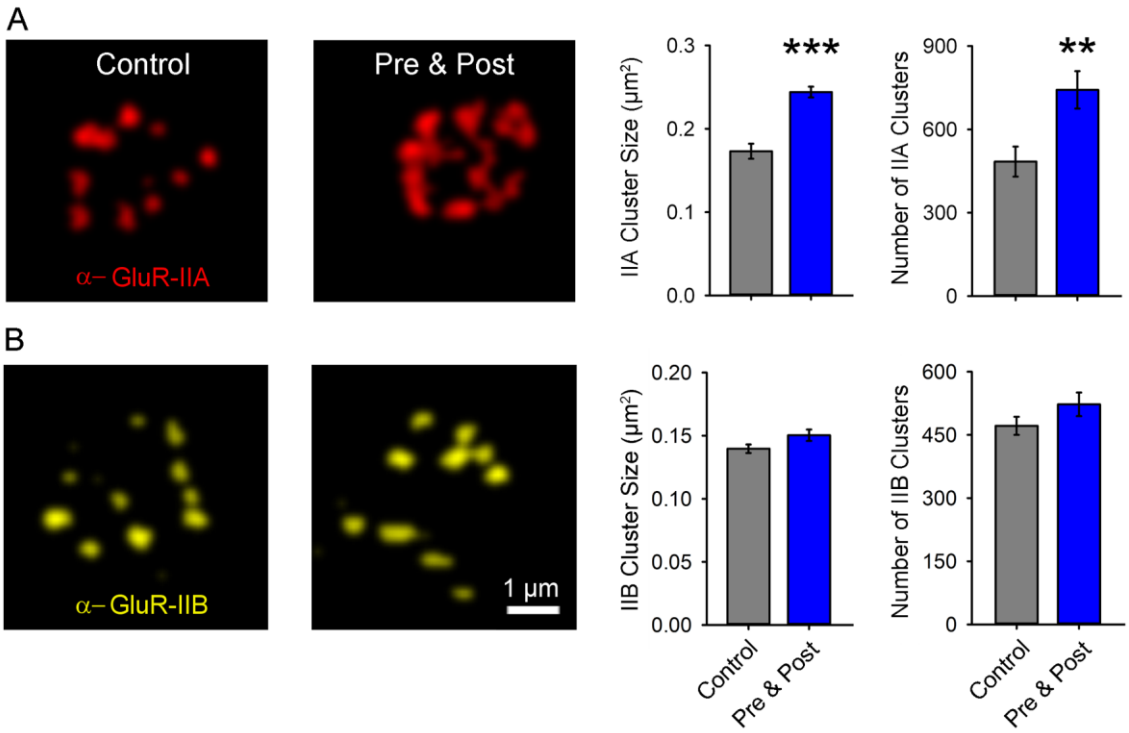

Figure 16 Specific incorporation of GluR-IIA type receptors upon 'Pre & Post' photo-stimulation. Larvae were raised under standard conditions and subjected to standard stimulation. (A) Representative stainings (α-GluR-IIA, red) and quantification of GluR-IIA receptor fields (clusters) at the shared muscle 6/7 NMJ of the segments A2 and A3. After ChR2 photo-stimulation GluR-IIA clusters were significantly increased in size and number at 'Pre & Post' (blue) compared to control NMJs (grey). (B) Size and number of GluR-IIB clusters (α-GluR-IIB, yellow) remained unchanged. (Ljaschenko et al., 2013).

Thus, combined pre- and postsynaptic photo-stimulation led to a specific increase of GluR-IIA containing receptors in postsynaptic densities. Due to variability in background staining, the experiment was performed thrice in order to exclude a bias by the differential background subtraction. Hence the large sample size of IIA stainings. Importantly, each of the three experiments gave the same significant result. To prevent a bias resulting from a smaller sample size, the staining procedure was also repeated for the IIB staining.

In contrast to GluR-IIA, neither the number (**Figure 16B**; Control 472 ± 21 clusters, n = 30 NMJs; 'Pre and Post' 523 ± 28 clusters, n = 29, P = 0.152 t-test), nor the average size of GluR-IIB clusters (**Figure 16B**; Control 0.140 ± 0.003 μm^2, n = 30 NMJs; 'Pre & Post' 0.150 ± 0.005 μm^2, n = 29, P = 0.063 t-test) were significantly influenced by the standard photo-stimulation protocol.

5.8 Mean intensity and area of GluR-IIA receptor fields

In confocal imaging the area and intensity of a detected spot are not independent from each other. To investigate whether the measured area growth after long-pulse stimulation represents a real increase in GluR-IIA content after 'Pre & Post' stimulation, or a mere increase in receptor field area, while the mean intensity was reduced, intensities vs. areas of the same spots of receptor fields before and after standard photo-stimulation were plotted (**Figure 17**). All detected spots were pooled. After standard photo-stimulation bigger receptor field sizes were detected (**Figure 16A**). Additionally, the clusters tend to have stronger mean intensities (**Figure 17**), which speaks for a genuine increase in GluR-IIA content.

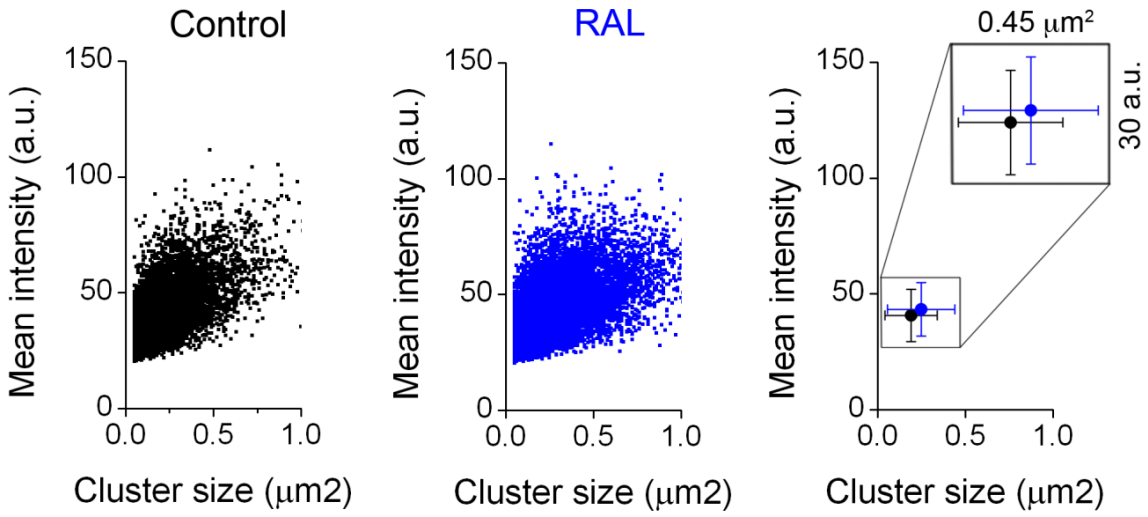

Figure 17 Correlation between GluR-IIA mean intensity and cluster size after standard 'Pre & Post' stimulation. Receptor fields of control animals are shown in black, of RAL-fed animals in blue. RAL fed animals show increased GluR-IIA area (Figure 16A) and tended to show stronger mean intensities. Error bars indicate standard deviations.

5.9 GluR-IIA content increase by short-pulse photo-stimulation

During the 'Pre & Post' photo-stimulation the net current flow over the postsynaptic membrane is larger than during isolated pre- or postsynaptic activation, which suggests itself as a possible explanation for GluR-IIA receptor field growth. Therefore, we set out to test whether GluR-IIA-mediated synaptic plasticity was caused by the higher net current flow on the postsynaptic side or induced by the correlative nature of the photo-stimulation. To this end, the length of the light pulses was reduced to 15 ms (instead of 2s; **Figure 18C**).

Now the current flow over the postsynaptic membrane was smaller than during the 'Pre' light-stimulation, the correlative nature of the light-stimulation, was however preserved. **Figure 18B** shows how two AP evoked EJCs reliably overlap with the postsynaptic depolarisation during the 15 ms pulse.

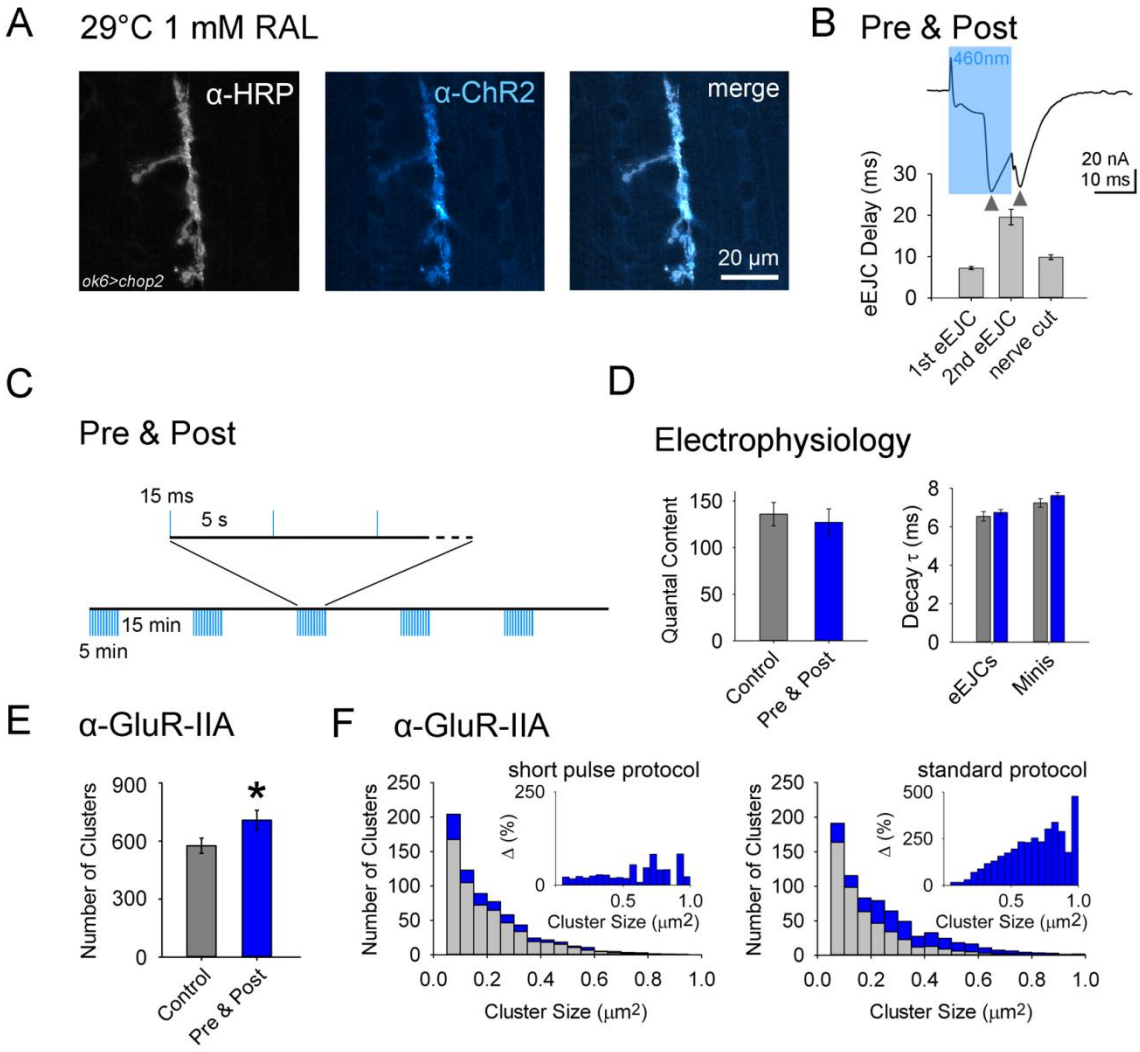

Figure 18 Synaptic plasticity evoked by brief paired light-stimulation. Larvae were raised under enhanced expression conditions (29°C, 1mM RAL). (A) α-HRP (grey) and α-ChR2 (blue) co-staining reveals ChR2 expression in motoneuron boutons, which was not the case under standard conditions (*ok6>chop2*; a 'Pre' NMJ is shown to avoid contamination by the postsynaptic ChR2 signal). (B) At 'Pre & Post' NMJs, a 15 ms, 1.7 mW/mm², light pulse (framed by LED on- and off artefacts) evoked two lEJCs (arrowheads) which superimpose on postsynaptically evoked muscle depolarisation. Below: quantification of lEJC delays relative to light application and compared to 'Pre' NMJs after severing motoneuron axons. (C) Scheme of short pulse light-stimulation protocol. (D) Mean quantal content, decay τ and (E) mean number of GluR-IIA clusters following light-stimulation at 'Pre & Post' (blue) and control NMJs (grey). More GluR-IIA clusters were detected at 'Pre & Post' NMJs compared to controls following brief paired photo-stimulation. (F) Distributions of GluR-IIA cluster sizes at 'Pre & Post' NMJs (blue) and controls (grey) following light-stimulation with the short pulse protocol (left) or standard protocol in larvae raised under standard conditions (right). Insets show relative change (Δ) in cluster numbers for a given cluster size. After the short pulse protocol the increase in cluster numbers is evenly distributed, after the standard protocol larger clusters increase disproportionally stronger. (Ljaschenko et al., 2013)

Strong LED light-stimulation (1.7 mW/mm^2) in 'Pre' animals, raised under standard conditions, would lead to a long latency of the onset of the first lEJC, photo-stimulation of 'Pre & Post' larvae would not lead to synchrony of lEJCs and the direct postsynaptic depolarisation during the 15 ms pulse. The direct postsynaptic depolarisation would be finished, while the first AP would not have been triggered yet. ChR2 expression was therefore reinforced, by raising larvae under enhanced expression conditions (29 °C, 1mM RAL). Now, directly induced postsynaptic depolarisation of the muscle coincided with two AP evoked lEJCs (latency first lEJC: 7.25 ± 0.36 ms, n = 4 NMJs; latency second: 19.53 ± 1.85 ms, n = 3; **Figure 18B**).

Interestingly, in contrast to standard expression, ChR2 (**Figure 12**) now also localised to presynaptic boutons (**Figure 18A**) and was not restricted to motoneuron cell bodies. When severing the motoneuron axon in a 'Pre' animal, raised under the same conditions and stimulated with the same light intensity, only one lEJC could be detected (latency of remaining lEJC: 9.88 ± 0.55 ms, n = 4). Taking ChR2 staining, which is present in boutons, into consideration, (**Figure 18A**), this indicates that in 'Pre & Post' larvae, raised under enhanced conditions, the first lEJC is triggered in the terminal axon segment, the second in the cell body.

'Pre & Post' larvae, raised under enhanced expression conditions, were subjected to the short pulse photo-stimulation protocol (**Figure 18C**). In contrast to the long pulse photo-stimulation protocol, this protocol did not produce a significant change in quantal content (**Figure 18D**; Control 136 ± 13 vesicles, n = 12 NMJs; 'Pre & Post' 127 ± 14, n = 12, P = 0.650 t-test). Moreover, neither the decay of eEJCs (Control 6.54 ± 0.24 ms, n = 12 NMJs; 'Pre & Post' 6.74 ± 0.15 ms, n = 12, P = 0.492 t-test), nor of minis (Control 7.24 ± 0.22 ms, n = 13 NMJs; 'Pre & Post' 7.63 ± 0.15 ms, n = 12, P = 0.201 rs-test) was significantly changed (**Figure 18D**). All other assessed electrophysiological parameters also remained below detection limit (Supplemental data **Table 4**).

The number of GluR-IIA receptor clusters, however, increased from 576 ± 39 in controls (n = 25 NMJs) to 708 ± 51 in 'Pre & Post' larvae (n = 17, P = 0.045 t-test, **Figure 18E**), while the mean receptor cluster size remained unchanged (Control 0.213 ± 0.009 μm2, n = 25 NMJs; 'Pre & Post' 0.216 ± 0.008 μm2, n = 17, P = 0.802 t-test). Brief correlated light-stimulation in contrast to the standard stimulation led to an evenly distributed increase in cluster numbers across all cluster sizes (**Figure 18F**). Therefore no change in the mean cluster size was expected.

5.10 Input specificity of GluR-IIA incorporation

Besides its correlative nature, a defining feature of Hebbian plasticity is its input-specific (synapse-specific) action (Abbott and Nelson, 2000). This means that plastic changes take place specifically at synapses, which participate in correlative activation, and do not spread globally to other synapses. In order to address this point, ChR2 was expressed presynaptically and additionally postsynaptically, but only in muscle 12 (Inaki et al., 2010).

Figure 19C shows a schematic depiction of the combined expression pattern of *ok6-GAL4* and *m12-GAL4* drivers. Live images (**Figure 19A**) of EGFP and immunohistochemical images against ChR2 (**Figure 19B**), expressed by the same drivers, show expression in motoneurons and selectively in muscle 12. The 'Pre & M12 Post' ChR2 genotype enabled us to compare activity-induced effects on synapses *in vivo*, including those formed by the same motoneuron (Hoang and Chiba, 2001), which experienced either solely presynaptic or combined pre- and postsynaptic light-stimulation. This experiment also provides an ideal control for variations arising from variability between individuals, since comparisons were made between neighbouring muscles within one individual.

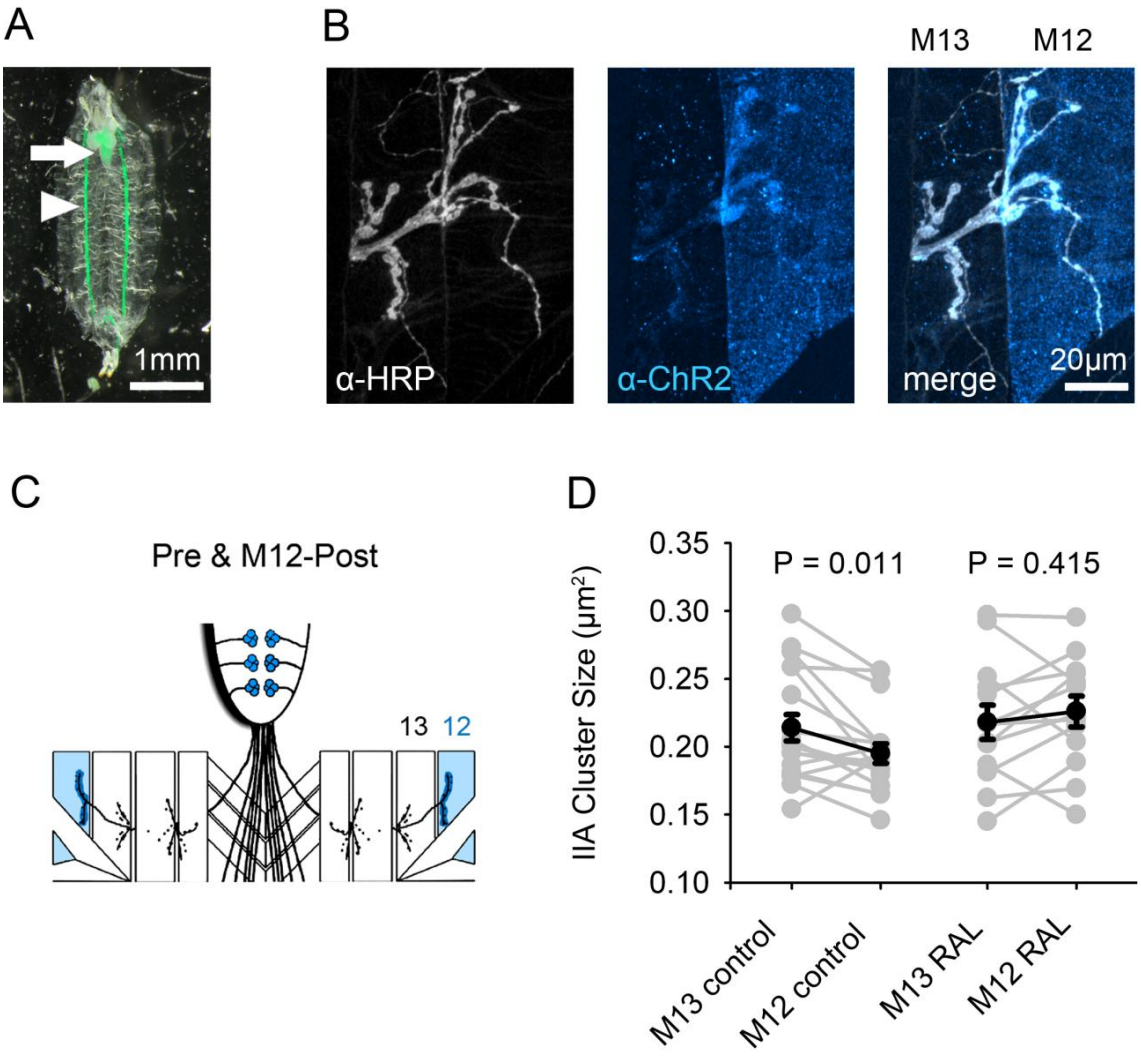

Figure 19 Input-specific induction of synaptic plasticity by paired photo-stimulation. Larvae were raised under enhanced expression conditions. (A) Dissected third instar larva, which expresses EGFP under control of *ok6-* & *m12-GAL4*. Arrow and arrowhead indicate CNS and muscle 12 respectively. (B) Double staining against HRP (grey) and ChR2 (blue) at 'Pre & M12-Post' NMJs of muscles 12 and 13. (C) Schematic distribution of ChR2 in 'Pre & M12-Post' larvae (D) Comparison between GluR-IIA cluster sizes on muscles 12 and 13 following the short pulse protocol in control and RAL fed 'Pre & M12-Post' larvae. Comparisons between adjacent muscles are indicated by a line (grey, individual larvae; black, mean values). GluR-IIA clusters were significantly smaller on M12 compared to M13 in controls, but attained an equal size in RAL fed 'Pre & M12-Post' larvae. (Ljaschenko et al., 2013).

Larvae ('Pre & M12-Post') were raised under enhanced expression conditions and subjected to the short pulse protocol *in vivo*. The mean GluR-IIA cluster sizes were compared in adjacent muscles 12 and 13 by paired t-tests. In control animals, GluR-IIA clusters were significantly smaller in muscle 12 than in adjacent muscle 13

(**Figure 19D**; M12: 0.195 ± 0.007 μm², n = 18 NMJs; M13: 0.214 ± 0.010 μm², n = 18, P = 0.011 paired t-test).

However, in RAL fed animals IIA cluster sizes on muscle 12, which received pre- and postsynaptic light-stimulation, grew selectively compared to the adjacent muscle 13 NMJs, which had received presynaptic photo-stimulation only (**Figure 19D**; M12: 0.226 ± 0.011 μm², n = 13 NMJs; M13: 0.218 ± 0.013 μm²; n = 13, P = 0.415 paired t-test).

6. Discussion

6.1 Hebbian plasticity

Paired photo-stimulation of the pre- and postsynaptic compartments led to a synapse specific increase in levels of postsynaptic GluR-IIA-type receptors (**Figure 16A**), which caused prolongation of synaptic currents at the level of quantal transmission (minis, **Figure 14D**) as well as at the level of evoked currents (eEJCs, **Figure 14D**). Consequently, the charge carried by eEJCs was restored to control level (**Figure 14B**), despite a strongly reduced quantal content (**Figure 14B**).

The isolated pre-, or postsynaptic photo-stimulation led to a strong quantal content reduction in both cases. Assuming a linear summation of the two effects, an even stronger reduction of the quantal content had been expected when the two stimulations were combined. However, the 'Pre & Post' photo-stimulation led to a non-linear change in synaptic function, increasing synaptic efficacy, rather than reducing it. This study presents to our knowledge the first description of a Hebbian form of synaptic plasticity at the *Drosophila* NMJ.

To check whether the supra-linear effect stemmed from the higher level of postsynaptic current during 'Pre & Post' photo-stimulation or the correlated nature of the stimulation, very brief light pulses (15 ms) were paired. This stimulation also led to an increase in postsynaptic GluR-IIA levels (**Figure 18E,F**). This was quite surprising, since only two lEJCs coincided with the postsynaptic depolarisation, which is 300 extra lEJCs paired with a 15 ms short direct postsynaptic depolarisation during 100 min of photo-stimulation. At the time of photo-stimulation (100 min) thousands of endogenously evoked motoneuron APs were probably fired during natural locomotion, which triggered thousands of eEJCS. This clearly demonstrates the power of the Hebbian mechanism of synaptic plasticity.

Interestingly, the short-pulse protocol did not lead to an increase in the mean cluster size. To extend and deepen the analysis, histograms, which illustrate the increase in

GluR-IIA cluster numbers at different cluster sizes were calculated. **Figure 18F** shows, that after the short-pulse photo-stimulation protocol GluR-IIA was incorporated in PSDs of all sizes. Clusters too small to be detected in control animals crossed the detection barrier. Therefore the mean size remained unchanged, while an increased number of detected clusters was observed.

The quantal content was also not significantly affected by the short-pulse photo-stimulation. In contrast, long-pulse photo-stimulation led a reduction of the quantal content in all three genotypes. Although it remains at present unclear whether the same pathway is responsible for reducing the quantal content during pre-, post, or paired photo-stimulation, the results obtained after the short pulse protocol in 'Pre & Post' animals, namely no reduction in quantal content, suggests that reduction in quantal content depends on the intensity of photo-stimulation. In contrast, the mechanism of GluR-IIA incorporation is more specific and sensitive to the precise nature of activity.

Following short 'Pre & Post' photo-stimulation no significant electrophysiological footprint of GluR-IIA incorporation was detected (Supplemental data **Table 4**), merely a tendency towards prolonged decay time constants of synaptic currents (**Figure 18D**). This can be understood by comparing the cluster size distribution of GluR-IIA clusters after the short pulse and the standard protocol (**Figure 18F**). The short pulse protocol led to an increase in GluR-IIA numbers across all cluster sizes, in contrast the standard light-stimulation protocol led to a great relative increase in numbers of large clusters. It was shown that neurotransmitter release probability varies across active zones at the same NMJ (Peled and Isacoff, 2011). Additionally, the size of glutamate receptor clusters is largest opposite high release probability active zones (Marrus and DiAntonio, 2004). Therefore, it is to be expected that electrophysiological recordings preferentially sample large receptor fields. The absolute number of large receptor fields was not strongly increased by the short pulse protocol compared to the standard protocol (**Figure 18F**), thus the NMJ preserved its electrophysiological properties.

Moreover, there was a limit to the absolute number of GluR-IIA clusters induced by 'Pre & Post' light-stimulation (both long and short pulses); it did not surpass markedly the number of IID clusters (IID after standard stimulation 697 ± 57; IIA after short pulse stimulation 708 ± 51; IIA after standard stimulation 742 ± 67). In view of the unchanged number of BRP spots, this indicates that paired photo-stimulation did not give rise to formation of many new synapses, but rather promoted GluR-IIA incorporation into existing receptor fields, with GluR-IIA levels below detection limit. Although it is important to remember that comparisons of data sets gathered in different imaging sessions should not be over-interpreted, the overall numbers of detected clusters however, should be a suitable parameter for a crude comparison.

6.2 Synapse specificity of GluR-IIA incorporation

A Hebbian mechanism demands synapse specificity of the effect (Abbott and Nelson, 2000). To investigate this point, the power and the availability of genetic tools in *Drosophila* were beneficial. ChR2 was expressed presynaptically and additionally postsynaptically, but only in muscle 12 (**Figure 19B,C**). As predicted by previous results, the short pulse protocol led to a specific increase of IIA, specifically in the muscle 12 NMJ (**Figure 19D**), which received pre- and postsynaptic photo-stimulation. Muscle 13, which was stimulated presynaptically only, did not show increased GluR–IIA cluster sizes.

The specific increase of IIA levels in M12 leads to the conclusion that the Hebbian mechanism acts locally enough to discriminate between synapses on two adjacent muscles, partially innervated by the same neurons.

6.3 Linking developmental and activity-dependent synaptic plasticity

An elegant *in vivo* imaging study suggests that during the development of the larval NMJ a mechanism initially promotes GluR-IIA incorporation during synapse growth and that GluR-IIA entry is specifically restrained during further maturation, while the rate of GluR-IIB recruitment remains constant (Schmid et al., 2008).

The physiological signals, which guide these dynamics, have been unknown, though it was thought that synaptic activity is important. Here we argue that the Hebbian mechanism presented in this work is the signal, which boosts GluR-IIA entry during synapse development. Furthermore, paired pre- and postsynaptic light-stimulation is able to override the inhibition of GluR-IIA incorporation at large, therefore probably mature receptor fields (**Figure 18F** right) and thus, restore a 'juvenile behaviour' of PSDs.

Future studies could help to clarify the nature of downstream signals, which regulate GluR-IIA abundance. The cAMP-pathway would be a candidate for that. New optogenetic tools like the photoactivated adenylyl cyclase (Bucher and Buchner, 2009; Stierl et al., 2011) could be used to manipulate cAMP *in vivo* and assess its effect on GluR-IIA abundance.

At the developing NMJ, receptor fields grow in synchrony with active zone maturation (Fouquet et al., 2009; Schmid et al., 2008). Correspondingly, large receptor fields are located opposite high release probability (p_r) active zones (Marrus and DiAntonio, 2004). Therefore, small, growing receptor fields, opposite immature low p_r release sites, are exposed to glutamate only during strong presynaptic depolarisation e.g. during trains of APs. Since many high p_r synapses will be already active, predepolarising the postsynapse, the glutamate release at a low p_r site will coincide with strong postsynaptic depolarisation. This leads to Hebbian GluR-IIA incorporation into the immature low p_r synapses (**Figure 20** left panel).

This mechanism predicts GluR-IIA recruitment at all simultaneously active synapses, independent of their size. Since 'Pre & Post' light-stimulation can pre-depolarise the postsynaptic cell independently of presynaptic release, the Hebbian protocol leads to incorporation of GluR-IIA into receptor fields of all active synapse, including the large, mature ones. Therefore, it seems that slot or space requirements within PSDs do not limit developmental IIA incorporation, which is slowed down at maturing synapses (Schmid et al., 2008).

Hence, a physiological model of GluR-IIA dynamics demands a signal to remove GluR-IIA from mature receptor fields, in order to prevent overgrowth of PSDs by IIA. We reason that the responsible physiological cue is provided by sparse, unsynchronised transmitter release, which does not trigger strong muscle depolarisation and should preferentially occur at high p_r sites (**Figure 20** right panel).

This hypothesis was experimentally supported by showing GluR-IIA removal from synapses at muscles where muscle depolarisation is prevented during neurotransmission (**Figure 11**). The accelerated decay measured in the experiment (**Figure 11B,21A**) does not seem to stem from a general break down phenomenon of the semi-intact preparation since the amplitudes of eEJCs during that experiment remained constant on average (**Figure 21B**). The decay reduction seems to kick in after an initial stationary phase of 1-2 minutes and proceed with a constant rate (**Figure 21C**).

Interestingly, 0.2 Hz stimulation alone already reduces GluR-IIA cluster sizes, even if the muscle is not voltage clamped (IIA clusters on the stimulated side are larger). This is likely due to the solitary nature of this stimulation, which does not lead to pronounced postsynaptic depolarisation.

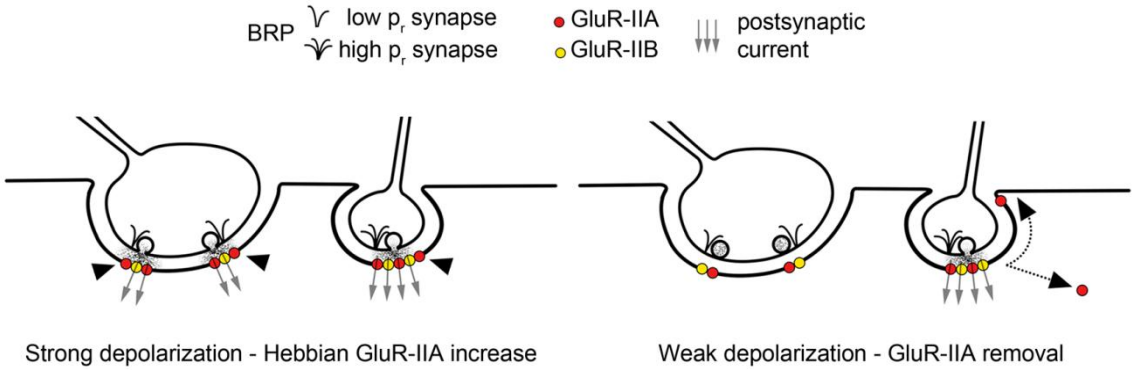

Figure 20 Model of activity-dependent GluR-IIA dynamics. Left: synchronous synaptic exocytosis induces strong muscle depolarisation and triggers Hebbian GluR-IIA incorporation at all simultaneously active synapses (arrowheads). Right: sparse activity (during minis or isolated AP firing) leads to neurotransmitter release only at high p_r sites (high BRP content). This triggers only weak muscle depolarisation and leads to GluR-IIA removal from active synapses. (Ljaschenko et al., 2013).

We introduce a physiological concept (**Figure 20**), where GluR-IIA levels are increased at simultaneously active synapses via a Hebbian mechanism and decreased at solitarily active synapses. Simultaneous activity occurs during AP trains. Solitary activity might be provided in living animals by minis or single APs. The physiological role of minis is matter of hot debate (Featherstone and Broadie, 2002; Saitoe et al., 2002; Verstreken and Bellen, 2002). We propose a function in controlling the molecular composition of PSDs by removing GluR-IIA from high p_r synapses with large receptor fields, which otherwise would overgrow. Putting a break on the Hebbian mechanism is a necessary feature of the synapse, discussed in "Synaptic plasticity: taming the beast" (Abbott and Nelson, 2000).

Our model accounts for developmental, synapse-specific receptor subunit dynamics and explains higher GluR-IIA levels opposite low p_r Ib boutons compared to high p_r sites in Is boutons (Schmid et al., 2008): the high p_r sites release neurotransmitter more readily during sparse activity, thus, reducing the GluR-IIA content of their PSDs. Low p_r sites release transmitter only during strong presynaptic depolarisations when many other sites already fire. Thus, low p_r synapses participate mainly in the Hebbian GluR-IIA incorporation events. Since the amount of

unsynchronised NT release is lower, the mechanism to curb GluR-IIA incorporation is activated less frequently, leading to higher IIA levels.

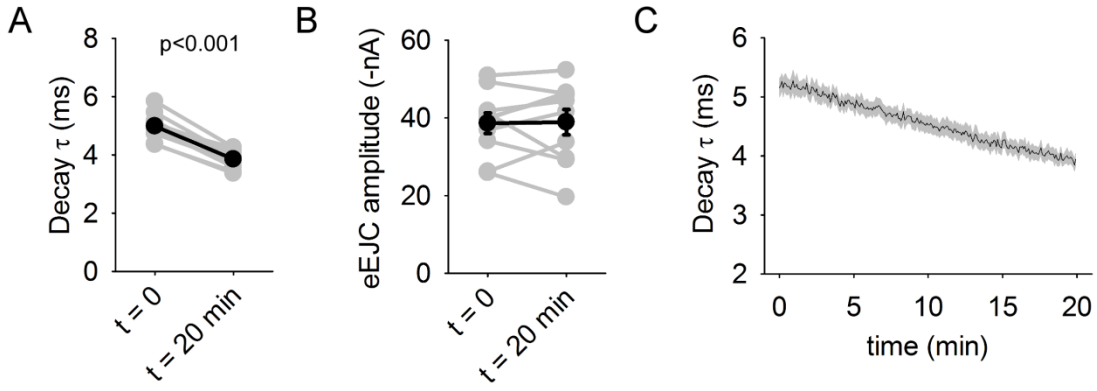

Figure 21 Dynamics of activity-dependent GluR-IIA removal. (A) Decay acceleration from TEVC measurements at 0.2 Hz electrical stimulation (see also Figure 11B). Black shows mean ± sem (very small in this case), grey shows decay acceleration in individual cells. (B) No change in average amplitude was measured after 20 min. Black shows mean ± sem, grey individual experiments. (C) Time course of decay acceleration. Black, mean; grey, sem.

Moreover, the present conceptual framework reconciles further independent and seemingly contradictory observations. The model predicts that homogeneous transmitter release promotes GluR-IIA incorporation, no matter whether the release probability is homogeneously increased or reduced.

BRP null mutant larval NMJs, for example, display a reduced release probability (Kittel et al., 2006), which means synapses should rather fire at high levels of presynaptic depolarisation, however, in synchrony, which may lead to the observed increase in GluR-IIA levels.

Similarly, the hyperactive potassium-channel mutant eag, Sh shows a reduced presynaptic activity. In this case, synapses might also fire rather synchronously at higher levels of activation, which might lead to observed increased occurrence of subsynaptic translation aggregates. These are associated with a significant increase in the postsynaptic GluR-IIA levels (Sigrist et al., 2000).

In contrast, during enhanced locomotion (Sigrist et al., 2003) the activity level is higher, but as long as it is increased to a more homogenous (synchronous) level the model again predicts higher levels of GluR-IIA, which was observed.

Thus, the proposed physiological concept, although speculative, provides an alternative hypothesis to models, which explain higher GluR-IIA levels with compensatory mechanisms in cases when neurotransmission in reduced, but which can't explain higher IIA levels in cases of increased presynaptic activity.

Interestingly, rapid GluR-IIA exit can be acutely provoked within 5 minutes (**Figure 21C**). Glutamate receptor dynamics on such a time scale were previously unknown at the *Drosophila* NMJ. These kinetics are reminiscent of fast glutamate receptor dynamics observed in mammals, which can even operate on time scales of minutes and well below (Heine et al., 2008; Lüscher et al., 1999; Tovar and Westbrook, 2002). However, they are concealed in time lapse imaging of live synapses in *Drosophila* during development *in vivo* because both removal and growth take place at the same time, while growth is the net direction observed during development (Rasse et al., 2005; Schmid et al., 2008). When one of the processes is accentuated like in 'Pre & Post' Hebbian growth of IIA receptor fields or electrical activity-induced removal of IIA, the speed of glutamate receptor kinetics at the NMJ come to light.

Taken together these considerations support the idea, that mechanisms of synaptic plasticity have been conserved during evolution (Glanzman, 2010).

6.4 Weak light-stimulation-induced plasticity

As expected, weak photo-stimulation of 'Pre' animals did not lead to strong changes in the electrophysiological footprint. The only parameter that changed in larvae stimulated with the weak lamp was a slightly, but significantly increased amplitude of minis, without influencing the quantal content (Supplemental data **Table 1**.). This

result is consistent with a previous publication, where ChR2 stimulation leads to a similar effect (Ataman et al., 2008). We hypothesise that Ataman and colleagues used a similarly low irradiance to induce photo-stimulation.

In the present work, the used 40 μW/mm² LED did not evoke visible muscle contractions; no APs seem to reach the muscle. Therefore, the stimulatory effect seems to take place at the cell soma and has to be transported to the synapse, since bigger mini amplitudes were observed. On the other hand it can be envisaged, that some APs reach the postsynapse if larvae are stimulated *in vivo*, without causing a visible contraction. The higher level of ambient glutamate in the haemolymph *in vivo* and therefore a higher level of postsynaptic receptor desensitization (Augustin et al., 2007) (Chen et al., 2009) might explain the missing contraction upon weak blue light stimulation. Taken together, attempts to find a mechanism at the present level of insight would be of a highly speculative nature.

Since neither contraction was seen, nor lEJCs were detected in the semi-intact preparation upon weak light stimulation, a much stronger LED (1.7 mW/mm²) was used for all other plasticity-inducing experiments. This irradiance caused both contractions in the free moving larva and lEJCs in the semi-intact preparation.

6.5 Level of activity determines presynaptic depression

In addition to the Hebbian mechanism of GluR-IIA incorporation in 'Pre and Post' animals, all three genotypes showed a strong depression, manifested in a heavily reduced quantal content, i.e. the number of released vesicles upon AP-like stimulation (**Figure 14B**).

In 'Pre' larvae, repeated light-induced neurotransmitter release from presynapses lead to depression (**Figure 14B**; Supplemental data **Table 2**). This was surprising at first, since 'Pre' stimulation lead to AP frequencies around 4 Hz. During breaks in the light-stimulation protocol, the larvae are allowed to crawl in the arena and

motoneurons most probably fire at higher AP rates. Budnik and colleagues show AP frequencies around 30 Hz (Budnik et al., 1990). In personal communication Prof. Chun-Fang Wu, an expert for "en passant" recordings of APs form motoneuron nerves, stated that: " [...] However, we do know they [motoneurons] can sustain maximum firing at a 7-8 millisecond inter-spike intervals (i.e. over 100 Hz). These are based on en passant recordings of spontaneous firings in mutants or wildtypes. [...]". However, motoneurons may fire at much higher rates when stimulated via ChR2 *in vivo* and do not necessarily move all the time during breaks.

The quantal content reduction after 'Pre' light stimulation also cannot be explained by an unspecific effect of RAL presence, since the same RAL concentration was used for larvae in the weak light stimulation experiment, where it did not lead to a quantal content reduction (Supplemental data **Table 1**).

Interestingly, the level of presynaptic activity seems to determine the extent of presynaptically induced depression, since no depression occurred with weak light stimulation. Analogously, short light pulse stimulation, in contrast to long pulse stimulation in 'Pre & Post' animals did not induce a quantal content change (**Figure 18D** versus **Figure 14D**). Although in 'Pre & Post' light-stimulation the mechanism of quantal content reduction may well be of different origin.

Taken together the present data indicate that the level of presynaptic activity determines the extent of synaptic depression. Correspondingly, results from Guo and colleagues showed that LTD in semi-intact preparation, which also works via a quantal content decrease, scaled with the frequency of electrical tetanic nerve stimulation (Guo and Zhong, 2006).

6.6 Retrograde signalling

The measured postsynaptic steady state current triggered by a 1.7 mW/mm² light-stimulation in 'Post' animals was surprisingly low, around -0.6 nA. For muscle 6, the

typical membrane resistance for a well-dissected animal is between 6 and 13 MΩ, which would result in a steady state depolarisation of only 3.6-7.8 mV, which does not sound like a lot. Stimulation of living, moving larvae by the same light however, triggers strong muscle contraction. This might be due to the fact that, *in vivo,* the membrane resistance is higher than measured in TEVC configuration (the cell is impaled by two electrodes), which would lead to a higher depolarisation. It is plausible that, for the Ca^{++}-dependent mechanism of muscle contraction, the prolonged influx of cations (2 s) is sufficient to trigger contraction, even at low amplitude. Such prolonged depolarisations should not occur during natural AP triggered locomotion.

Interestingly, 'Post' photo-stimulation also led to a reduction in quantal content, although postsynaptic depolarisation was evoked independently of synaptic transmission (**Figure 14B**). This strongly suggests a retrograde signal, which is triggered by the postsynapse to influence presynaptic neurotransmitter release properties.

Such a mechanism is reminiscent of homeostatic retrograde signalling of inverted polarity, which has been extensively studied at the *Drosophila* NMJ (Davis, 2006; Petersen et al., 1997). There, a retrograde pathway is activated to increase quantal content, responding to a reduction in muscle excitability. This homeostatic pathway can be triggered by chronically hyperpolarising muscles through over-expression of potassium channels (Paradis et al., 2001), by blocking postsynaptic GluR channels with philanthotoxin-433 (Frank et al., 2006), an insect glutamate receptor antagonist purified from wasp venom (Eldefrawi et al., 1988; Karst and Piek, 1991), or by overexpression of a dominant negative pore mutant of DGluRIIA which leads to a decreased mini size (DiAntonio et al., 1999).

It is possible that the 'Post' light-stimulation protocol employed in the present study triggers a related retrograde pathway of inverted polarity. However, we did not find a molecular correlate for this change (**Figure 15**). With help of STED microscopy it was shown that BRP rearrangements at the level of single active zones are involved

in homeostatic retrograde signalling following the blockade of glutamate receptors (Weyhersmüller et al., 2011). In this work, however, no hints towards an involvement of this protein were observed at confocal resolution. Here, super resolution techniques like *direct* Stochastic Optical Reconstruction Microscopy, *d*STORM, (Heilemann et al., 2008; van de Linde et al., 2011) might help to clarify that point.

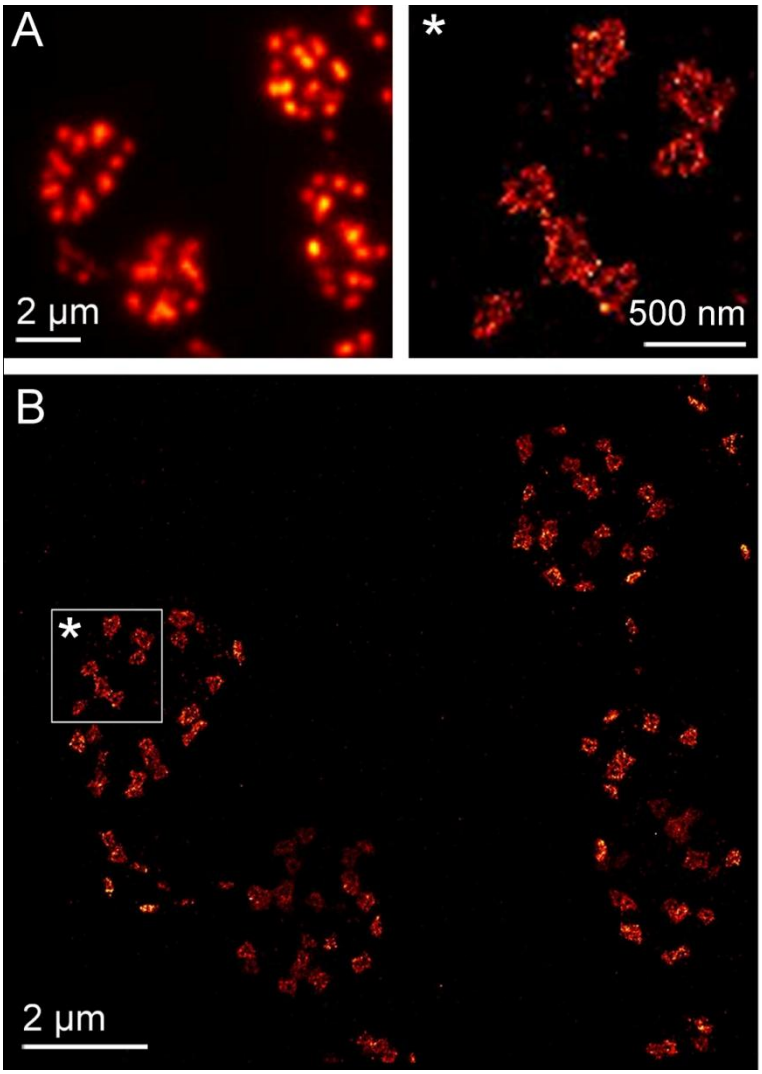

Figure 22 Comparison between epifluorescence and *d*STORM image of Bruchpilot. (A) While in an epifluorescence image the BRP spots are visible as diffraction limited spots only, (B) the sub diffraction distribution of BRP epitopes (same area enlarged) is discernible in the *d*STORM image. Asterisk marks zoomed area (white rectangle). (Ehmann et. al., submitted, see Appendix)

To illustrate the power of this technique, a comparison between an epifluorescence image and a *d*STORM image of nc82 labelled larvae is shown in **Figure 22** (nc82 stains the C-terminal part of BRP; Fouquet et al., 2009; Hofbauer et al., 2009). With its explicit single molecule resolution, it is possible to count the number of BRP molecules present in one active zone (Ehmann et. al., submitted, see Appendix) and maybe, thus, find a structural correlate of homeostatic effects on the presynaptic side. It would also be of interest to test whether the molecular players, which are involved in homeostatic upregulation of release (Dickman and Davis, 2009), are also involved in the opposite pathway, observed in the present study.

7. Supplemental data

'Pre' weak lamp	Control	RAL	P value t-test/ rs-test
mini amplitude	0.74 ± 0.05	0.81 ± 0.03	n.a.
	(11)	(13)	0.040
mini rise time	1.12 ± 0.09	1.05 ± 0.02	n.a.
	(11)	(13)	0.724
mini decay τ	6.15 ± 0.26	6.04 ± 0.19	0.737
	(11)	(11)	0.451
mini frequency	1.18 ± 0.12	1.33 ± 0.08	0.286
	(11)	(13)	0.235
eEJC amplitude	66.9 ± 4.5	59.5 ± 4.4	0.256
	(9)	(10)	0.236
eEJC rise time	1.03 ± 0.08	0.89 ± 0.04	n.a.
	(9)	(10)	0.067
eEJC decay τ	5.26 ± 0.26	5.36 ± 0.13	n.a.
	(9)	(10)	0.775
quantal content	122 ± 11	98 ± 9	0.107
	(9)	(10)	0.131
paired pulse ratio	1.17 ± 0.05	1.25 ± 0.04	0.243
	(9)	(10)	0.307

Table 1 Electrophysiological quantification of synaptic currents after weak light-stimulation of 'Pre' larvae. Amplitude (-nA), rise-time (ms), decay τ (ms), of minis and eEJCs, additionally mini frequency (s^{-1}), quantal content and paired pulse ratios from TEVC recordings in larvae (muscle 6, segments A2 and A3), raised under standard conditions and subjected to the standard photo-stimulation protocol with the weak LED lamp (40 $\mu W/mm^2$ at 460 nm). The values are presented as mean ± sem, the number of averaged NMJs is shown in brackets. Statistical comparisons were performed with the t-test and the rank sum test (rs-test). n.a. indicates the non-applicability of the t-test due to non-normal distribution of data or different variabilities between the two groups.

	'Pre'			**'Post'**			**'Pre & Post'**		
	Control	RAL	P value t-test/ rs-test	Control	RAL	P value t-test/ rs-test	Control	RAL	P value t-test/ rs-test
mini amplitude	0.83 ± 0.02 (13)	0.82 ± 0.04 (14)	n.a. 0.356	0.85 ± 0.03 (11)	0.91 ± 0.04 (11)	0.214 0.324	0.59 ± 0.02 (11)	0.65 ± 0.03 (11)	0.090 0.131
mini charge	8.33 ± 0.43 (13)	8.05 ± 0.68 (14)	0.739 0.396	7.56 ± 0.24 (11)	8.99 ± 0.95 (11)	n.a. 0.470	3.87 ± 0.33 (11)	6.13 ± 0.58 (11)	n.a. 0.009
mini rise-time	1.08 ± 0.025 (13)	1.04 ±0.033 (14)	0.325 0.476	0.95 ± 0.03 (11)	0.97 ± 0.040 (11)	0.601 0.730	1.06 ± 0.04 (11)	1.14 ± 0.03 (11)	0.103 0.110
mini decay τ	6.55 ± 0.18 (13)	6.39 ± 0.20 (14)	0.570 0.216	6.05 ± 0.13 (11)	6.50 ± 0.25 (11)	n.a. 0.293	4.72 ± 0.40 (11)	6.05 ± 0.42 (11)	n.a. 0.010
mini frequency	1.56 ±0.18 (13)	1.73 ± 0.19 (14)	n.a. 0.662	2.24 ± 0.17 (11)	1.97 ± 0.24 (11)	0.367 0.358	1.48 ± 0.20 (11)	1.85 ± 0.23 (11)	0.235 0.293

	'Pre'			'Post'			'Pre & Post'		
	Control	RAL	P value t-test/ rs-test	Control	RAL	P value t-test/ rs-test	Control	RAL	P value t-test/ rs-test
eEJC amplitude	73.9 ± 8.4 (10)	46.9 ± 6.7 (10)	0.022 0.017	67.8 ± 4.6 (11)	50.7 ± 4.0 (11)	0.012 0.018	69.9 ± 4.7 (11)	58.5 ± 8.0 (10)	0.224 0.062
eEJC charge	754 ± 77 (10)	445 ± 61 (10)	0.006 0.005	631 ± 63 (11)	458 ± 40 (11)	n.a. 0.018	483 ± 52 (11)	514 ± 67 (10)	n.a. 0.504
eEJC rise-time	1.03 ± 0.05 (10)	0.98 ± 0.07 (10)	0.560 0.439	0.76 ± 0.03 (11)	0.87 ± 0.04 (11)	n.a. 0.014	0.93 ± 0.06 (11)	1.01 ± 0.05 (10)	n.a. 0.208
eEJC decay τ	5.66 ± 0.17 (10)	5.37 ± 0.15 (10)	0.205 0.140	5.76 ± 0.85 (11)	5.06 ± 0.15 (11)	n.a. 0.948	3.87 ± 0.23 (11)	5.08 ± 0.32 (10)	0.006 0.007
quantal content	105±13 (10)	66±11 (10)	n.a. 0.021	98 ± 6 (11)	68 ± 6 (11)	0.002 0.004	150 ± 10 (11)	109 ± 13 (10)	0.020 0.027
paired-pulse ratio	1.27 ± 0.06 (10)	1.37 ± 0.06 (10)	0.233 0.273	1.16 ± 0.02 (11)	1.33 ± 0.04 (10)	0.001 0.002	1.16 ± 0.025 (9)	1.29 ± 0.06 (10)	n.a. 0.111

Table 2 Electrophysiological quantification of synaptic currents after standard photo-stimulation of three genotypes. Amplitude (-nA), charge (pC), rise-time (ms), decay τ (ms), of minis and eEJCs, additionally mini frequency (s^{-1}), quantal content and paired pulse ratios from TEVC recordings in larvae (muscle 6, segments A2 and A3), raised under standard conditions and subjected to the standard photo-stimulation protocol with the strong LED lamp (1.7 mW/mm^2 at 460 nm). The values are presented as mean ± sem, the number of averaged NMJs is shown in brackets. Statistical comparisons were performed with the t-test and the rank sum test (rs-test). n.a. indicates the non-applicability of the t-test due to non-normal distribution of data or different variabilities between the two groups. Adapted from (Ljaschenko et al., 2013).

	'Pre'			'Post'			'Pre & Post'		
	Control	RAL	P value t-test/ rs-test	Control	RAL	P value t-test/ rs-test	Control	RAL	P value t-test/ rs-test
BRP number	679 ± 55	681 ± 47	0.98	545±35	531±32	n.a.	812 ± 53	827 ± 60	0.86
	(11)	(11)	1	(8)	(10)	0.89	(12)	(12)	0.93
BRP area	0.248 ± 0.014	0.253 ± 0.010	0.766	0.303 ± 0.009	0.306 ± 0.006	0.829	0.263 ± 0.007	0.273±0.006	0.275
	(11)	(11)	0.844	(8)	(10)	0.965	(12)	(12)	0.285
GluR-IID	638 ± 49	743 ± 98	n.a.	525 ± 43	472 ± 33	n.a.	650 ± 42	697 ± 57	0.509
number	(11)	(11)	0.743	(7)	(10)	0.223	(12)	(12)	0.707
GluR-IID area	0.343 ± 0.024	0.308 ± 0.035	0.416	0.431 ± 0.024	0.432 ± 0.012	0.966	0.272 ± 0.010	0.306 ± 0.021	0.175
	(11)	(11)	0.694	(7)	(10)	0.961	(12)	(12)	0.148
HRP area	746 ± 48	699 ± 77	0.494	487 ± 49	431 ± 32	0.334	723 ± 56	803 ± 70	0.410
	(11)	(11)	0.293	(7)	(10)	0.407	(9)	(12)	0.546

Table 3 Immunohistochemical quantification of synaptic structure with major synaptic markers (BRP, GluR-IID and HRP). Maximum projections of confocal stacks of muscle 6/7 NMJs in segments A2 and A3 were analysed. 3rd instar larvae were raised under standard conditions and subjected to the standard light-stimulation protocol with the strong LED (1.7 mW/mm² at 460 nm). The values are given as mean ± sem, number of averaged NMJs are shown in brackets. The areas are given in µm². Statistical comparisons were performed with the t-test and the rank sum test (rs-test). n.a. indicates the non-applicability of the t-test due to non-normal distribution of data or different variabilities between the two groups. (Ljaschenko et al., 2013).

'Pre & Post' short pulses	control	RAL	P value t-test/ rs-test
mini amplitude	0.73 ± 0.03	0.69 ± 0.034	0.290
	(13)	(12)	0.253
mini rise time	1.12 ± 0.047	1.16 ± 0.08	n.a.
	(13)	(12)	0.760
mini decay τ	7.24 ± 0.22	7.63 ± 0.15	n.a.
	(13)	(12)	0.201
mini frequency	0.87 ± 0.12	0.92 ± 0.11	0.797
	(13)	(12)	0.913
eEJC amplitude	74.8 ± 7.8	64.3 ± 7.2	0.335
	(12)	(12)	0.403
eEJC rise time	1.18 ± 0.06	1.10 ± 0.07	n.a.
	(12)	(12)	0.279
eEJC decay τ	6.54 ± 0.24	6.741 ± 0.15	0.492
	(12)	(12)	0.371
quantal content	135 ± 13	127 ± 14	0.650
	(12)	(12)	0.624
paired pulse ratio	1.23 ± 0.04	1.27 ± 0.05	0.538
	(12)	(12)	0.624

Table 4 Electrophysiological quantification of synaptic currents after short light pulse stimulation of 'Pre & Post' larvae. Amplitude (-nA), rise-time (ms), decay τ (ms), of minis and eEJCs, additionally mini frequency (s^{-1}), quantal content and paired pulse ratios from TEVC recordings in larvae (muscle 6, segments A2 and A3), raised under enhanced expression conditions and subjected to the short pulse photo-stimulation protocol with the strong LED lamp (1.7 mW/mm^2 at 460 nm). The values are presented as mean ± sem, the number of averaged NMJs is shown in brackets. Statistical comparisons were performed with the t-test and the rank sum test (rs-test). n.a. indicates the non-applicability of the t-test due to non-normal distribution of data or different variabilities between the two groups.

8. References

Abbott, L.F., and Nelson, S.B. (2000). Synaptic plasticity: taming the beast. Nat Neurosci 3, 1178-1183.

Adams, F. (1849). The genuine works of Hippocrates (London: printers C. and J. Adlard, printed for the Sydenham society).

Adams, M.D., Celniker, S.E., Holt, R.A., Evans, C.A., Gocayne, J.D., Amanatides, P.G., Scherer, S.E., Li, P.W., Hoskins, R.A., Galle, R.F*., et al.* (2000). The genome sequence of *Drosophila melanogaster*. Science 287, 2185-2195.

Antonov, I., Antonova, I., Kandel, E.R., and Hawkins, R.D. (2003). Activity-dependent presynaptic facilitation and hebbian LTP are both required and interact during classical conditioning in *Aplysia*. Neuron 37, 135-147.

Arshavsky, Y.I. (2006). "The seven sins" of the Hebbian synapse: can the hypothesis of synaptic plasticity explain long-term memory consolidation? Prog Neurobiol 80, 99-113.

Ashburner, M., Golic, K.G., and Hawley, S.R. (2005). Life cycle. In *Drosophila* a laboratory manual (New York: Cold Spring Harbor Laborytory Press).

Ashburner, M., and Roote, J. (2007). Culture of *Drosophila*: the laboratory setup. CSH protocols 2007, pdb ip34.

Aszodi, A., Muller, U., Friedrich, P., and Spatz, H.C. (1991). Signal convergence on protein kinase A as a molecular correlate of learning. Proc Natl Acad Sci USA 88, 5832-5836.

Ataman, B., Ashley, J., Gorczyca, M., Ramachandran, P., Fouquet, W., Sigrist, S.J., and Budnik, V. (2008). Rapid activity-dependent modifications in synaptic structure and function require bidirectional Wnt signaling. Neuron 57, 705-718.

Atwood, H.L., Govind, C.K., and Wu, C.F. (1993). Differential ultrastructure of synaptic terminals on ventral longitudinal abdominal muscles in *Drosophila* larvae. J Neurobiol 24, 1008-1024.

Atwood, H.L., and Wojtowicz, J.M. (1999). Silent synapses in neural plasticity: current evidence. Learn Mem 6, 542-571.

Augustin, H., Grosjean, Y., Chen, K., Sheng, Q., and Featherstone, D.E. (2007). Nonvesicular release of glutamate by glial xCT transporters suppresses glutamate receptor clustering *in vivo*. J Neurosci 27, 111-123.

Bailey, C.H., and Chen, M. (1988). Long-term sensitization in *Aplysia* increases the number of presynaptic contacts onto the identified gill motor neuron L7. Proc Natl Acad Sci USA 85, 9356-9359.

Bear, M.F., Connors, B.W., and Paradiso, M.A. (2007a). Memory Systems. In Neuroscience exploring the brain (Baltimore: Lippincott Williams & Willkins).

Bear, M.F., Connors, B.W., and Paradiso, M.A. (2007b). Synaptic Transmission. In Neuroscience exploring the brain (Baltimore: Lippincott Willams & Willkins).

Bellen, H.J., Tong, C., and Tsuda, H. (2010). 100 years of *Drosophila* research and its impact on vertebrate neuroscience: a history lesson for the future. Nat Rev Neurosci 11, 514-522.

Beumer, K., Matthies, H.J., Bradshaw, A., and Broadie, K. (2002). Integrins regulate DLG/FAS2 via a CaM kinase II-dependent pathway to mediate synapse elaboration and stabilization during postembryonic development. Development 129, 3381-3391.

Bliss, T.V., and Lømo, T. (1973). Long-lasting potentiation of synaptic transmission in the dentate area of the anaesthetized rabbit following stimulation of the perforant path. J Physiol 232, 331-356.

Borst, J.G. (2010). The low synaptic release probability *in vivo*. Trends Neurosci 33, 259-266.

Brand, A.H., and Perrimon, N. (1993). Targeted gene expression as a means of altering cell fates and generating dominant phenotypes. Development 118, 401-415.

Bucher, D., and Buchner, E. (2009). Stimulating PACalpha increases miniature excitatory junction potential frequency at the *Drosophila* neuromuscular junction. J Neurogenet 23, 220-224.

Budnik, V., and Ruiz-Canada, C. (2006). The Fly Neuromuscular Junction: Structure and Function, Vol 75 (San Diego: Elsevier).

Budnik, V., Zhong, Y., and Wu, C.F. (1990). Morphological plasticity of motor axons in *Drosophila* mutants with altered excitability. J Neurosci 10, 3754-3768.

Burrell, B.D., and Sahley, C.L. (2004). Multiple forms of long-term potentiation and long-term depression converge on a single interneuron in the leech CNS. J Neurosci 24, 4011-4019.

Byrne, J.H., and Kandel, E.R. (1996). Presynaptic facilitation revisited: state and time dependence. J Neurosci 16, 425-435.

Cai, D., Chen, S., and Glanzman, D.L. (2008). Postsynaptic regulation of long-term facilitation in *Aplysia*. Curr Biol 18, 920-925.

Castellucci, V., Pinsker, H., Kupfermann, I., and Kandel, E.R. (1970). Neuronal mechanisms of habituation and dishabituation of the gill-withdrawal reflex in *Aplysia*. Science 167, 1745-1748.

Castellucci, V.F., and Kandel, E.R. (1974). A quantal analysis of the synaptic depression underlying habituation of the gill-withdrawal reflex in *Aplysia*. Proc Natl Acad Sci USA 71, 5004-5008.

Chen, K., Augustin, H., and Featherstone, D.E. (2009). Effect of ambient extracellular glutamate on *Drosophila* glutamate receptor trafficking and function. Journal of comparative physiology A, Neuroethology, sensory, neural, and behavioral physiology 195, 21-29.

Clegg, D.O., Wingerd, K.L., Hikita, S.T., and Tolhurst, E.C. (2003). Integrins in the development, function and dysfunction of the nervous system. Frontiers in bioscience : a journal and virtual library 8, d723-750.

Contractor, A., Rogers, C., Maron, C., Henkemeyer, M., Swanson, G.T., and Heinemann, S.F. (2002). Trans-synaptic Eph receptor-ephrin signaling in hippocampal mossy fiber LTP. Science 296, 1864-1869.

Corkin, S., Amaral, D.G., Gonzalez, R.G., Johnson, K.A., and Hyman, B.T. (1997). H. M.'s medial temporal lobe lesion: findings from magnetic resonance imaging. J Neurosci 17, 3964-3979.

Dash, P.K., Hochner, B., and Kandel, E.R. (1990). Injection of the cAMP-responsive element into the nucleus of *Aplysia* sensory neurons blocks long-term facilitation. Nature 345, 718-721.

Davis, G.W. (2006). Homeostatic control of neural activity: from phenomenology to molecular design. Annu Rev Neurosci 29, 307-323.

Davis, R.L. (2005). Olfactory memory formation in *Drosophila*: from molecular to systems neuroscience. Annu Rev Neurosci 28, 275-302.

DiAntonio, A., Petersen, S.A., Heckmann, M., and Goodman, C.S. (1999). Glutamate receptor expression regulates quantal size and quantal content at the *Drosophila* neuromuscular junction. J Neurosci 19, 3023-3032.

Dickman, D.K., and Davis, G.W. (2009). The schizophrenia susceptibility gene dysbindin controls synaptic homeostasis. Science 326, 1127-1130.

Drain, P., Folkers, E., and Quinn, W.G. (1991). cAMP-dependent protein kinase and the disruption of learning in transgenic flies. Neuron 6, 71-82.

Eldefrawi, A.T., Eldefrawi, M.E., Konno, K., Mansour, N.A., Nakanishi, K., Oltz, E., and Usherwood, P.N. (1988). Structure and synthesis of a potent glutamate receptor antagonist in wasp venom. Proc Natl Acad Sci USA 85, 4910-4913.

Featherstone, D., and Broadie, K. (2002). Response: meaningless minis? Trends Neurosci 25, 386-387.

Featherstone, D.E., Rushton, E., Rohrbough, J., Liebl, F., Karr, J., Sheng, Q., Rodesch, C.K., and Broadie, K. (2005). An essential *Drosophila* glutamate receptor subunit that functions in both central neuropil and neuromuscular junction. J Neurosci 25, 3199-3208.

Feeney, C.J., Karunanithi, S., Pearce, J., Govind, C.K., and Atwood, H.L. (1998). Motor nerve terminals on abdominal muscles in larval flesh flies, Sarcophaga bullata: comparisons with *Drosophila*. J Comp Neurol 402, 197-209.

Feldman, D.E. (2012). The spike-timing dependence of plasticity. Neuron 75, 556-571.

Feng, Y., Ueda, A., and Wu, C.F. (2004). A modified minimal hemolymph-like solution, HL3.1, for physiological recordings at the neuromuscular junctions of normal and mutant *Drosophila* larvae. J Neurogenet 18, 377-402.

Foster M., S.C.S. (1897). A text book of Physiology Part III, Vol 3, 7 edn (London: MacMillan and co., Limited).

Fouquet, W., Owald, D., Wichmann, C., Mertel, S., Depner, H., Dyba, M., Hallermann, S., Kittel, R.J., Eimer, S., and Sigrist, S.J. (2009). Maturation of active zone assembly by *Drosophila* Bruchpilot. J Cell Biol 186, 129-145.

Frank, C.A., Kennedy, M.J., Goold, C.P., Marek, K.W., and Davis, G.W. (2006). Mechanisms underlying the rapid induction and sustained expression of synaptic homeostasis. Neuron 52, 663-677.

Glanzman, D.L. (2010). Common mechanisms of synaptic plasticity in vertebrates and invertebrates. Curr Biol 20, R31-36.

Glanzman, D.L., Kandel, E.R., and Schacher, S. (1990). Target-dependent structural changes accompanying long-term synaptic facilitation in *Aplysia* neurons. Science 249, 799-802.

Grutzendler, J., Kasthuri, N., and Gan, W.B. (2002). Long-term dendritic spine stability in the adult cortex. Nature 420, 812-816.

Guo, H.F., and Zhong, Y. (2006). Requirement of Akt to mediate long-term synaptic depression in *Drosophila*. J Neurosci 26, 4004-4014.

Hallermann, S., Heckmann, M., and Kittel, R.J. (2010a). Mechanisms of short-term plasticity at neuromuscular active zones of *Drosophila*. HFSP journal 4, 72-84.

Hallermann, S., Kittel, R.J., Wichmann, C., Weyhersmuller, A., Fouquet, W., Mertel, S., Owald, D., Eimer, S., Depner, H., Schwarzel, M.*, et al.* (2010b). Naked Dense Bodies Provoke Depression. J Neurosci 30, 14340-14345.

Hawkins, R.D., Abrams, T.W., Carew, T.J., and Kandel, E.R. (1983). A cellular mechanism of classical conditioning in *Aplysia*: activity-dependent amplification of presynaptic facilitation. Science 219, 400-405.

Hebb, D.O. (1949). The organization of behavior. (New York: John Wiley & Sons Inc).

Heilemann, M., van de Linde, S., Schuttpelz, M., Kasper, R., Seefeldt, B., Mukherjee, A., Tinnefeld, P., and Sauer, M. (2008). Subdiffraction-resolution fluorescence imaging with conventional fluorescent probes. Angew Chem Int Ed Engl 47, 6172-6176.

Heine, M., Groc, L., Frischknecht, R., Beique, J.C., Lounis, B., Rumbaugh, G., Huganir, R.L., Cognet, L., and Choquet, D. (2008). Surface mobility of postsynaptic AMPARs tunes synaptic transmission. Science 320, 201-205.

Hertweck, H. (1931). Anatomie und Variabilität des Nervensystems und er Sinnesorgane von *Drosophila melanogaster*. Zeitschrift für wissenschaftliche Zoologie 139, 559-663.

Hille, B. (2001). Ligand-gated channels of fast chemical synapses. In Ion channels of excitable membranes, B. Hille, ed. (Sunderland: Sinauer).

Hoang, B., and Chiba, A. (2001). Single-cell analysis of *Drosophila* larval neuromuscular synapses. Dev Biol 229, 55-70.

Hochner, B., Brown, E.R., Langella, M., Shomrat, T., and Fiorito, G. (2003). A learning and memory area in the *Octopus* brain manifests a vertebrate-like long-term potentiation. J Neurophysiol 90, 3547-3554.

Hofbauer, A., Ebel, T., Waltenspiel, B., Oswald, P., Chen, Y.C., Halder, P., Biskup, S., Lewandrowski, U., Winkler, C., Sickmann, A.*, et al.* (2009). The Wuerzburg hybridoma library against *Drosophila* brain. J Neurogenet 23, 78-91.

Hormuzdi, S.G., Filippov, M.A., Mitropoulou, G., Monyer, H., and Bruzzone, R. (2004). Electrical synapses: a dynamic signaling system that shapes the activity of neuronal networks. Biochim Biophys Acta 1662, 113-137.

Inaki, M., Shinza-Kameda, M., Ismat, A., Frasch, M., and Nose, A. (2010). *Drosophila* Tey represses transcription of the repulsive cue Toll and generates neuromuscular target specificity. Development 137, 2139-2146.

Jahn, R., and Fasshauer, D. (2012). Molecular machines governing exocytosis of synaptic vesicles. Nature 490, 201-207.

Jan, L.Y., and Jan, Y.N. (1976a). L-glutamate as an excitatory transmitter at the *Drosophila* larval neuromuscular junction. The Journal of physiology 262, 215-236.

Jan, L.Y., and Jan, Y.N. (1976b). Properties of the larval neuromuscular junction in *Drosophila melanogaster*. The Journal of physiology 262, 189-214.

Jan, L.Y., and Jan, Y.N. (1982). Antibodies to horseradish peroxidase as specific neuronal markers in *Drosophila* and in grasshopper embryos. Proc Natl Acad Sci USA 79, 2700-2704.

Kandel, E.R. (2001). The molecular biology of memory storage: a dialogue between genes and synapses. Science 294, 1030-1038.

Kandel, E.R., and Siegelbaum, S.L. (2012). Cellular mechanisms of implicit memory storage and the biological basis of individuality. In Principles of neural science, E.R. Kandel, J.H. Schwartz, T.M. Jessell, S.L. Siegelbaum, and A.J. Hudspeth, eds. (Mcgraw-Hill Professional).

Kano, T., Brockie, P.J., Sassa, T., Fujimoto, H., Kawahara, Y., Iino, Y., Mellem, J.E., Madsen, D.M., Hosono, R., and Maricq, A.V. (2008). Memory in *Caenorhabditis elegans* is mediated by NMDA-type ionotropic glutamate receptors. Curr Biol 18, 1010-1015.

Karst, H., and Piek, T. (1991). Structure-activity relationship of philanthotoxins--II. Effects on the glutamate gated ion channels of the locust muscle fibre membrane. Comparative biochemistry and physiology C, Comparative pharmacology and toxicology 98, 479-489.

Kennedy, M.B. (1997). The postsynaptic density at glutamatergic synapses. Trends Neurosci 20, 264-268.

Kessels, H.W., and Malinow, R. (2009). Synaptic AMPA receptor plasticity and behavior. Neuron 61, 340-350.

Kittel, R.J., Wichmann, C., Rasse, T.M., Fouquet, W., Schmidt, M., Schmid, A., Wagh, D.A., Pawlu, C., Kellner, R.R., Willig, K.I.*, et al.* (2006). Bruchpilot promotes active zone assembly, Ca2+ channel clustering, and vesicle release. Science 312, 1051-1054.

Koh, Y.H., Popova, E., Thomas, U., Griffith, L.C., and Budnik, V. (1999). Regulation of DLG localization at synapses by CaMKII-dependent phosphorylation. Cell 98, 353-363.

Koon, A.C., Ashley, J., Barria, R., DasGupta, S., Brain, R., Waddell, S., Alkema, M.J., and Budnik, V. (2011). Autoregulatory and paracrine control of synaptic and behavioral plasticity by octopaminergic signaling. Nat Neurosci 14, 190-199.

Krueger, S., and Fitzsimonds, R.M. (2006). Remodeling the plasticity debate: the presynaptic locus revisited. Physiology (Bethesda) 21, 346-351.

Lahey, T., Gorczyca, M., Jia, X.X., and Budnik, V. (1994). The *Drosophila* tumor suppressor gene dlg is required for normal synaptic bouton structure. Neuron 13, 823-835.

Li, H.L., Huang, B.S., Vishwasrao, H., Sutedja, N., Chen, W., Jin, I., Hawkins, R.D., Bailey, C.H., and Kandel, E.R. (2009). Dscam mediates remodeling of glutamate receptors in *Aplysia* during de novo and learning-related synapse formation. Neuron 61, 527-540.

Li, Q., Roberts, A.C., and Glanzman, D.L. (2005). Synaptic facilitation and behavioral dishabituation in *Aplysia*: dependence on release of Ca2+ from postsynaptic intracellular stores, postsynaptic exocytosis, and modulation of postsynaptic AMPA receptor efficacy. J Neurosci 25, 5623-5637.

Li, W., Tully, T., and Kalderon, D. (1996). Effects of a conditional *Drosophila* PKA mutant on olfactory learning and memory. Learn Mem 2, 320-333.

Lin, X.Y., and Glanzman, D.L. (1994). Hebbian induction of long-term potentiation of *Aplysia* sensorimotor synapses: partial requirement for activation of an NMDA-related receptor. Proceedings Biological sciences / The Royal Society 255, 215-221.

Ljaschenko, D., Ehmann, N., and Kittel, R.J. (2013). Hebbian plasticity guides maturation of glutamate receptor fields *in vivo*. Cell Reports 3, 1407-13.

Lüscher, C., Xia, H., Beattie, E.C., Carroll, R.C., von Zastrow, M., Malenka, R.C., and Nicoll, R.A. (1999). Role of AMPA receptor cycling in synaptic transmission and plasticity. Neuron 24, 649-658.

Malenka, R.C., and Bear, M.F. (2004). LTP and LTD: an embarrassment of riches. Neuron 44, 5-21.

Marrus, S.B., and DiAntonio, A. (2004). Preferential localization of glutamate receptors opposite sites of high presynaptic release. Curr Biol 14, 924-931.

Marrus, S.B., Portman, S.L., Allen, M.J., Moffat, K.G., and DiAntonio, A. (2004). Differential localization of glutamate receptor subunits at the *Drosophila* neuromuscular junction. J Neurosci 24, 1406-1415.

Martens, S., and McMahon, H.T. (2008). Mechanisms of membrane fusion: disparate players and common principles. Nat Rev Mol Cell Biol 9, 543-556.

Menzel, R., and Manz, G. (2005). Neural plasticity of mushroom body-extrinsic neurons in the honeybee brain. J Exp Biol 208, 4317-4332.

Montarolo, P.G., Goelet, P., Castellucci, V.F., Morgan, J., Kandel, E.R., and Schacher, S. (1986). A critical period for macromolecular synthesis in long-term heterosynaptic facilitation in *Aplysia*. Science 234, 1249-1254.

Murphy, G.G., and Glanzman, D.L. (1997). Mediation of classical conditioning in *Aplysia californica* by long-term potentiation of sensorimotor synapses. Science 278, 467-471.

Nagel, G., Szellas, T., Huhn, W., Kateriya, S., Adeishvili, N., Berthold, P., Ollig, D., Hegemann, P., and Bamberg, E. (2003). Channelrhodopsin-2, a directly light-gated cation-selective membrane channel. Proc Natl Acad Sci USA 100, 13940-13945.

Nusslein-Volhard, C., and Wieschaus, E. (1980). Mutations affecting segment number and polarity in *Drosophila*. Nature 287, 795-801.

O'Kane, C.J., and Gehring, W.J. (1987). Detection in situ of genomic regulatory elements in *Drosophila*. Proc Natl Acad Sci USA 84, 9123-9127.

Osborne, M.P. (1967). The fine structure of neuromuscular junctions in the segmental muscles of the blowfly larva. J Insect Physiol 13, 827-833.

Paradis, S., Sweeney, S.T., and Davis, G.W. (2001). Homeostatic control of presynaptic release is triggered by postsynaptic membrane depolarization. Neuron 30, 737-749.

Pavlov, I., Petrovich (1927). Conditional Reflexes. (New York: Dover Publications).

Pawlu, C., DiAntonio, A., and Heckmann, M. (2004). Postfusional control of quantal current shape. Neuron 42, 607-618.

Peled, E.S., and Isacoff, E.Y. (2011). Optical quantal analysis of synaptic transmission in wild-type and rab3-mutant *Drosophila* motor axons. Nat Neurosci 14, 519-526.

Petersen, S.A., Fetter, R.D., Noordermeer, J.N., Goodman, C.S., and DiAntonio, A. (1997). Genetic analysis of glutamate receptors in *Drosophila* reveals a retrograde signal regulating presynaptic transmitter release. Neuron 19, 1237-1248.

Prokop, A. (1999). Integrating bits and pieces: synapse structure and formation in *Drosophila* embryos. Cell Tissue Res 297, 169-186.

Qin, G., Schwarz, T., Kittel, R.J., Schmid, A., Rasse, T.M., Kappei, D., Ponimaskin, E., Heckmann, M., and Sigrist, S.J. (2005). Four different subunits are essential for expressing the synaptic glutamate receptor at neuromuscular junctions of *Drosophila*. J Neurosci 25, 3209-3218.

Rasse, T.M., Fouquet, W., Schmid, A., Kittel, R.J., Mertel, S., Sigrist, C.B., Schmidt, M., Guzman, A., Merino, C., Qin, G.*, et al.* (2005). Glutamate receptor dynamics organizing synapse formation *in vivo*. Nat Neurosci 8, 898-905.

Regehr, W.G., Carey, M.R., and Best, A.R. (2009). Activity-dependent regulation of synapses by retrograde messengers. Neuron 63, 154-170.

Rose, J.K., Kaun, K.R., Chen, S.H., and Rankin, C.H. (2003). GLR-1, a non-NMDA glutamate receptor homolog, is critical for long-term memory in *Caenorhabditis elegans*. J Neurosci 23, 9595-9599.

Royer, S., Coulson, R.L., and Klein, M. (2000). Switching off and on of synaptic sites at *Aplysia* sensorimotor synapses. J Neurosci 20, 626-638.

Saitoe, M., Schwarz, T.L., Umbach, J.A., Gundersen, C.B., and Kidokoro, Y. (2002). Response: meaningless minis? Trends Neurosci 25, 385-386.

Schacter, D.L., and Wagner, A.D. (2012). Learning and memory. In Principles of neural science, E.R. Kandel, J.H. Schwartz, T.M. Jessell, S.L. Siegelbaum, and A.J. Hudspeth, eds. (Mcgraw-Hill Professional).

Schmid, A., Hallermann, S., Kittel, R.J., Khorramshahi, O., Frölich, A.M., Quentin, C., Rasse, T.M., Mertel, S., Heckmann, M., and Sigrist, S.J. (2008). Activity-dependent site-specific changes of glutamate receptor composition *in vivo*. Nat Neurosci 11, 659-666.

Schmid, A., and Sigrist, S.J. (2008). Analysis of Neuromuscular Junctions. Histology and *In Vivo* Imaging. In Methods in molecular biology: *Drosophila*: Methods and Protocols, C. Dahmann, ed. (Totowa: Humana Press).

Schroll, C., Riemensperger, T., Bucher, D., Ehmer, J., Völler, T., Erbguth, K., Gerber, B., Hendel, T., Nagel, G., Buchner, E., and Fiala, A. (2006). Light-induced activation of distinct modulatory neurons triggers appetitive or aversive learning in *Drosophila* larvae. Curr Biol 16, 1741-1747.

Schuster, C.M. (2006). Experience-Dependent Potentiation of Larval Neuromuscular Synapses. In The Fly Neuromuscular Junction: Structure and Function V. Budnik, and C. Ruiz-Canada, eds. (San Diego: Elsevier).

Schuster, C.M., Davis, G.W., Fetter, R.D., and Goodman, C.S. (1996). Genetic dissection of structural and functional components of synaptic plasticity. II. Fasciclin II controls presynaptic structural plasticity. Neuron 17, 655-667.

Schuster, C.M., Ultsch, A., Schloss, P., Cox, J.A., Schmitt, B., and Betz, H. (1991). Molecular cloning of an invertebrate glutamate receptor subunit expressed in *Drosophila* muscle. Science 254, 112-114.

Schwartz, J.H., and Javitch, J.A. (2012). Neurotransmitters. In Principles of neural science, E.R. Kandel, J.H. Schwartz, T.M. Jessell, S.L. Siegelbaum, and A.J. Hudspeth, eds. (Mcgraw-Hill Professional).

Sejnowski, T.J. (1999). The book of Hebb. Neuron 24, 773-776.

Shomrat, T., Zarrella, I., Fiorito, G., and Hochner, B. (2008). The *Octopus* vertical lobe modulates short-term learning rate and uses LTP to acquire long-term memory. Curr Biol 18, 337-342.

Sigrist, S.J., Reiff, D.F., Thiel, P.R., Steinert, J.R., and Schuster, C.M. (2003). Experience-dependent strengthening of *Drosophila* neuromuscular junctions. J Neurosci 23, 6546-6556.

Sigrist, S.J., Thiel, P.R., Reiff, D.F., Lachance, P.E., Lasko, P., and Schuster, C.M. (2000). Postsynaptic translation affects the efficacy and morphology of neuromuscular junctions. Nature 405, 1062-1065.

Sigrist, S.J., Thiel, P.R., Reiff, D.F., and Schuster, C.M. (2002). The postsynaptic glutamate receptor subunit DGluR-IIA mediates long-term plasticity in *Drosophila*. J Neurosci 22, 7362-7372.

Steinert, J.R., Kuromi, H., Hellwig, A., Knirr, M., Wyatt, A.W., Kidokoro, Y., and Schuster, C.M. (2006). Experience-dependent formation and recruitment of large vesicles from reserve pool. Neuron 50, 723-733.

Stewart, B.A., Atwood, H.L., Renger, J.J., Wang, J., and Wu, C.F. (1994). Improved stability of *Drosophila* larval neuromuscular preparations in haemolymph-like physiological solutions. J Comp Physiol A 175, 179-191.

Stierl, M., Stumpf, P., Udwari, D., Gueta, R., Hagedorn, R., Losi, A., Gartner, W., Petereit, L., Efetova, M., Schwarzel, M.*, et al.* (2011). Light modulation of cellular cAMP by a small bacterial photoactivated adenylyl cyclase, bPAC, of the soil bacterium Beggiatoa. J Biol Chem 286, 1181-1188.

Tansey, E.M. (1997). Not committing barbarisms: Sherrington and the synapse, 1897. Brain Res Bull 44, 211-212.

Molecular Devices (2008). The axon guide: A guide to electrophysiology & biophysics laboratory techniques, 3 edn.

Thorndike, E.L. (1901). Animal intelligence: An experimental study of the associative processes in animals. . Psychological Review Monograph Supplement, 2, 1–109.

Tovar, K.R., and Westbrook, G.L. (2002). Mobile NMDA receptors at hippocampal synapses. Neuron 34, 255-264.

Trujillo-Cenóz, O. (1969). Some aspects of the structural organization of the medulla in muscoid flies. Journal of Ultrastructure Research 27, 533-553.

van de Linde, S., Loschberger, A., Klein, T., Heidbreder, M., Wolter, S., Heilemann, M., and Sauer, M. (2011). Direct stochastic optical reconstruction microscopy with standard fluorescent probes. Nature protocols 6, 991-1009.

Verstreken, P., and Bellen, H.J. (2002). Meaningless minis? Mechanisms of neurotransmitter-receptor clustering. Trends Neurosci 25, 383-385.

Wagh, D.A., Rasse, T.M., Asan, E., Hofbauer, A., Schwenkert, I., Durrbeck, H., Buchner, S., Dabauvalle, M.C., Schmidt, M., Qin, G.*, et al.* (2006). Bruchpilot, a protein with homology to ELKS/CAST, is required for structural integrity and function of synaptic active zones in *Drosophila*. Neuron 49, 833-844.

Walters, E.T., and Byrne, J.H. (1983). Associative conditioning of single sensory neurons suggests a cellular mechanism for learning. Science 219, 405-408.

Weiner, J. (2000). Time, Love, Memory: A Great Biologist and His Quest for the Origins of Behavior (New York: Vintage).

Weyhersmüller, A., Hallermann, S., Wagner, N., and Eilers, J. (2011). Rapid active zone remodeling during synaptic plasticity. J Neurosci 31, 6041-6052.

Wolf, M.J. (2012). Modeling dilated cardiomyopathies in *Drosophila*. Trends in cardiovascular medicine 22, 55-61.

Xia, S., Miyashita, T., Fu, T.F., Lin, W.Y., Wu, C.L., Pyzocha, L., Lin, I.R., Saitoe, M., Tully, T., and Chiang, A.S. (2005). NMDA receptors mediate olfactory learning and memory in *Drosophila*. Curr Biol 15, 603-615.

Yin, J.C., Wallach, J.S., Del Vecchio, M., Wilder, E.L., Zhou, H., Quinn, W.G., and Tully, T. (1994). Induction of a dominant negative CREB transgene specifically blocks long-term memory in *Drosophila*. Cell 79, 49-58.

Yoshihara, M., and Littleton, J.T. (2002). Synaptotagmin I functions as a calcium sensor to synchronize neurotransmitter release. Neuron 36, 897-908.

Zhai, R.G., and Bellen, H.J. (2004). The architecture of the active zone in the presynaptic nerve terminal. Physiology (Bethesda) 19, 262-270.

Zito, K., Fetter, R.D., Goodman, C.S., and Isacoff, E.Y. (1997). Synaptic clustering of Fascilin II and Shaker: essential targeting sequences and role of Dlg. Neuron 19, 1007-1016.

Zuo, Y., Lin, A., Chang, P., and Gan, W.B. (2005). Development of long-term dendritic spine stability in diverse regions of cerebral cortex. Neuron 46, 181-189.

9. Abbreviations and definitions

AMPA	α-amino-3-hydroxy-5-methyl-4-isoxazolepropionic acid
AP	action potential
a.u.	arbitrary unit
BRP	Bruchpilot
CD8	cluster of differentiation 8 or cluster of designation 8
CNS	central nervous system
CREB	cAMP response element binding protein
C/EBP	CCAAT enhancer binding protein
*d*STORM	*direct* stochastic optical reconstruction microscopy
e.g.	for example, Latin exempli gratia
EGFP	enhanced green fluorescent protein
GluR-IIx	glutamate receptor subunit of the x type: A, B, C or D
chop2	Channelopsin-2
ChR2	Channelrhodopsin-2
eEJC	evoked excitatory junctional current
eEJP	evoked excitatory junctional potential
GFP	green fluorescent protein
lEJC	light-evoked junctional current

LTD	long-term depression
LTP	long-term potentiation
HL3/3.1	haemolymph like solution 3/3.1
min	minutes
mini	miniature excitatory junctional current
mEJP	miniature excitatory junctional potential
n.a.	not available
ND	neutral density
NGS	normal goat serum
NMDA	N-methyl-D-aspartate
PBS	phosphate buffered saline
PBT	phosphate buffered saline with Triton
PKA	protein kinase A
PKC	protein kinase C
PSD	postsynaptic density
p_r	release probability of single active zone
RAL	All-*trans*-retinal
sem	standard error of the mean
STDP	spike timing dependent plasticity
TEM	transmission electron microscopy

TEVC	Two-electrode voltage clamp
UAS	upstream activating sequence
V	volt
v/v	a measure for concentration: volume of a fluid per total volume of solution (%)
W	watt
w/v	a measure for concentration: weight of a solid per total volume of solution (%), 1% w/v corresponds to one gram solid in 100ml solution

10. Table of figures and tables

11. Solution formulas

Laying medium

25 l	Water
125 g	Agar-agar
450 g	Baker's yeast
250 g	Soy flour
2 kg	Maize flour
35 g	Methylparaben (Sigma Aldrich H5501)
125 ml	Ethanol (Roth 9065.4)
800 g	Malt sugar syrup
440 g	Sugar beet syrup
130 ml	Propanoic acid (Roth 6026.3)

Dissolve agar in 15 l of water, cook for 5 min. Dissolve yeast and soy flour in 4 l of water. Dissolve maize flour in another 4 l of water. Warm up malt sugar and sugar beet syrups. Mix Agar solutions with the syrups, cook for 5 min at middle temperature. Add soy flour solution and cook for 5min while stirring at middle temperatures. Add maize flour solution and flush with the remaining 2 l of water. Heat up to 90°C and cook for 10 min at this temperature while stirring. Dissolve methylparaben in ethanol. Add methylparaben solution and propanoic acid to the warm mash as soon as the mash is cooled down to 65°C.

HL-3/HL-3.1 without Ca^{++}

70 mmol/l	NaCl (Merck 1.06404)
5 mmol/l	KCl (Merck 1.04933)
20 (HL-3) /5 (HL-3.1) mmol/l	$MgCl_2$ (Merck 1.05833)
10 mmol/l	$NaHCO_3$ (Sigma Aldrich S6297)
5 mmol/l	D-(+)-Trehalose (Sigma Aldrich T5251)
115 mmol/l	Sucrose (Sigma Aldrich S9378)
5 mmol/l	HEPES (Sigma Aldrich 54457)
	adjust to pH 7.2

pH of 7.2 was adjusted with 1 mol/l NaOH or 1mol/l HCl solutions.

Phosphate buffered saline (PBS)

8 g	NaCl (Merck 1.06404)
1.15 g	Na_2HPO_4 (Merck 1.06580)
0.2 g	KCl (Merck 1.04933)
0.2 g	KH_2PO_4 (Merck 1.05108)
1 l	fill up to with H_2O

pH of 7.4 was adjusted with 1 mol/l NaOH or 1mol/l HCl solutions.

4% (w/v) polyformaldehyde (PFA) in PBS

8 g PFA (Merck 1.04005) was dissolved in 150 ml H_2O for 15 min at 50-60°, a minute amount of NaOH (2 mol/l) was added till the solution became clear. 20 ml 10x PBS was added and filled up to 200 ml with H_2O.

pH of 7.4 was adjusted with 1 mol/l NaOH or 1mol/l HCl solutions.

Phosphate buffered solution with 0.05% (v/v) Triton X100 (PBT)

8 g	NaCl (Merck 1.06404)
1.15 g	Na_2HPO_4 (Merck 1.06580)
0.2 g	KCl (Merck 1.04933)
0.2 g	KH_2PO_4 (Merck 1.05108)
1 l	fill up to with H_2O
500µl	Triton X100 (Sigma Aldrich T9284)

pH of 7.4 was adjusted with 1 mol/l NaOH or 1mol/l HCl solutions before adding Triton X100.

12. Appendix

12.1 Publications

Ljaschenko, D., Ehmann, N., and Kittel, R.J. (2013). Hebbian plasticity guides maturation of glutamate receptor fields *in vivo*. Cell Reports 3, 1407-13

Stock, P.*, Ljaschenko, D.*, Heckmann, M., Dudel J. Agonists binding nicotinic receptors elicit specific channel opening patterns at αγ or αδ sites. *Submitted.*

Dawydow, A.*, Gueta, R.,*, Ljaschenko, D., Hermann, M., Fiala, A., Langenhan, T., Nagel, G., Kittel, R.J. An improved channelrhodopsin for behavioural neuroscience *Submitted.*

Ehmann, N.*, van de Linde, S.*, Ljaschenko, D., Keung, X.Z., Holm, T., Weyhersmüller, A., DiAntonio, A., Hallermann, S., Heckmann, M., Sauer, M., Kittel, R.J. Quantitative Super-Resolution Imaging of Active Zone States. *Submitted.*

*Equal contribution

12.2 Academic Curriculum Vitae

Education

10/2008 - present	University of Wuerzburg, PhD thesis in neuroscience, on synaptic plasticity
10/2002 - 6/2008	University of Wuerzburg, "Diplom" in Biology Main focus: neuroscience (functional electrophysiology) Focus: bioinformatics (Perl programming, SQL data base programming) Focus: biotechnology (cryobiology, electro manipulation, waste water treatment)

Skills & Experience

2004-present	**Programming**: automated image analysis plugins, PERL programming for bioinformatics applications, SQL programming for biological data bases
02/2013	**Poster Award** at the annual international congress of the German Physiological Society in Heidelberg
03/2012	**Oral presentation** at the annual international congress of the German Physiological Society in Dresden
10/2012	**Oral presentation** at the international symposium of the Graduate School of Life Sciences University of Wuerzburg in Wuerzburg, Germany
07/2010	**Oral presentation** at the international meeting "Communicating Physiology" in Maribor, Slovenia

Languages

English (business fluent), German (native language), Russian (native language), French (reading)